From Weather Forecasts to Impact-Based Flood Warning Systems - a Modelling Perspective

Inauguraldissertation
der Philosophisch-naturwissenschaftlichen Fakultät
der Universität Bern

vorgelegt von

Markus Mosimann

von Signau

LeiterInnen der Arbeit:

Prof. Dr. Andreas Zischg
Prof. Dr. Olivia Romppainen-Martius

Geographisches Institut der Universität Bern, Mobiliar Lab für Naturrisiken,
Oeschger-Zentrum für Klimaforschung

From Weather Forecasts to Impact-Based Flood Warning Systems - a Modelling Perspective

Inauguraldissertation
der Philosophisch-naturwissenschaftlichen Fakultät
der Universität Bern

vorgelegt von

Markus Mosimann

von Signau

LeiterInnen der Arbeit:

Prof. Dr. Andreas Zischg
Prof. Dr. Olivia Romppainen-Martius

Geographisches Institut der Universität Bern, Mobiliar Lab für Naturrisiken,
Oeschger-Zentrum für Klimaforschung

Von der Philosophisch-naturwissenschaftlichen Fakultät angenommen.

Bern, 28. Mai 2024

Der Dekan:
Prof. Dr. Marco Herwegh

In any moment of decision, the best thing you can do is the right thing, the next best thing is the wrong thing, and the worst thing you can do is nothing.

–Theodore Roosevelt

Abstract

Climate change is exacerbating devastating flood events and has thus increased the critical need for effective flood risk management strategies. Traditional flood warnings often fall short in communicating specific impacts to communities, leading to poor preparedness and weak responses. This PhD thesis addresses this shortcoming by enhancing the early warning framework for fluvial floods in Switzerland. Translating weather forecasts into impact forecasts requires (i) the development of vulnerability models, (ii) the capability for near real-time computation of hazards and their impacts, and (iii) comprehensive understanding and integration of uncertainties. Finally, it needs (iv) cartographic and graphical visualizations to transfer the modelling perspective, namely the impact assessment derived from weather forecasts to decision-makers.

The first paper in this thesis focuses on the often-overlooked aspect of household contents damage. This paper presents two regression models that analyze insurance claim records to estimate monetary damage and the degree of damage to household contents from that to building structure. These models are robust and enable the degree of damage model to be transferred as well. They are therefore valuable tools for improving the estimation of financial flood impacts. The findings underscore the significant contribution of contents damage to total building damage and challenge current flood damage assessments to broaden their scope beyond structural damage.

The second paper introduces a novel library-based surrogate flood model designed for real-time impact-based warnings. The surrogate model was tested in northern Switzerland's river and lake network and benchmarked against high-resolution transient flood simulations with reduced computational efficiency, and it demonstrates a high agreement with flood impacts assessed for buildings, people, and workplaces. In nine scenarios derived from hindcast archives, the surrogate model achieves a critical success index for area between 0.74 and 0.90 and for exposed people between 0.77 and 0.93 and thus proves its potential for real-time flood impact prediction at national scale. This optimization of the trade-off between spatial resolution and computational efficiency signifies a substantial advancement in impact-based flood forecasting.

The third study explores the quantification of impact sensitivity to changes in flood magnitudes in floodplains. This paper introduces the floodplain sensitivity index (FSI), which integrates slope and curvature metrics, to provide a nuanced understanding of how floodplains respond to various flood scenarios. An analysis with the FSI demonstrates the nonlinearity and region-specific nature of the relationship between flood magnitude and impacts. The FSI aids in identifying significant magnitude thresholds both for short-term impact-based warnings and for and long-term climate-change-influenced flood risk mitigation. It defines ranges with high or low sensitivity of impacts to increases in magnitude and enhances the formulation and precision of impact-based warnings.

Fourthly, by integrating and visualizing the models and methods developed in these studies into web tools, this thesis contributes to risk communication and shows the

potential of web-based solutions for impact-based flood warning systems to bridge the gap between hydrometeorological forecasting and practical flood risk mitigation.

In conclusion, this doctoral thesis introduces innovative modelling approaches that enhance impact-based forecast and warning services and provides valuable insights into critical aspects of flood risk management to help face the challenges of an anticipated increase of extreme flood events with severe impacts. The modelling perspective thus allows model chains to be extended from weather forecasts to impact forecasts. Impact forecasts can only be made with models for dynamic hazard and impact assessments that are coupled with weather forecast models. This perspective also facilitates the evaluation of simulation techniques for real-time applications. Besides addressing unresolved scientific questions, the focus on Switzerland and the web-based communication of its findings illustrates the practical applicability of this approaches , which aligns with the latest standards in web-based technology to expand the current early warning framework in Switzerland.

Keywords: Impact-based flood warnings; flood vulnerability assessment; real-time flood forecasting; floodplain impact sensitivity; web-based flood impact visualization; flood risk management

Contents

List of Figures

List of Tables

1 Introduction

River floods are among the most prevalent natural disasters and are responsible for significant economic, environmental, and human losses globally. According to the Global Assessment Report on Disaster Risk Reduction, on average, global annual damages caused by flood risk amount to US$ 104 billion (UNISDR, 2015). Recent flood events exemplify their disruptive potential. For instance, floods in Western and Central Europe in 2021 caused more than 180 fatalities overall. The flooding of the Ahr River in Germany led to discussions about responsibilities which concluded that the gap in communication between weather services and the authorities was one reason for the weak response that led to this high number of fatalities (Fekete & Sandholz, 2021). Further examples of extreme flood events followed globally: In August 2022, an extreme flood event in Pakistan caused 1280 fatalities (Shehzad, 2023). In 2023, floods in California, USA, flooding of the Emilia-Romagna region in Italy, and an extreme flood event involving Slovenia, Austria, and Croatia together resulted in hundreds of fatalities and billions in damage . In this context, the question arises how far the occurrence of floods can be attributed to climate change (e.g., Faranda et al., 2022; Clarke et al., 2022).

Across a wide range of regions, including Western and Central Europe, projections consistently anticipate that flood risk will increase as a result of climate change. More intense and changing weather patterns lead to more severe rainfall and thus increase the likelihood and severity of floods and of flood hazard (Intergovernmental Panel on Climate Change, 2021; CH2018, 2018). Consequently, areas that may have been considered low risk in the past will face or already face higher risks of flooding, and regions already vulnerable to flooding will experience even greater challenges.

Besides hazard, exposure and vulnerability are key components of flood risk that determine which elements are at risk, such as the numbers of exposed buildings and people , and their susceptibility to floods. In the past, socio-economic development and human interventions have influenced all of these intertwined components (Zischg et al., 2018b). Projections Iindicate that trends in these components will lead to a severe increase in flood risk (Jongman et al., 2012). Anthropogenic interventions such as levee constructions have created supposedly protected areas that are now occupied by new buildings for a growing population. This has increased the potential impacts of extreme flood events (Elmer et al., 2012; Cammerer & Thieken, 2013; Fuchs et al., 2015, 2017; Nicholls & Crompton, 2017; Zischg et al., 2018b). These developments are even more critical because they combine with an expected increase of extreme events that exceed the design standards for these levees (Dottori et al., 2018), and with, as Fischer et al. (2021) stated in the general context of climate extremes, "extremes unprecedented in the observational period often have substantial impacts due to a tendency to adapt to the highest intensities, and no higher, experienced during a lifetime."

An effective strategy for reducing the impacts of river floods particularly when structural defenses such as levees do not meet the full scope of flood challenges, is by increasing

Fig. 1.1: Examples of key IBFWS user groups (World Meteorological Organization, 2021)

flood awareness and perception through the implementation of early warning systems. Poor responses to flood warnings from national meteorological and hydrological service s (NMHSs) led the World Meteorological Organization (WMO) to launch guidelines for the development of impact-based warning (IBW) and impact forecast (IF) services (World Meteorological Organization, 2015). These guidelines state that IBWs are designed to inform target users about the impacts of forecasted weather events expected from known vulnerabilities. IFs enhance this approach by incorporating detailed information about individual and community-level exposure. This enhancement aims to support informed decision-making to optimize short-term prevention and risk management tailored to specific target groups (see examples of key user groups in Figure 1.1). In its updated guidelines (World Meteorological Organization, 2021), the WMO has merged the concepts of IBW and IF into the term impact-based forecast and warning services (IBFWSs).

This thesis explores innovative modelling approaches to be implemented in IBFWSs and thus enhance flood impact mitigation in Switzerland. By addressing hazard, exposure, and vulnerability, this thesis aims to find solutions associated with the challenges in forecasting the impacts of anticipated fluvial extreme flood events. The current trends in climate change and socio-economic development will render these increasingly important. Moreover, by developing publicly accessible, interactive web tools, this thesis contributes to increasing the risk awareness of professionals, politicians, and the general public to enhance prevention and preparedness for flood events.

1.1 Background and problem statement

Recent studies have demonstrated the effectiveness of IBFWSs in enhancing response actions and risk perception during extreme weather events (Weyrich et al., 2018; Casteel,

2018; Potter et al., 2018; Meléndez-Landaverde et al., 2020). Despite their proven effectiveness, a significant need remains for improvement in the collection and management of impact data and the refinement of technical standards to enhance or establish the operational efficacy of IBFWSs for floods (Meléndez-Landaverde et al., 2020; Potter et al., 2021). Therefore, methodologies are needed that are capable of laying the analytical groundwork for accurately identifying fluvial flood hazards, assessing flood exposure, and defining potential impacts of vulnerabilities to floods. Such methodologies are essential to bridge the gap between the forecasts provided by NMHSs and the various target users effectively .

Modelling approaches facilitate the anticipation of potential impacts of flood events. These approaches support the formulation of impact-based warnings for potentially affected communities and provide detailed insights for effective decision-making. Nevertheless, several gaps in current modelling approaches limit their appropriateness for early warning applications; these gaps are explained subsequently.

1.1.1 Model chains: From weather prediction to impact assessment

Model chains from weather to impacts involve a multistep process in which meteorological data are first used to predict weather conditions. These conditions are then fed into hydrological models to forecast river flows, lake levels, and potential flooding and then generate hydrographs containing the estimation of discharge or lake levels over time. These provide input to hydrodynamic models that simulate the flood dynamics, including water depth and flow velocity over time and across the landscape, which is referred to as floodplain. This detailed information allows flood extents to be mapped and the exposure of infrastructure and populations to be assessed. The final step involves analyzing the socio-economic consequences of hazard and exposure from the vulnerability of the elements at risk, such as financial damage, displacement, and interruption of roads. Each step in the modelling chain requires specialized expertise and represents distinct research domains. This integrated approach provides a comprehensive understanding of the cascading effects of weather events on human and natural systems.

Numerous studies have used model chains for flood risk assessment and thus highlighted their potential value (van Dyck & Willems, 2013; Ward et al., 2013; Falter et al., 2015; Foudi et al., 2015; Moncoulon et al., 2014; Alfieri et al., 2016; Felder et al., 2018). However, the emphasis in these studies is not on near-real-time application. For instance, their computation times can exceed the lead times required for actionable warnings, making them unsuitable for use in early warning systems. Computational efficiency needs to be optimized to meet the demands of timely and effective flood forecasting and response actions.

Operationally, numerous countries have established NMHSs to offer forecasts on expected flood magnitudes, such as discharge and lake levels, and to alert populations about potential hazards. In Switzerland, the Federal Office for the Environment (FOEN) issues hydrological forecasts for "rivers and lakes of national interest" (FOEN, 2024b). These forecasts are updated daily and more frequently during flood events. This service provides early warnings to both authorities and the public and categorize potential hazards into five levels by their severity thresholds for specific sections of the main rivers and lakes in Switzerland. Level 1 indicates no or low danger and level 5 signifies very

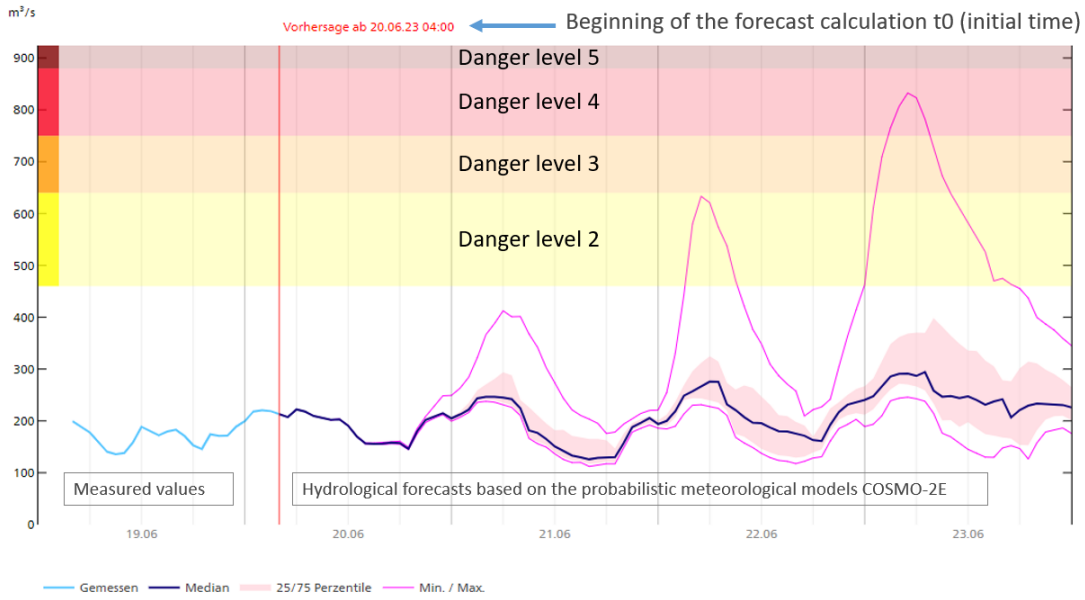

Fig. 1.2: The hydrological forecasts for the station Rhône–Porte-du-Scex exemplifies the forecast given by the Federal Office for the Environment (FOEN), provided by FOEN (2024a). Explanatory notes on the legend—*Gemessen* (=measured): Discharge measured at the station. Median: Median forecast among all 21 model outputs. 25/75 Percentile: interquartile range. Min./Max.: Range spanned by maximum and minimum estimation.

high danger (Figure 1.2). The warnings provide information about potential impacts and behavioral recommendations, such as avoiding driving on flooded roads. Nevertheless, these warnings tend to be broad and cover extensive areas, and they lack the information at individual and community level that is required by many target groups of IBFWSs.

As this thesis focuses on Switzerland, the point from which approaches for improving IBFWSs need to start is at the outputs of hydrological models estimated from NMHSs. Although hydrological forecasts at the national level can already be produced in a timeframe suitable for early warnings, the next step in the model chain, the hydrodynamic simulation, requires the trade-off between high resolution and computation time to be resolved (Savage et al., 2016). This is the chief reason why flood risk assessment approaches cannot yet be implemented in early warning services.

1.1.2 Hydrodynamic modelling

One-dimensional (1D) flood models simulate water flow within river channels with cross-sectional data at high computational efficiency. Two-dimensional (2D) models are more complex and suited for detailed flood risk mapping. Combining these, 1D-2D coupled models integrate river flow with floodplain inundation, which is valuable for complex flood scenarios (Neal et al., 2012). Recent studies have demonstrated the capability of high-resolution (10m) raster-based 2D flood models, which use GPU technology for early warning applications across large areas (Ming et al., 2020; Apel et al., 2004). These employ fixed grid cells, potentially oversimplifying complex terrains even at a resolution of 10m. For instance, the top edges of levees in Switzerland typically span only a few

meters in width, indicating that a resolution of 10 meters is inadequate for accurately representing these structures. Flexible mesh models adjust resolution dynamically and thus offer precision around and discretization of critical features without significantly increasing computational load (Horritt & Bates, 2002; Zischg et al., 2018c).

The implementation of hydrodynamic models in warning systems is even more critical because hydrometeorological forecasts are derived from ensemble weather predictions, as illustrated by the range spanned by the lines indicating the minimum and maximum estimations of discharge in Figure 1.2. To navigate these uncertainties, a service supporting IBFWs must be applicable to a range of forecasts, a requirement that intensifies the trade-off between computational efficiency and spatial resolution.

Library-based surrogate flood models have the potential to resolve this issue and optimize this trade-off (Zischg et al., 2018a). They are particularly applied to surface water floods (Bermúdez et al., 2018; Aldridge et al., 2020; Cox et al.). Impact forecasts are derived from precalculated flood simulations stored, for instance, in a database. When a flood forecast occurs, the system selects a simulation that exhibits similar peak discharge or lake level. Library-based surrogate models are also referred to as metamodels or models of models (Razavi et al., 2012). The term surrogate model is also used to refer to deep learning models that replace numerical simulations, an emerging technique in flood modelling.

1.1.3 Exposure and vulnerability

Two other key components in risk assessment are exposure and vulnerability. Exposure refers to the elements at risk, such as people, property, and infrastructure, and vulnerability is the susceptibility of these elements (World Meteorological Organization, 2015). Vulnerability can be physical when related to building and infrastructure damage and social when related, for instance, to communities' ability to respond to and recover from flood events. The WMO guidelines for IBFWSs emphasize these concepts and advocate warnings that not only predict meteorological events but also forecast their potential impacts on exposed and vulnerable elements to enhance preparedness and response actions.

Whereas exposure is often simplified as the intersection of the extent of flood hazards and, for instance, building footprints (e.g., Rothlisberger et al., 2017; Zischg et al., 2018c), vulnerability can encompass a wider array of factors beyond physical attributes, including socio-economic conditions, community resilience, and adaptive capacities, encapsulated as social vulnerability (Fuchs & Thaler, 2018). These aspects influence how communities anticipate, cope with, respond to, and recover from the impacts of flood events. Understanding both physical and social vulnerability is crucial to developing effective IBFWSs.

This thesis particularly focuses on physical vulnerability. In combination with exposure, physical vulnerability plays a critical role in prioritization during decision-making processes and therefore affects social vulnerability. The analysis of physical vulnerability helps in identifying areas and communities at higher risk. Such information is the basis for planning mitigation measures and allocating resources accordingly (World Meteorological Organization, 2021).

A central point in flood risk management is the estimation of monetary damage. For buildings, vulnerability is defined as the monetary damage relative to the value of a building, also described as the degree of loss, or degree of damage. This concept is important when linking flood magnitude parameters, such as flow depth and velocity, to empirical damage data through vulnerability or stage-damage functions. Although these are primarily developed for assessing building structure vulnerability (e.g., Fuchs et al., 2012; Papathoma-Köhle et al., 2011), they also provide systematic oversight of the impact on household content vulnerability. Nevertheless, Thieken et al. (2005) notes the considerable proportion of household content damage in total building damage and emphasizes the need for empirical data for developing reliable vulnerability functions. Studies of vulnerability functions for building and content damage often have regional character and remain specific to the regions from which the damage data stem (Molinari et al., 2020).

1.1.4 Building resilience: leveraging risk awareness and perception for flood prevention and preparedness

A widely recognized and described phenomenon is that society's memory of flood events is limited, and longer periods without floods lower the awareness of flood risk, and therefore flood perception, prevention, and preparedness (e.g., Munz et al., 2023; Fischer et al., 2021), whether or not general information about flood hazard is available (Glaus et al., 2020). In Switzerland, areas with high flood hazard cover a large proportion of the settled area. In personal discussions, I often experience skepticism on the issue, particularly about areas classified as dangerous. People often remark that no flood has occurred in the last 20 or 30 years. This view is also highlighted by a Swiss study on "what makes flood protection projects successful" (Thomi et al., 2015), which demonstrates that mitigation measures mainly gain acceptance in society after the occurrence of a flood event.

The communication of flood risks via their impacts offers a promising approach to enhancing flood risk awareness and to bridging the gap between hydrometeorological forecasts and decision-makers. Consequently, using visualizations in communication strategies can improve the comprehension of potential flood impacts among a wide audience, including decision-makers who often are not experts in natural hazards. Optimally, the development of such visualizations is accompanied by target users such that the final product meets their needs (Munz et al., 2023; Percival et al., 2020). The WMO encourages and recommends using websites and other media sources to communicate IBFWSs (World Meteorological Organization, 2021, Chapter 2).

1.2 Aims and scope of the thesis

Extreme river flood events are projected to be exacerbated by trends in climate change and socio-economic development. Additionally, unprecedented flood events often result in weak mitigation responses. Consequently, this thesis aims to lay a technical foundation for IBFWSs for floods and to bridge the gap between hydrometeorological warning services (Figure 1.2) and their potential target users (Figure 1.1) in Switzerland. It aims to leverage and improve state-of-the art techniques in hydrodynamic and vulnerability

modelling for IBFWSs and therefore to enhance the physical model chain from weather forecasts to IBFWSs. Moreover, this thesis aims to improve public awareness of flood risks by communicating results from research in openly accessible and interactive web tools. Besides showing the potential of web-based tools for IBFWSs, this thesis aims to increase flood risk awareness and to enhance social resilience. The specific objectives of this thesis are these:

1. **Modelling the vulnerability and damage of household contents**

   The first aim of this thesis is to enhance flood damage estimation by providing a robust modelling approach that integrates the vulnerabilities of household contents. The approach should provide a more holistic understanding of flood impacts and thus improve the accuracy of damage assessments. The estimation of household content damage aids the prioritization process during an extreme flood event (Chapter 2).

2. **Development of a surrogate flood model for real-time flood impact forecasts**

   The second aim is to explore and optimize the efficiency of hydrodynamic models to meet the requirements of near-real-time IBFWSs. By optimizing the trade-off between spatial resolution and computational efficiency, this chapter aims to develop a flood modelling approach that meets the requirements of early warning systems and enables them to deliver timely and detailed flood warnings to various target users (Chapter 3).

3. **Assessment of impact sensitivity in floodplains**

   The third part of this thesis focuses on the sensitivity of impacts to uncertainties in hydrometeorological forecasts. By introducing a floodplain sensitivity index (FSI) derived from the magnitude–impact relationship of floodplains and highlighting magnitude ranges with a high sensitivity of impacts, this thesis seeks to improve the formulation of flood warnings for specific target groups. Additionally, the FSI is also applicable for uncertainties of climate-change projections and therefore supports decision-making in the short and long term (Chapter 4).

4. **Enhancing flood risk awareness through interactive web tools**

   Lastly, this thesis aims to show how interactive web tools can enhance flood risk awareness by integrating data, models, and insights gained from the research presented in Chapters 2 to 4. The tools developed focus on the impact-oriented communication of consequences of physically plausible extreme weather and flood events and showcase the potential of web-based visualization solutions in transferring impact-based warnings from NMHSs to target users (Chapter 5).

The insights derived from Chapters 2 to 5 are synthesized in Chapter 6 along with a brief outlook on further research and steps needed for the integration of the methodologies presented into Switzerland's current national early warning system. Despite the Swiss focus of this thesis, the methods developed in this thesis are aligned to the WMO's guidelines and designed for adaptation and implementation in other regions facing similar challenges. This research contributes to the broader field of disaster risk reduction by offering modelling solutions that meet the requirements of IBFWSs.

References

Aldridge, T., Gunawan, O., Moore, R. J., Cole, S. J., Boyce, G., & Cowling, R. (2020). Developing an impact library for forecasting surface water flood risk. *Journal of Flood Risk Management*, *13*. doi:10.1111/jfr3.12641.

Alfieri, L., Feyen, L., Salamon, P., Thielen, J., Bianchi, A., Dottori, F., & Burek, P. (2016). Modelling the socio-economic impact of river floods in europe. *Natural Hazards and Earth System Science*, *16*, 1401–1411. doi:10.5194/nhess-16-1401-2016.

Apel, H., Thieken, A. H., Merz, B., & Blöschl, G. (2004). Flood risk assessment and associated uncertainty. *Natural Hazards and Earth System Science*, *4*, 295–308. doi:10.5194/nhess-4-295-2004.

Bermúdez, M., Ntegeka, V., Wolfs, V., & Willems, P. (2018). Development and comparison of two fast surrogate models for urban pluvial flood simulations. *Water Resources Management*, *32*, 2801–2815. doi:10.1007/s11269-018-1959-8.

Cammerer, H., & Thieken, A. H. (2013). Historical development and future outlook of the flood damage potential of residential areas in the alpine lech valley (austria) between 1971 and 2030. *Regional Environmental Change*, *13*, 999–1012. doi:10.1007/s10113-013-0407-9.

Casteel, M. A. (2018). An empirical assessment of impact based tornado warnings on shelter in place decisions. *International Journal of Disaster Risk Reduction*, *30*, 25–33. doi:10.1016/j.ijdrr.2018.01.036.

CH2018 (2018). Ch2018 - climate scenarios for switzerland, technical report. National Centre for Climate Services. URL: https://www.nccs.admin.ch/nccs/en/home/data-and-media-library/data/ch2018---climate-scenarios-for-switzerland.html.

Clarke, B., Otto, F., Stuart-Smith, R., & Harrington, L. (2022). Extreme weather impacts of climate change: an attribution perspective. *Environmental Research: Climate*, *1*, 012001. doi:10.1088/2752-5295/ac6e7d.

Cox, T., Hampson, R., Hooper, R., Hunter, N., Porter, I.-H., Revilla-Romero, B., Stroud, R., & Wylde, R. (). Real-time flood impacts mapping: Technical report. Environment Agency. URL: https://assets.publishing.service.gov.uk/media/6037956ae90e070563e5a6da/Real-time_flood_impacts_mapping_-_report__1_.pdf.

Dottori, F., Szewczyk, W., Ciscar, J.-C., Zhao, F., Alfieri, L., Hirabayashi, Y., Bianchi, A., Mongelli, I., Frieler, K., Betts, R. A., & Feyen, L. (2018). Increased human and economic losses from river flooding with anthropogenic warming. *Nature Climate Change*, *8*, 781–786. doi:10.1038/s41558-018-0257-z.

Elmer, F., Hoymann, J., Düthmann, D., Vorogushyn, S., & Kreibich, H. (2012). Drivers of flood risk change in residential areas. *Natural Hazards and Earth System Science*, *12*, 1641–1657. doi:10.5194/nhess-12-1641-2012.

Falter, D., Schröter, K., Dung, N. V., Vorogushyn, S., Kreibich, H., Hundecha, Y., Apel, H., & Merz, B. (2015). Spatially coherent flood risk assessment based on long-term continuous simulation with a coupled model chain. *Journal of Hydrology*, *524*, 182–193. doi:10.1016/j.jhydrol.2015.02.021.

Faranda, D., Bourdin, S., Ginesta, M., Krouma, M., Noyelle, R., Pons, F., Yiou, P., & Messori, G. (2022). A climate-change attribution retrospective of some impactful weather extremes of 2021. *Weather and Climate Dynamics*, *3*, 1311–1340. doi:10.5194/wcd-3-1311-2022.

Fekete, A., & Sandholz, S. (2021). Here comes the flood, but not failure? lessons to learn after the heavy rain and pluvial floods in germany 2021. *Water*, *13*, 3016. doi:10.3390/w13213016.

Felder, G., Gómez-Navarro, J. J., Zischg, A. P., Raible, C. C., Röthlisberger, V., Bozhinova, D., Martius, O., & Weingartner, R. (2018). From global circulation to local flood loss: Coupling models across the scales. *The Science of the total environment*, *635*, 1225–1239. doi:10.1016/j.scitotenv.2018.04.170.

Fischer, E. M., Sippel, S., & Knutti, R. (2021). Increasing probability of record-shattering climate extremes. *Nature Climate Change*, *11*, 689–695. doi:10.1038/s41558-021-01092-9.

FOEN (2024a). Explanatory notes on forecast plots. Federal Office for the Environment FOEN. URL: https://www.hydrodaten.admin.ch/en/erlauterungen-zu-den-vorhersage-plots.

FOEN (2024b). Forecasts and flood alerts: stations with forecasts. Federal Office for the Environment FOEN. URL: https://www.hydrodaten.admin.ch/en/messstationen-vorhersage. Last accessed: 04.04.2024.

Foudi, S., Osés-Eraso, N., & Tamayo, I. (2015). Integrated spatial flood risk assessment: The case of zaragoza. *Land Use Policy*, *42*, 278–292. doi:10.1016/j.landusepol.2014.08.002.

Fuchs, S., Birkmann, J., & Glade, T. (2012). Vulnerability assessment in natural hazard and risk analysis: current approaches and future challenges. *Natural Hazards*, *64*, 1969–1975. doi:10.1007/s11069-012-0352-9.

Fuchs, S., Keiler, M., & Zischg, A. (2015). A spatiotemporal multi-hazard exposure assessment based on property data. *Natural Hazards and Earth System Science*, *15*, 2127–2142. doi:10.5194/nhess-15-2127-2015.

Fuchs, S., Röthlisberger, V., Thaler, T., Zischg, A., & Keiler, M. (2017). Natural hazard management from a coevolutionary perspective: Exposure and policy response in the european alps. *Annals of the American Association of Geographers*, *107*, 382–392. doi:10.1080/24694452.2016.1235494.

Fuchs, S., & Thaler, T. (Eds.) (2018). *Vulnerability and Resilience to Natural Hazards*. Cambridge University Press.

Glaus, A., Mosimann, M., Röthlisberger, V., & Ingold, K. (2020). How flood risks shape policies: flood exposure and risk perception in swiss municipalities. *Regional Environmental Change*, *20*, 120. doi:10.1007/s10113-020-01705-7.

Horritt, M. S., & Bates, P. D. (2002). Evaluation of 1d and 2d numerical models for predicting river flood inundation. *Journal of Hydrology*, *268*, 87–99. doi:10.1016/S0022-1694(02)00121-X.

Intergovernmental Panel on Climate Change (2021). *Climate Change 2021: The physical science basis : summary for policymakers : working group I contribution to the sixth Assessment report of the Intergovernmental Panel on Climate Change*. Geneva, Switzerland: Intergovernmental Panel on Climate Change.

Jongman, B., Ward, P. J., & Aerts, J. C. (2012). Global exposure to river and coastal flooding: Long term trends and changes. *Global Environmental Change*, *22*, 823–835. doi:10.1016/j.gloenvcha.2012.07.004.

Meléndez-Landaverde, E. R., Werner, M., & Verkade, J. (2020). Exploring protective decision–making in the context of impact–based flood warnings. *Journal of Flood Risk Management*, *13*. doi:10.1111/jfr3.12587.

Ming, X., Liang, Q., Xia, X., Li, D., & Fowler, H. J. (2020). Real–time flood forecasting based on a high–performance 2–d hydrodynamic model and numerical weather predictions. *Water Resources Research*, *56*. doi:10.1029/2019WR025583.

Molinari, D., Scorzini, A. R., Arrighi, C., Carisi, F., Castelli, F., Domeneghetti, A., Gallazzi, A., Galliani, M., Grelot, F., Kellermann, P., Kreibich, H., Mohor, G. S., Mosimann, M., Natho, S., Richert, C., Schroeter, K., Thieken, A. H., Zischg, A. P., & Ballio, F. (2020). Are flood damage models converging to "reality"? lessons learnt from a blind test. *Natural Hazards and Earth System Sciences*, *20*, 2997–3017. URL: https://nhess.copernicus.org/articles/20/2997/2020/. doi:10.5194/nhess-20-2997-2020.

Moncoulon, D., Labat, D., Ardon, J., Leblois, E., Onfroy, T., Poulard, C., Aji, S., Rémy, A., & Quantin, A. (2014). Analysis of the french insurance market exposure to floods: a stochastic model combining river overflow and surface runoff. *Natural Hazards and Earth System Science*, *14*, 2469–2485. doi:10.5194/nhess-14-2469-2014.

Munz, L., Kauzlaric, M., Mosimann, M., Fehlmann, A., Martius, O., & Zischg, A. P. (2023). Participatory development of storymaps to visualize the spatiotemporal dynamics and impacts of extreme flood events for disaster preparedness. *International Journal of Disaster Risk Reduction*, *98*, 104039. doi:10.1016/j.ijdrr.2023.104039.

Neal, J., Schumann, G., & Bates, P. (2012). A subgrid channel model for simulating river hydraulics and floodplain inundation over large and data sparse areas. *Water Resources Research*, *48*, 619. doi:10.1029/2012WR012514.

Nicholls, S., & Crompton, J. L. (2017). The effect of rivers, streams, and canals on property values. *River Research and Applications*, *33*, 1377–1386. doi:10.1002/rra.3197.

Papathoma-Köhle, M., Kappes, M., Keiler, M., & Glade, T. (2011). Physical vulnerability assessment for alpine hazards: state of the art and future needs. *Natural Hazards*, *58*, 645–680. doi:10.1007/s11069-010-9632-4.

Percival, S. E., Gaterell, M., & Hutchinson, D. (2020). Effective flood risk visualisation. *Natural Hazards*, *104*, 375–396. doi:10.1007/s11069-020-04173-8.

Potter, S., Harrison, S., & Kreft, P. (2021). The benefits and challenges of implementing impact-based severe weather warning systems: Perspectives of weather, flood, and emergency management personnel. *Weather, Climate, and Society*, *13*, 303–314. doi:10.1175/WCAS-D-20-0110.1.

Potter, S. H., Kreft, P. V., Milojev, P., Noble, C., Montz, B., Dhellemmes, A., Woods, R. J., & Gauden-Ing, S. (2018). The influence of impact-based severe weather warnings on risk perceptions and intended protective actions. *International Journal of Disaster Risk Reduction*, *30*, 34–43. doi:10.1016/j.ijdrr.2018.03.031.

Razavi, S., Tolson, B. A., & Burn, D. H. (2012). Review of surrogate modeling in water resources. *Water Resources Research*, *48*. doi:10.1029/2011WR011527.

Rothlisberger, V., Zischg, A. P., & Keiler, M. (2017). Identifying spatial clusters of flood exposure to support decision making in risk management. *The Science of the total environment*, *598*, 593–603. doi:10.1016/j.scitotenv.2017.03.216.

Savage, J. T. S., Bates, P., Freer, J., Neal, J., & Aronica, G. (2016). When does spatial resolution become spurious in probabilistic flood inundation predictions? *Hydrological Processes*, *30*, 2014–2032. doi:10.1002/hyp.10749.

Shehzad, K. (2023). Extreme flood in pakistan: Is pakistan paying the cost of climate change? a short communication. *The Science of the total environment*, *880*, 162973. doi:10.1016/j.scitotenv.2023.162973.

Thieken, A. H., Müller, M., Kreibich, H., & Merz, B. (2005). Flood damage and influencing factors: New insights from the august 2002 flood in germany. *Water Resources Research*, *41*. doi:10.1029/2005WR004177.

Thomi, L., Zischg, A., & Suter, H. (2015). *Was macht Hochwasserschutzprojekte erfolgreich? Eine Evaluation der Risikoentwicklung, des Nutzens und der Rolle privater Geldgeber*. Bern: Geographisches Institut.

UNISDR (2015). *Global assessment report on disaster risk reduction (GAR) 2015: Making development sustainable : the future of disaster risk management*. New York: United Nations.

van Dyck, J., & Willems, P. (2013). Probabilistic flood risk assessment over large geographical regions. *Water Resources Research*, *49*, 3330–3344. doi:10.1002/wrcr.20149.

Ward, P. J., Jongman, B., Weiland, F. S., Bouwman, A., van Beek, R., Bierkens, M. F. P., Ligtvoet, W., & Winsemius, H. C. (2013). Assessing flood risk at the global scale: model setup, results, and sensitivity. *Environmental Research Letters*, *8*, 044019. doi:10.1088/1748-9326/8/4/044019.

Weyrich, P., Scolobig, A., Bresch, D. N., & Patt, A. (2018). Effects of impact-based warnings and behavioral recommendations for extreme weather events. *Weather, Climate, and Society*, *10*, 781–796. doi:10.1175/WCAS-D-18-0038.1.

World Meteorological Organization (2015). Wmo guidelines on multi-hazard impact-based forecast and warning services, . URL: https://library.wmo.int/doc_num.php?explnum_id=7901.

World Meteorological Organization (2021). *WMO guidelines on multi-hazard impact-based forecast and warning services: Part II: Putting Multi-hazard IBFWS into Practice* volume no. 1150 of *WMO*. Geneva, Switzerland: World Meteorological Organization.

Zischg, A. P., Felder, G., Mosimann, M., Röthlisberger, V., & Weingartner, R. (2018a). Extending coupled hydrological-hydraulic model chains with a surrogate model for the estimation of flood losses. *Environmental Modelling & Software*, *108*, 174–185. doi:10.1016/j.envsoft.2018.08.009.

Zischg, A. P., Hofer, P., Mosimann, M., Röthlisberger, V., Ramirez, J. A., Keiler, M., & Weingartner, R. (2018b). Flood risk (d)evolution: Disentangling key drivers of flood risk change with a retro-model experiment. *The Science of the total environment*, *639*, 195–207. doi:10.1016/j.scitotenv.2018.05.056.

Zischg, A. P., Mosimann, M., Bernet, D. B., & Röthlisberger, V. (2018c). Validation of 2d flood models with insurance claims. *Journal of Hydrology*, *557*, 350–361. doi:10.1016/j.jhydrol.2017.12.042.

2 A Robust and Transferable Model for the Prediction of Flood Losses on Household Contents

Markus Mosimann[1, 2, 3], Linda Frossard[1, 2, 3], Margreth Keiler[1, 2], Rolf Weingartner[1, 2, 3], Andreas Paul Zischg [1, 2, 3]

[1] *Institute of Geography, University of Bern, Hallerstrasse 12, 3012 Bern, Switzerland*

[2] *Mobiliar Lab for Natural Risks, University of Bern, Hallerstrasse 12, 3012 Bern, Switzerland*

[3] *Oeschger Centre for Climate Change Research, University of Bern, Hochschulstrasse 4, 3012, Bern, Switzerland*

Water (MDPI), 10, 1596, https://doi.org/10.3390/w10111596
Submitted: 3 October 2018; Accepted: 1 November 2018; Published: 7 November 2018

Abstract

Beside the flood hazard analysis, a comprehensive flood risk assessment requires the analysis of the exposure of values at risk and their vulnerability. Currently, the main focus of such analysis is on losses on building structure. However, loss on household contents accounts for up to 30% of the total losses on buildings due to floods. Based on insurance claim records, we developed and (cross-)validated two functions. The models based on linear regressions estimate the monetary loss and the degree of loss of household contents by the monetary and degree of loss for building structure, respectively. The main focus herein is to develop functions which provide robustness in prediction and transferability to other regions. Both models generate appropriate results with a comparative advantage of the relative over the absolute loss model. Our results indicate that the ratio of household content to building structure loss is decreasing relatively in regions with comparatively high losses or degrees of loss. A detailed examination of the model residuals, shows that the Box-Cox transformation works well to accurately fit a standard regression model to general right-skewed loss data as the transformed data meet the assumptions of a regression model.

Keywords: flood loss estimation; vulnerability functions; loss on household content; flood impact modelling; linear regression; Box-Cox transformation; transferability

2.1 Introduction

Floods are one of the most frequent natural hazards worldwide, affecting more people than any other hazard and being responsible for one third of the global expected annual average loss of USD 314 billion (UNISDR, 2015). Therefore, the assessment of flood risk (defined by hazard, exposure and vulnerability (Intergovernmental Panel on Climate Change, 2012)) and thus the analysis of losses due to floods constitutes a substantial public interest. Several studies assess flood risk on a global scale coping with low-resolution data (Ward et al., 2013; Sampson et al., 2015; Alfieri et al., 2018) to for instance make projections to future flood risk scenarios (Hirabayashi et al., 2013) or to find regions that should be prioritized for river-flood protection investments (Ward et al., 2017). Floods are also a topical issue on national (CH), regional (cantons) and local (municipalities) scale. Based on a database from 1946 to 2015, flood ranks third in the list of most fatal catastrophes related to natural hazards in Switzerland (Badoux et al., 2016). According to Swiss Re (2012), floods accounted for 71% of the total loss due to natural hazards in Switzerland over the period 1973 to 2011. Compared to windstorm (15%), hailstorm (11%) and other perils (3%), this indicates the relevance of national, regional and even local flood risk assessment. The destructive potential was also shown in August 2005, when floods and debris flows in Switzerland led to financial losses of more than CHF 3 billion (roughly EUR 2 billion) (Andres & Badoux, 2017).

However, on local scale, namely for Swiss municipalities, the resolution used in the global studies mentioned is to coarse to also consider creaks and mesoscale catchments representatively. The availability of spatially and temporally high resolved flood models and the possibility to develop flood scenarios lead to new perspectives in detecting regions or even single buildings with a high loss potential. Especially, flood losses are increasingly estimated at the scale of single buildings (Staffler et al., 2008; Ernst et al., 2010; Zischg et al., 2013; Fuchs et al., 2015, 2017; Zischg et al., 2018). Because inundations rarely lead to a total destruction of buildings, e.g., Papathoma-Köhle et al. (2011) and Fuchs & Thaler (2018) use the term "(physical) vulnerability" to describe the ratio of the monetary loss to the value of a building and thus, this term corresponds to the relative loss occurring on a building (loss divided by insurance sum). Synonymously, the term "degree of loss" is widely used (Fuchs et al., 2012; Papathoma-Köhle, 2016; Akbas et al., 2009; UNDRO, 1980). Most often mathematical functions are used to link parameters of flood magnitude (mainly flow depth, less frequently flow velocity or duration of exposition) to empirical flood loss data by fitting a vulnerability or stage-damage curve to observed data. Thereunder, the diversity of such functions is manifold and ranges from univariate functions, e.g., based on Weibull distribution functions (Totschnig et al., 2011; Papathoma-Köhle et al., 2015) or root functions (Hydrotec, 2001; Dutta et al., 2003), over to multivariate functions, e.g., graduated models (Jonkman et al., 2008; FOEN, 2015) or complex models considering exposure variables like building type, footprint area etc. as well as hazard variables (Dottori et al., 2016; Kreibich et al., 2010).

Although such functions are mainly developed to assess building structure vulnerability, Dutta et al. (2003), Jonkman et al. (2008), the Federal Office of Environment

(FOEN) (FOEN, 2015) and Kreibich et al. (2010) also present stage-damage curves for flood vulnerabilities of household contents. Especially univariate models or models considering only hazard variables systematically neglect a possible effect of the structural vulnerability on the vulnerability of contents.

Thieken et al. (2005) examined the influence of several factors on flood loss on building structures and contents for about 1000 flood-affected households, with information gained by computer-aided telephone interviews. They analysed the influence of different variables in the lower and upper loss quartiles by principle component analyses and the results indicate that flood impact variables (water level, flood duration and contamination by sewage, chemicals or petrol/oil) are the most important factors, followed by variables describing the size and value of the affected buildings or flats. Similar significant variables were obtained for all combinations of loss type (monetary, relative loss) and object type (contents, structure). Thieken et al. (2005) also described an interrelation between content and building structure losses, especially in the case of higher losses and degrees of loss. Although the monetary loss was provided by the interviewed persons, the values of buildings and contents were estimated by a model. Further it is shown that considering absolute household content loss is relevant, since the mean absolute loss on contents (EUR 16 335) amounts to 39% of the mean absolute loss on building structures (EUR 42 093). Assuming the mean total loss on a building would consist of the mean building structure loss and the mean household content loss, the share of the latter in the mean total building loss is 28%, whereas the mean loss ratio for household contents (0.296) is more than twice the mean loss ratio for buildings (0.123) (Thieken et al., 2005).

In an analysis of the flood event in August 2005, the Federal Office of Water and Geology (FOWG) (FOWG, 2005) provides an overview of the estimated losses based on insurance data. The report mentions an even larger fraction of the mean household content loss of CHF 32,100 (EUR 20,700, calculated according to the website of PoundSterlingLive (PSL) (PSL, 2018); total: CHF 700 (EUR 450) millions; 21,783 claim records) relative to the mean building structure loss of CHF 55,800 (EUR 36,000; total: CHF 250 (EUR 160) millions; 4483 claim records), resulting in a ratio of 58% (share of the mean household content loss in the mean total building loss, assumed to consist of the mean loss on building structure and the mean loss on household contents: 36.5%).

Studies on flood losses on household contents are subject to restrictions concerning the availability of empirical data needed for developing vulnerability functions or for assessing model reliability. In case of missing loss data, proxies for values at risk and losses are used. One example are data on flood losses compiled by interviews with persons affected by a flood event (Thieken et al., 2008; Kreibich et al., 2010; Chinh et al., 2017). To derive relative losses, the values of building structure and household content are modelled. Another example uses forms to generate the required datasets to derive (only) monetary flood losses on household contents (Carisi et al., 2018). Both data gathering approaches introduce uncertainties in the resulting flood loss models. The developed models are often lacking information about model uncertainties, for instance in terms of the (in)dependence of errors. In addition, most models are not tested for their robustness in prediction by validation (Papathoma-Köhle et al., 2011; Gerl et al., 2016). Another issue mentioned in literature (Cammerer & Thieken, 2013; Amadio et al., 2016) is the transferability of such models, meaning that they are only valid for regions the data was collected in, or which at least show similar characteristics.

In summary, although putting effort in the estimation of losses on building structures, the role of potential losses on household contents should not be underestimated. There is still a lack of knowledge concerning the statistical correlation of losses on household contents with the corresponding losses on building structures and in robustness and transferability of vulnerability functions for household contents. Therefore, the main objective of this study is to develop a model for estimating flood losses on household contents based on observed and reliable data. The main focus herein is to develop functions which provide robustness in prediction and transferability to other regions. This also comprises the question whether the loss on household contents can better be predicted by a relative loss model, looking at the relation of the loss ratios occurring on buildings and contents, or by a direct loss model connecting monetary loss on building structure with monetary loss on household contents.

As we derive flood losses on household contents from losses on building structure, developing a classical vulnerability function linking flow parameters (flow depth) with the loss itself is not the objective. Therefore, an analysis of the relation between content and structure losses is possible. Further, characteristics of the building structure that has an influence on the flood susceptibility of contents (a stronger damaged house will presumably allow a higher amount of water to enter the house to affect contents) is already covered within the (relative) building loss. This implies that these type of functions are supposed to be more transferable than vulnerability curves depending on flood intensities, as they can be linked with often locally validated vulnerability functions. Compared to the classical model, the *indirect model* set up presented here (also mentioned in Carisi et al. (2018) can also be used to complete loss estimations when loss data on structure is known, for instance to provide total loss estimations for flood events.

Hereafter, we will use the terms “degree of loss” (=relative loss, vulnerability) and “monetary loss” (=absolute loss). The “relative loss model” will describe the model, which predicts degrees of loss on household contents based on degrees of loss on building structure. The “monetary loss model” will predict monetary loss on household contents based on monetary loss on building structures.

2.2 Material and Methods

This study relies on a data set from the private *Swiss Mobiliar Insurance Company*. In Switzerland, 19 out of 26 cantons have public insurance companies for buildings with monopoly positions. Hence, different insurers are responsible for losses on building structures and for losses on household content. Data about monetary losses on building structures and on household contents are only available for the cantons without a monopoly position, namely Geneva, Uri, Schwyz, Ticino, Appenzell Inner-Rhodes, Valais and Obwalden.

After the description of the data in the first subsection, we describe the development of the vulnerability function in the subsequent section.

2.2.1 Data

The used data set (anonymised, as valid for December 2016) consists of the damage date, product information (distinction between households, small enterprises and medium enterprises), type of building describing its purpose (holiday homes, single-family house, apartment house with maximum three or more than three units, etc.) and the type of construction (solid or not). The timespan of the data covers January 2004 to December 2016. Here, we focus on residential data only. As key elements for this study, the data set includes information on the insurance sum of building structures and household contents, as well as damage claim records on structures and contents at the time of the occurrence of the loss. We did not correct the data with respect to inflation or modifications. The claim data are distinguished by the cause of loss. Losses due to leakages in pipes and groundwater effects are recorded as "water losses" and losses caused by riverine floods as "elementary losses". Based on this distinction, losses due to water entering the structure at ground level (="water losses") can be identified and excluded. The availability of insurance sum and loss allows a more reliable calculation of the degree of loss (DoL = loss divided by insurance sum). As a contract ID and the address including X-Y coordinates for a major part of the records are also available, it is possible to reliably link loss data of building structures with those of household contents. For the data analysis, we used the software R (R Core Team, 2016).

2.2.1.1 Quality Check

Not all entries in the data set were valid for the proposed analysis. Thus, the data had to be preprocessed and filtered to ensure a homogeneous data set. The loss data were provided separately for elementary losses on building structures and household contents. To compare the degree of loss observed on a building structure with that on household content, the single entries for structures and contents had to be matched. For the data from the *Swiss Mobiliar Insurance Company*, this was possible by matching the anonymous loss IDs. For every record, the address was used to check the accordance of the matched entries. Residential buildings from single-family houses up to apartment buildings with maximum three units and holiday homes were considered. Buildings with more than three apartments are defined as small and medium enterprises by the *Swiss Mobiliar Insurance Company* and were excluded from the analysis.

Some loss values in the claim records of the *Swiss Mobiliar Insurance Company* were remarkably and implausibly low, resulting in outliers. These values might have been caused by e.g., the magnitude of franchise or costs for administrative work. To exclude these outliers, the experts from the *Swiss Mobiliar Insurance Company* advised to only consider values above CHF 100 for the analysis. In total, this concerns eight entries of the matched subsets. Furthermore, entries for on "household" products could include buildings like summer or bee houses with a very low insurance sum and systematically higher degrees of loss than residential buildings. In consultation with the experts from the *Swiss Mobiliar Insurance Company*, entries with insurance sums lower than CHF 100,000 (six cases) were excluded. This ensures analysing a comparable class of buildings with residential purpose. After the quality check, there were 16,946 records of household content loss and 1662 records of building structure loss left. The number of loss records for building structure is the limiting data set for the number of claims occurring in

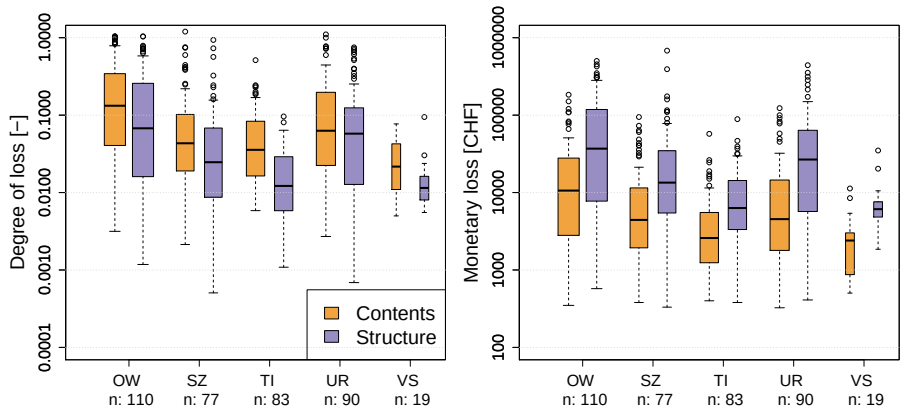

Fig. 2.1: Canton-wise distribution of records in the data sets used for the analyses. (**Left**): Degree of loss [-], (**right**): monetary loss [CHF]; both on log-scale. Sample size is given by "n:" and illustrated by the width of the box plots. Due to the low number of claim records, data recorded in Geneva and Appenzell Inner-Rhodes are not presented.

combination because buildings are insured by monopolists in 19 out of 26 cantons, whereas for household contents this is only the case in the two cantons of Vaud and Nidwalden. For roughly one fourth (384) of all buildings insured by the *Swiss Mobiliar Insurance Company* with occurrence of structure loss, a loss claim of household content was recorded too. Hereafter, we only refer to those 384 *paired claim records*, where *paired* indicates buildings with a claim record for structure and content. As already mentioned, the loss data corresponded to the amount of money paid by the insurance and thus the franchise was originally not included. Since the amounts and rates of franchise in Switzerland are legally anchored and the temporal information on the occurrence of the loss is provided, we were able to reproduce the effective loss.

2.2.1.2 Data Distribution

The canton-wise distributions of all paired monetary flood losses and degrees of loss within the period from January 2004 to December 2016 is presented in Figure 2.1. The cantons of Geneva and Appenzell Inner-Rhodes are not shown because there were available only two and three records, respectively. One can observe that the distribution of monetary losses and degrees of loss is different among cantons. In Obwalden (OW) and Uri (UR), the cost of claim was highest, whereas in Ticino (TI) and Valais (VS) it was lowest. Compared to them, Schwyz (SZ) shows intermediate costs. This pattern is shown by the distributions of losses and degrees of loss on contents and in almost the same manner for structures.

As we are interested in the role of content losses and vulnerability compared to structural losses, we calculate as a first overview the shares of content losses and insurance sums on total (structure + content) building losses and building values (see Figure 2.2). This will help us to make comparisons with other studies and reports of past events.

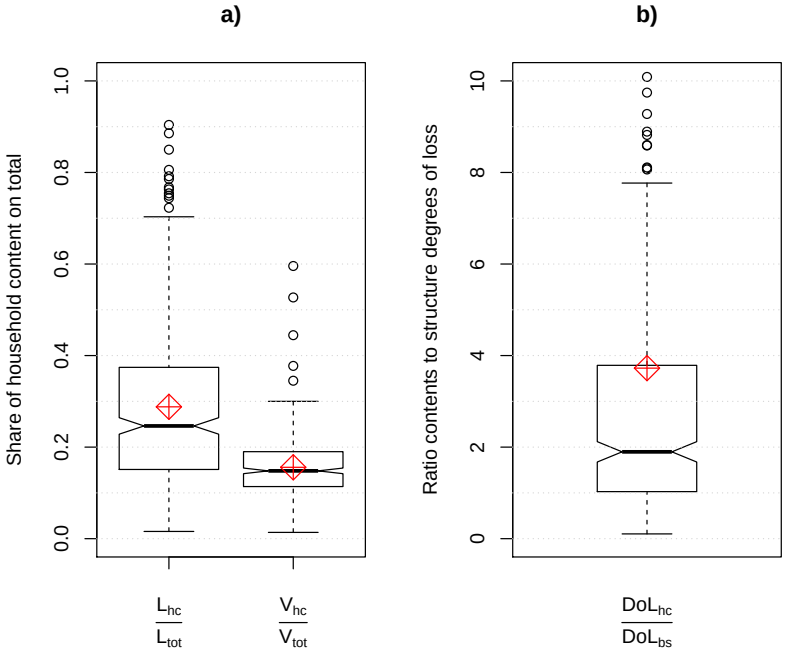

Fig. 2.2: (**a**) **Left**: Share of the household content loss (L_{hc}) on the total building loss (L_{tot} = structure loss + content loss). **Right**: Share of the insurance sum of household contents (V_{hc}) on the total insurance sum of a building (V_{tot}). (**b**) Ratio of the degree of loss on household contents (DoL_{hc}) to the degree of loss on structure (DoL_{bs}) for the same building. The red diamond symbols indicate the corresponding mean values.

2.2.2 Regression Model

In this study, we used a linear regression (Weisberg, 2005c; Good & Hardin, 2003) for the estimation of losses on household contents caused by flood events. The main objective of the regression analysis is to derive losses on household contents (as monetary [CHF] loss and as degree of loss [-]) from losses occurring on building structures at the same location and caused by the same event. Consequently, we use respectively the monetary loss and the degree of loss on household contents as the dependent variable and the corresponding type of loss on building structures as the only independent input to estimate the intercept and the slope parameter of the regression.

2.2.2.1 Data Transformation and Fitting

As indicated by Figure 2.1, the distributions of monetary losses and degrees of loss are even on the log scale both characterized by a right skew and therefore not normally distributed, nor do they follow a log-normal distribution (i.e., the logarithm of a variable is normally distributed). As normality of the involved variables themselves is not a prerequisite in classical linear regression analysis (Greene, 2012) (p. 92), this issue was not further examined. Instead we focus on the characteristics of the residuals produced by the linear model. This requires the consideration of heteroscedasticity, which is given when the variability of the response is not constant across the range of the explanatory

variables. It can for example be adressed, visually with diagnostic plots or more formally by the Breusch-Pagan (BP) test (Breusch & Pagan, 1979). Further, the assumption of normally distributed residuals has to be met as well (Weisberg, 2005b; Greene, 2012) and will be tested by the Shapiro-Wilks (SW) test for normality (Royston, 1982). We will also use diagnostic plots as visual aids for interpretations. Gaussian linear regression models with non-normally distributed residuals might lead to inaccurate confidence and prediction intervals and biased predictions. Not considering either of these assumptions will lead to an inaccurate estimation of the regression parameters.

For data initially not satisfying these properties, power transformations are common methods to achieve normality and an approximately constant residual variance in Gaussian linear regressions. Out of this family, the Box-Cox transformation, defined for $y \geq 0$ as

$$y^{(\lambda)} = \begin{cases} \frac{y^{\lambda}-1}{\lambda}, & \lambda \neq 0, \\ \log(y), & \lambda = 0, \end{cases} \tag{2.1}$$

where $\lambda \in \mathbb{R}$ is the power parameter and $y^{(\lambda)}$ denotes the transformed version of y, is a special case (Box & Tidwell, 1962; Box & Cox, 1964; Carroll & Ruppert, 1984; Weisberg, 2005c; Maciejewski et al., 2013; Ruppert & Matteson, 2015). To return to the original scale of the data, the values can be back-transformed by using

$$y = \begin{cases} \left(1 + \lambda y^{(\lambda)}\right)^{\frac{1}{\lambda}}, & \lambda \neq 0, \\ \exp\left(y^{(\lambda)}\right), & \lambda = 0. \end{cases} \tag{2.2}$$

The advantages of this transformation compared to other members of the power family are the systematic determination of the power parameter λ by maximum likelihood estimation (Perry & Walker, 2015) (p. 278) and the continuity at $\lambda = 0$ (Ruppert & Matteson, 2015) (p. 67). Consider the linear regression model with a single covariate x given by

$$y = \beta_0 + \beta_1 x + \varepsilon, \tag{2.3}$$

where y and x denote response and covariate respectively, β_0 and β_1 are the regression coefficients to be estimated and the error ε is assumed to be normally distributed with variance σ^2. Originally the Box-Cox transformation would be applied to the response variable y so that y in Equation (2.3) is replaced by $y^{(\lambda)}$, but an application to other non-negative quantities is of course also possible. Carroll & Ruppert (1984) and Ruppert & Matteson (2015) introduced the transform-both-sides (TBS) method, which consists in transforming the response y and the deterministic part of the regression equation with the same power parameter λ so that the model Equation (2.3) becomes

$$y^{(\lambda)} = \left(\beta_0 + \beta_1 x\right)^{(\lambda)} + \varepsilon. \tag{2.4}$$

This approach was actually developped for cases where the response y is known to theoretically satisfy a given non-linear function of x and some unknown parameters β_i, but where the residuals from the corresponding model on original scale would not

satisfy normality and/or homoscedasticity. In our application of this model, we chose the linear structure because it does not seem too bad based on a scatterplot of the data and because we had no other a priori guess for the relation between y and x for the loss data. To nevertheless account for possible non-linearity between the two quantities, we also applied another model we termed pseudo-transform-both-sides (PTBS). It consists of the same linear regression structure applied to Box-Cox transformations of y and x, i.e.,

$$y^{(\lambda)} = \beta_0 + \beta_1 x^{(\lambda)} + \varepsilon. \tag{2.5}$$

In a first step we used the same power parameter λ for both transformations as given here, but due to slightly sub-optimal model diagnostics especially for the absolute loss data, we also fitted the following extension of the PTBS model with two different power parameters for x and y (later referred to as PTBS.seplam):

$$y^{(\lambda_y)} = \beta_0 + \beta_1 x^{(\lambda_x)} + \varepsilon. \tag{2.6}$$

For all three models, the complete parameter set can be estimated by maximum likelihood estimation, so that standard errors and confidence intervals for all parameters are easily obtained.

The Bonferroni Outlier Test was used to detect exceptional data points (Weisberg, 2005b). We also calculated Cook's distance, leverage and defined large residuals. Once the regression parameters are estimated and all model assumptions verified, the edited regression has to be back-transformed to retrieve the original and interpretable unit, resulting for the PTBS model in:

$$y = \left(1 + \lambda\beta_0 - \beta_1 + \beta_1 x^{\lambda}\right)^{\frac{1}{\lambda}}. \tag{2.7}$$

The back-transformation being non-linear for the PTBS and PTBS.seplam models, the residuals are not any more normally distributed as they were in transformed form (Duan, 1983; Taylor, 1986; Sakia, 1990; Perry & Walker, 2015). In addition, mean and median of the back-transformed distribution no longer coincide. When $\lambda < 1$, the power parameter for the back-transformation becomes > 1 which means that the normal distribution of the residuals on the transformed scale gets right-skewed on the original scale (Rothery, 1988). The right skew implies a discrepancy between the median and the mean of the back-transformed distribution such that the former systematically underestimates the latter. Taylor (1986) derived an approximation for the conditional mean of the untransformed response variable y in terms of the model parameters β_0, β_1, σ^2, λ for the original Box-Cox model, where $y^{(\lambda)}$ is linear in x, i.e., $y^{(\lambda)} = \beta_0 + \beta_1 x + \varepsilon$. Adopted to the PTBS model it reads

$$E[Y|x] \approx \left(1 + \lambda\beta_0 + \lambda\beta_1 x^{(\lambda)}\right)^{\frac{1}{\lambda}} \times \left(1 + \frac{\sigma^2(1-\lambda)}{2(1 + \lambda\beta_0 + \lambda\beta_1 x^{(\lambda)})^2}\right) =: \psi \tag{2.8}$$

where the unknown residual value is set to zero. Replacing the parameters β_0, β_1, σ^2, λ in (2.8) by their maximum likelihood estimates yields an estimate $\hat{\psi}$ for the mean of the original variable Y. The variance of $\hat{\psi}$ can then be estimated by the delta method (e.g. Weisberg (2005a)) and confidence intervals (and prediction intervals) for ψ can be based on the asymptotic normality of the maximum likelihood estimator.

2.2.2.2 Cross-Validation

To test the predictive accuracy of our models and their robustness in terms of variance and bias, a leave-one-out cross-validation was applied (Davison & Hinkley, 2013; Hastie et al., 2009). For each model type (PTBS, PTBS.seplam, TBS as well as relative or monetary loss), every single observation y_i is predicted as either the median or the mean from the model fitted to the data set without observation y_i. For the resulting sample of predictions, the aggregate prediction error is computed as the mean of the prediction errors for the individual observations y_i. In addition we computed the standard deviations for each prediction error sample as a measure of the spread of the individual prediction errors. To compare the prediction quality and accuracy of the different models we considered four different error metrics for each case: bias [CHF], relative bias [%], absolute error [CHF] and relative absolute error [%] (Walther & Moore, 2005).

For comparisons in terms of accuracy, the results of both the monetary loss model and the model based on degrees of loss need to describe the same unit and scale. We use the unit [CHF] for evaluating the models. To do so, predicted degrees of loss on household contents are multiplied by the insurance sum of the content, provided by the insurance company.

2.2.2.3 Assessment of Transferability

Based on Wenger & Olden (2012), who suggest non-random cross-validation by splitting data into geographic regions, we analysed the performance of our models in terms of transferability. We applied the non-random cross-validation based on monetary losses to data from five out of seven available cantons. The cantons of Geneva and Appenzell Inner-Rhodes were neglected because only few claims were found with both structure and content loss. The transferability assessment for our models was tested for Obwalden ($n = 110$), Ticino (83), Uri (90), Schwyz (77) and Valais (19).To make sure that the unbalanced sample sizes of the cantons do not impact the results, we applied non-random K-fold cross-validation for several numbers of folds K between 2 and 20. In the last case, the fold sizes are similar to the "outlying" Valais sample size. We used the same error metrics for this analysis as for the leave-one-out cross-validation.

As a further assessment of transferability, we carried out an analysis of variance (anova) (Weisberg, 2005a; Sokal & Rohlf, 1969) on the transformed data, assuming λ fixed. More particularly, we tested whether a model with individual regression lines for each canton (differing either only in the intercept or in intercept and slope) fits the data better than the simpler model with a single line. Good transferability of the current simple model is then achieved if the more complex version with individual regression lines leads to *no* significantly improve fit.

2.3 Results

2.3.1 On the Role of Household Contents

The box plots of the shares of household content loss (left) and insurance sum (right) on total building loss and insurance sum are shown in Figure 2.2a. The mean share

Table 2.1: The role of household contents in five Swiss Cantons. OW: Obwalden, SZ: Schwyz, TI: Ticino, UR: Uri, VS: Valais. * Share of the summed content loss on the summed total (structure + content) loss per canton. ** Means and medians of observed shares of content loss on total loss. *** Means and medians of the observed ratios of degrees of loss of contents to degrees of loss of structure

	OW	**SZ**	**TI**	**UR**	**VS**
Share of content loss on total building loss*	0.22	0.23	0.32	0.21	0.26
Mean/median loss fraction **	0.27/0.22	0.31/0.28	0.33/0.28	0.25/0.24	0.28/0.24
Mean/median DoL rati o ***	2.8/1.67	3.81/1.94	6.22/2.62	2.69/1.81	2.32/1.49

of content loss amounts to 0.29 (=29%), whereas the median is roughly 25%. With respect to the share on the total building value (mean: 0.16; median: 0.15), this is disproportionately high. Accordingly, the degree of loss of contents is generally higher than the degree of loss of building structure, as shown in Figure 2.2b. The interquartile range lies between 1.03 and 3.73 (median = 1.9, mean $\approx$ 3.7), which implies that in nearly three quarters of all losses, household content is more vulnerable than building structure.

The same quantities as seen in Figure 2.2 are shown in Table 2.1, but instead of considering the complete data set, values are shown separately for each canton. We see that in Obwalden and Uri, contents show generally lower fractions and shares of content loss to total building loss.

2.3.2 Model Fitting

As mentioned in Section 2.2.2.1, we fitted different models to both types of loss data. Although the model fit is slightly advantageous for the TBS and the PTBS.seplam model, we define the PTBS model (regression function fitted after transformation by the same λ for both sides) as the best model, due to its better performance in terms of predictive power. Therefore, in the following two subsections, we will only present results for this specific model.

2.3.2.1 Data Transformation

The 95% confidence interval (CI) for λ obtained by profile maximum likelihood estimation indicates a range with plausible values for λ. For degrees of loss, the method proposes to use $\lambda = 0.205$, CI: $(0.144, 0.265)$ as transformation parameter. Weisberg (2005c) recommends to use a rounded value for λ. Because none of the suggested values $\{-1, -1/2, 0, 1/3, 1/2, 1\}$ lies within the range of our CI, we select the exact estimate of λ. Indeed we do not consider $y^{1/5}$, which would be covered by the CI, to be more easily interpretable in terms of the original variable y than $y^{0.205}$.

For monetary loss, the best estimate and 95% CI of λ are 0.131 and $(0.068, 0.193)$, respectively. We use the exact value of λ for the same reasons as before.

2.3.2.2 Regression Model

The result of the PTBS approach and the regression based on transformed degrees of loss can be examined in Figure 2.3a. Kendall's τ (0.556) and Spearman's ρ (0.746) suggest to reject the null hypothesis of non-correlation of the degree of loss of building structure and household content. The F-statistic of the model indicates significant linearity and the adjusted R^2 reaches 0.668. Here, the CI of the intercept parameter β_0 is $(-0.255, 0.060)$ which indicates that the regression line goes roughly through the origin and the intercept parameter is not significant. A visual insight into the diagnostic plots for the model based on degrees of loss is given in Figure 2.5 in the Appendix. Based on the patternless scatter of the standardised residuals plotted against the fitted values (Figure 2.5, top right), the standardized residuals following a normal distribution (Figure 2.5, top left) and emphasized by the Shapiro-Wilks test (SW: p-value = 0.385), normality cannot be rejected. In addition, the Breusch-Pagan test indicates that the null hypothesis of the residuals being homoscedastic cannot be rejected either (BP: p-value = 0.742), which is also indicated by the scale-location plot (Figure 2.5, bottom right) not showing severe changes in variance. The monetary loss model also meets the requirements of a linear regression relatively reasonably. The model produces residuals which are not significantly different from a normal distribution (SW: p-value = 0.245) and not significantly heteroscedastic (BP: p-value = 0.221). Linearity is significant as well (adj. $R^2 = 0.618$, see Figure 2.3c), the diagnostic plots are shown in Figure 2.6. Note that there is a slight pattern in residuals plotted against the fitted values, indicating a minor lack of fit. An overview of all parameter estimates ($\hat{\beta}_0$, $\hat{\beta}_1$, $\hat{\sigma}$ and $\hat{\lambda}$) is given with Table 2.2, their confidence intervals (95%-CI) and statistical measures for the resulting models indicating the model quality (Shapiro-Wilks and Breusch-Pagan tests, Spearman's ρ, Kendall's τ and the coefficient of determination (adj. R^2)).

After substitution of the model parameters in Equation (2.7) and (2.8), respectively, the regression is not linear any more, because the back-transformation of the Box-Cox method leads to a non-linear function. Figure 2.3b,d show the final results of the model optimization process on the original scale. In Figure 2.3b, the concavity of the regression function points out that especially for objects where a low degree of loss was observed, the ratio of degree of loss of contents to the degree of loss of structure is generally higher than in cases, where high vulnerabilities were recorded. The major part of the household contents shows higher degrees of loss than the building structures.

The monetary loss model, which allows a direct estimation of loss on household contents based on the loss that occurred on building structure, shows that structure loss is in general considerably higher than the corresponding household content loss (see Figure 2.3d). Poor predictive power is found on higher magnitudes (building structure losses > ca. 320,000 CHF). Here, the model underestimates the content loss.

2.3.3 Cross-Validation

The metrics resulting from the leave-one-out cross-validation are presented in Figure 2.4: (i) bias; (ii) relative bias; (iii) mean absolute error and (iv) relative absolute error. Here, results for the alternative models (TBS and PTBS.seplam) are presented as well. The position of the black symbols indicates the aggregated prediction error of the

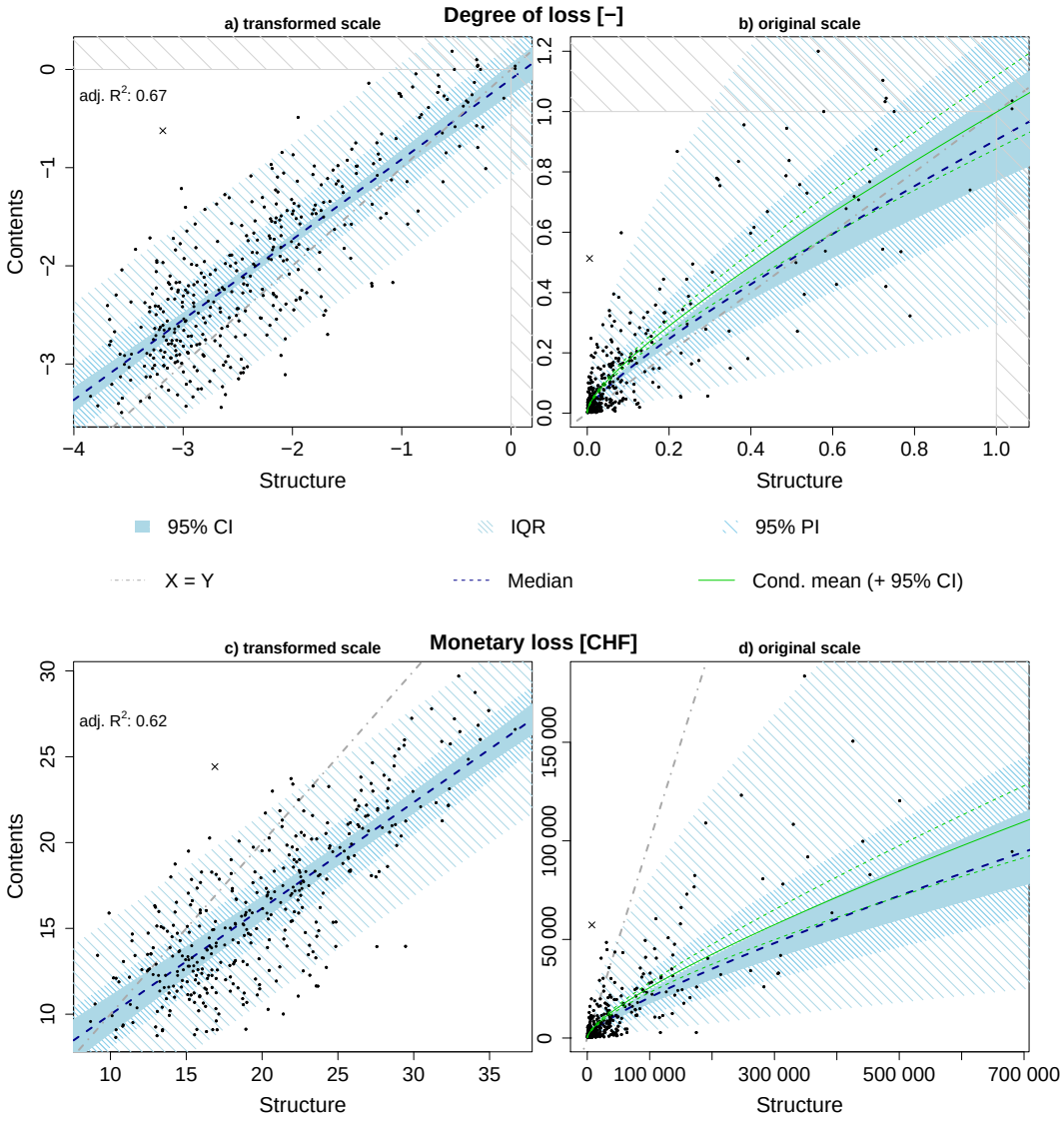

Fig. 2.3: Loss models based on degrees of loss (**a**,**b**) and monetary loss in CHF (**c**,**d**). In plots (**a**,**c**), the models based on transformed input values are presented, whereas in (**b**,**d**) the model results are shown on the original scale after back-transformation. CI: Confidence Interval; IQR: Inter-Quartile Range; PI: Prediction Interval. Note that the mean in plots (**a**,**c**) coincides with the median. Cross symbol: Outlier excluded before model fitting.

cross-validation, the dots along the dashed blue line indicate the standard deviation of the individual prediction errors. To compare model accuracy in the same unit (CHF), the predicted degrees of loss (DoL) on household contents were multiplied by the insurance sum.

In terms of bias (Figure 2.4i), we first of all see that there is a clear improvement from median to mean estimation for both, the relative and absolute loss models. Second, we observe that the relative loss model with median estimation performs better, whereas there is no clear "overall" pattern for the mean estimates. Within the the groups (Loss.med, DoL.med, Loss.mean, DoL.mean), differences in performance are rather small. Apparently, the relative loss models show lower mean absolute prediction errors (Figure 2.4iii). Regarding this particular metric, we can say that estimations by median perform slightly better than by mean. Interestingly, the standard errors of the TBS and PTBS absolute loss models and for the PTBS relative model lower mean prediction, whereas the metric itself gets higher. Looking at the two relative metrics (Figure 2.4ii,iv), we see that they are very similar to each other. On one hand, we can observe that median prediction is in terms of these relative metrics more accurate and on the other hand that the TBS and PTBS.seplam model supply roughly the same quality-better than the PTBS model. Figure 2.9 also shows, that relative errors (Figure 2.4ii,iv) are mainly large for lower loss values, whereas large absolute errors (Figure 2.4i,iii) rather occur in estimations of high losses. This in turn is not surprising, as the loss is, relative to the loss magnitude, larger for smaller losses. Hence a prediction of a small loss more easily misses the target by a few orders of magnitudes, resulting in a relative prediction error of several hundred percent while its absolute prediction error in CHF is still rather small compared to the larger loss values in the data. On the other hand, a small percentage (relative error) of a large loss can correspond to a large amount of money (absolute error). We also tested the behaviour of the Box-Cox transformation in the re-sampling process and found that the estimation of λ is robust.

In this study, we focus on the estimation of monetary flood losses, so we prioritize absolute to relative accuracy of the models. In the following summary describing the major findings concerning the absolute and relative loss models, we just mention absolute bias and mean absolute error: (a) The accuracy of predicting monetary loss is higher when derived by the relative loss model instead of the monetary loss model; (b) The standard deviation in the error samples show that prediction variance is lower for the relative loss models which is accompanied by higher robustness; (c) Although median estimation is able to compete with the mean estimation in terms of mean absolute error, it has clear disadvantages concerning bias. In the end, the fact that the PTBS model shows highest robustness and the best predictive accuracy, we selected this model to focus on and finally present in this study. We will use this model for the relative and absolute loss model although for the latter, the TBS model showed slight, for us not meaningful competitive advantages. Please also note that prioritization of relative metrics would lead to a different, but also plausible choice.

2.3.4 Transferability

The analysis of variance for the relative loss model on transformed scale indicates a significant improvement in the overall fit for both PTBS models when separating the

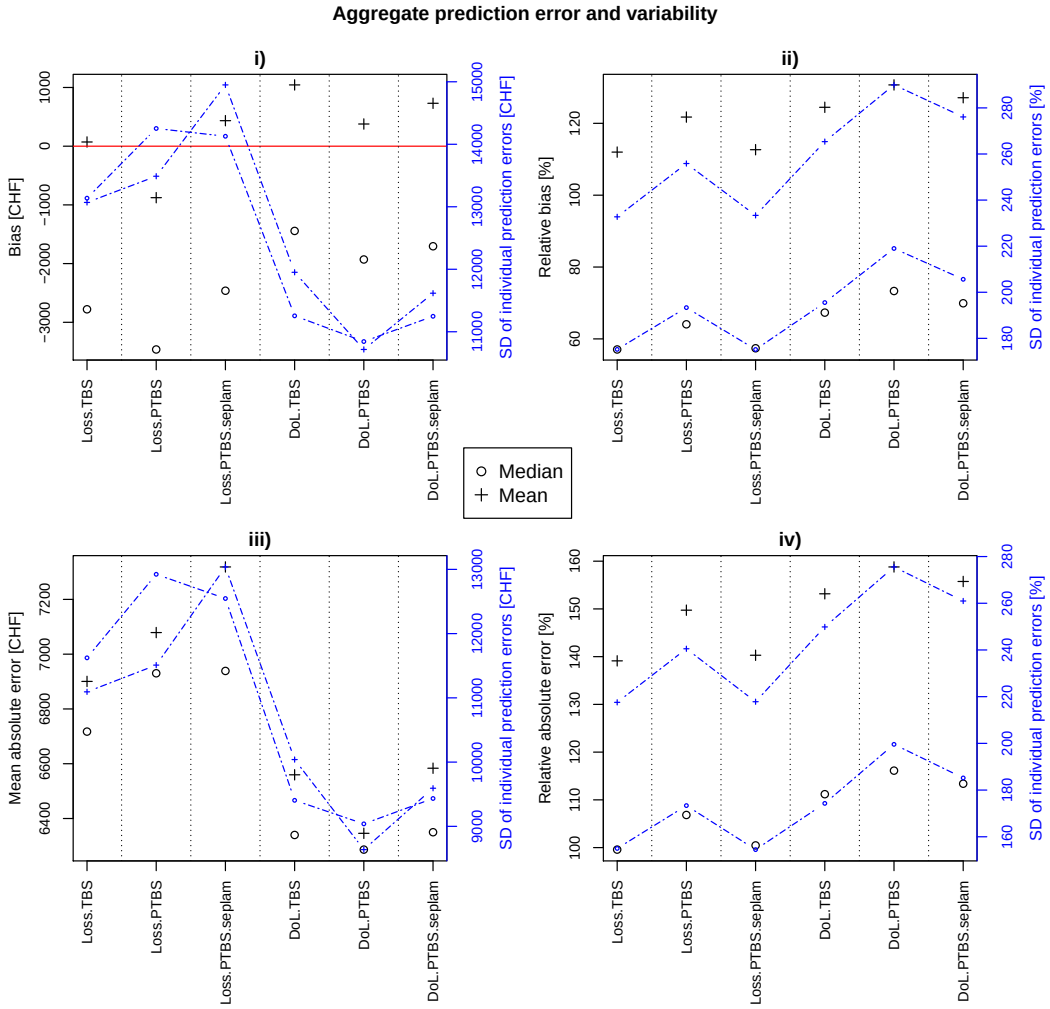

Fig. 2.4: Cross-validation results for the model combinations based on leave-one-out cross-validation. ○: Aggregated prediction error with median prediction; +: Aggregated prediction error with mean prediction. The blue line indicates the standard deviation of the individual prediction errors; (**i**) Bias [CHF]; (**ii**) Relative bias [%]; (**iii**) Mean absolute error [CHF]; (**iv**) Relative absolute error [CHF].

intercept according to cantons (likelihood ratio test at 5% level) while such a seperation is not significant for the TBS model. However, this is not the case for the slope, meaning that there is only a shift of the regression line (on transformed scale) along the vertical axis. The non-significance of the slope parameter implies that the relative increase of the vulnerability of household contents to an increase of the vulnerability of the building structure stays stable and is not significantly different across cantons.

In view of the apparently significant difference between the intercepts and thus the overall magnitudes of degrees of loss for cantons, one would want to detect which cantons (or groups of cantons) are most different from others. A first straightforward, but rather innocent approach would be to assess the significance of all differences between pairs of intercepts by performing a t-test at a given level for each of them. Yet we believe that properly answering this question involves so-called *a posteriori* comparisons Sokal & Rohlf (1969) (Chapter 9), all the more that we had no a prioi guess on which cantons might exhibit the largest differences before looking at the data. Performing such comparisons falls into the large field of *multiple testing* or *multiple comparisons*, which roughly speaking means that to reach an overall uncertainty level of α on several tests, the single sub-tests have to be carried out at much smaller significance levels than α. This in turn means that less significances tend to be found. We applied most approaches to this problem described in Sokal & Rohlf (1969), but they did not lead to coherent results. Moreover, the whole matter is complicated because the sample sizes of the different cantons are not equal and their variances (still on transformed scale) seem to be significantly different, whereas many multiple comparison methods do strictly speaking not apply without the assumption of sample sizes and constant variances for all groups. We therefore do not present any further "results" of this analysis here because they are in our opinion not sufficiently well-founded, but refer to the discussion in Section 2.4. Interestingly, the difference in the intercept is only observed for the relative and not for the absolute loss model, although both models rely on the same loss data set.

As our model with only one covariate is rather simple, the tendency for over-fitting as described by Wenger & Olden (2012) is expected to be rather small. This is indeed confirmed by the results of the non-random cross-validation, which are very similar to those found with the leave-one-out cross-validation (see Figure 2.10). Here, the models with high prediction accuracy thus also show the best performance in terms of transferability.

2.4 Discussion

With approximately 29%, the mean share of content loss on the total loss of residential buildings (structure + household contents) is similar to those found by Thieken et al. (2005) (28%) or FOWG (2005) (36.5%). Although we found comparable results in terms of the share of content loss on the total building loss, the data (monetary losses and degrees of loss) in our study were distributed over a lower range of magnitudes than in the analysis of Thieken et al. (2005) for the Elbe and Danube floods. As mentioned in Section 2.3.1, regions with lower loss magnitudes showed in general a higher share of content loss on total building losses. This is emphasised by the facts, that the share on the loss is disproportionately high compared to the share of the content value to the

total building value and, as seen by the linear regression in Figure 2.3a,b, the content loss to structure loss ratio is high especially for lower magnitudes. Therefore, as the loss magnitudes given by Thieken et al. (2005) are higher, the mean share of content loss on the total building loss is rather high based on the findings in this study. Possible reasons are manifold and should be further studied, for instance different vulnerabilities of the buildings due to their type, differences of the hazard process (suspension load, dynamic or static inundation, caused by flooding of rivers in inclined topographies and inundation by a raising lake level, respectively, time of exposure, forecast accuracy of the event etc.). Preparedness may matter in this case as well: As insuring structure and contents in the regions analysed here is voluntary, contractors of insurance companies might be in general more sensitive to flood risks than others, and thus might be more resilient to such events. To our knowledge, this was not the case in the studies of Thieken et al. (2005). Another explanation for the differences in Thieken et al. (2005) and FOWG (2005) might be that in their studies content and structure losses need not necessarily be linked to each other. So the structure and content data sets do not have the same origin and thus, their results are not directly comparable with those of this study.

Uncertainty exists because information on the total number of flood-affected buildings and household contents is missing. This implies that we cannot make comparisons of loss frequency for building structure and household contents, respectively. Thus, we leave open the question of how probable a household content loss occurs when building structure is affected (and vice versa). Moreover we did not consider either that one building might consist of more than one household (in this study up to three). Depending on how the building is arranged, for instance with one apartment on the ground floor and two on upper floors (or vice versa), where water levels rarely rise to, content losses might get less (or more) relevant in the total building loss. Residents from upper floors storing contents on the underground floor might play a role in this context as well. We neglected those points and focused on examples where only both in combination, building structure and household content losses, occurred. In terms of total loss prediction, we point out that this is a crucial issue and that those points can make the difference between successful and failed predictions.

Furthermore, there are some methodical restrictions that have to be addressed. As we filtered the data by insurance sum, monetary loss and product type, the results are just valid for buildings with an insurance sum higher than CHF 100,000, losses above CHF 100 and with a residential purpose with maximum three apartments. Hence, attention has to be paid when comparing our results or applying the presented models to other data.

By applying the transform-both-sides (TBS) methodology after Carroll & Ruppert (1984) to our data, we found a way to meet the assumptions of Gaussian linear regression models concerning homoscedasticity and normality in the distribution of the residuals. There is one minor disadvantage: Due to the challenges of the back-transformation to make inferences in the original scale, a correction factor has to be calculated to derive the estimated mean. This makes the equation more laborious than other approaches, but reproducibility is still given. Alternatively to the proposed method of our study to find a mean estimation, one could also try to fit a generalized linear model. In addition, a quantile regression approach (see Davino et al. (2014)) could be potentially useful. So far, in vulnerability and flood loss prediction, the presented method was never used

before and the benefits are shown by its reproducibility, the possibility for a systematic application in other study areas and considering the prediction uncertainties. Our models indicate a high robustness of estimating λ, ensuring normality and homoscedasticity for the residuals resulting from the subsequent linear regressions.

One objective of this study was to deduce whether the prediction of household content losses performs better by a loss model based on degrees of loss, looking at the relation of loss ratio (loss/insurance sum) occurring on content and structure or by a direct loss model connecting monetary loss on household content with the loss on building structure. For the model based on degrees of loss, we found one basic similarity as already presented by Jonkman et al. (2008): for the lower intensity level on structure, with the increase of the degree of loss of structure, the degree of loss on household contents comparatively increases following a concave function. This leads to a larger ratio of degrees of loss of contents to degrees of loss of structure at low levels. This emphasises the findings mentioned above, that especially for losses with low magnitudes, household contents are more vulnerable to floods than building structure and here, the role of losses on household contents might be essential.

As a consequence of the model characteristics mentioned and as a punctuating element of this statement, the regression of the monetary loss model shows a concave characteristic as well. This implies that the ratio of the monetary household content losses relative to the building structure losses is higher in low magnitudes compared to high ones. Although the model statistically meets all demanded requirements (normality, homoscedasticity, robustness and, to some restrictions we discuss afterwards, also transferability), we see in Figure 2.3 that for the highest structure losses, the predicted content loss is underrated systematically. This could also be the reason that leads to the (slight) tendency for negative bias and underestimation of the total loss we found in (non-)random cross-validation. As these high values mainly occurred in the canton of Obwalden, we cannot clearly say if this issue originates in methodical inadequacies or just local conditions. With respect to the analyses done by Carisi et al. (2018), we didn't only select our model by the best performance concerning error metrics, but also in compliance with statistical requirements. As we also did not need to predefine the type of transformation, the method used in this study has advantages in it's flexibility and strong adaptiveness.

Comparing the quality of the two PTBS models, the accuracy of the model based on degrees of loss is advantageous as shown by the model fit, the absolute bias and the mean absolute error. This includes tests for normality and homoscedasticity (Table 2.2 and Figures 2.5 and 2.6), robustness (Figure 2.4) and transferability (Figure 2.10, absolute errors). Concerning the analysis of variance, several uncertainties remain. First of all, the application for the TBS approach turned out to be very complex and there is still potential for improvement. We can clearly say that for the relative loss model based on degrees of loss, a difference in the intercept parameter exists, but we cannot clearly define the source that leads to the differences. With a variety of correction methods for the anova, we found that only differences between a combination of three groups are significant, but not between any pair of cantons. We mention that there are also uncertainties in the proceeding and methodical correct utilization of the methods in detecting the relevant differences, not least because of unequal group sizes and variances; see also Section 2.3.4. As mentioned, there is no improvement by distinguishing the origin of the losses in the absolute loss model. Here, it is plausible that the higher variance and

the lower model fit prevents the intercept parameter from being significantly different. To conclude, although uncertainties exist, we still would interpret the relative loss model as transferable, justified in accordance with the intercept parameter statistically not being significant in model fitting, but we also point out, that further analysis and improvements are required. In particular, we acknowledge that a more in-depth statistical analysis of these uncertain aspects is not infeasible and would most likely also lead to improved answers, but simply was beyond the scope of this study.

The random cross-validation underlines the relative loss model being more robust than the monetary model, by returning lower error standard deviation and improved accuracy concerning the absolute error types. In addition, we expect advantages of the relative loss model concerning reliability, being independent of the value of an object. This means in detail that for the monetary loss model a constant ratio of content and structure values is assumed, whereas the relative loss model is independent of the variety of possible value-combinations, e.g., valuable contents being located in low-priced buildings etc. The dependence of the monetary loss on the value is also shown by Thieken et al. (2005), where variables describing value and size are highly relevant for monetary losses, whereas for the degree of loss this effect is remarkably reduced by putting the monetary loss value in relation to the monetary value of the object. We suppose that this could be the reason why variance and the model fit in the relative loss model are more accurate. We point out that with degree of loss and monetary loss of structure as only input variables, the relative and monetary models are able to explain 67% and 62% of the variance in degrees of loss and monetary loss of contents, respectively. We explain these high values with two out of three main components (flood variables and preparedness) found by Thieken et al. (2005) being neutralized through our approach: As we analysed contents and structure being part of the same building, the interacting flood variables are the same and thus neglectable. The same is valid for preparedness: We linked contracts of contents and structure referring to the same person with obviously the same preparedness. In conclusion, indirect models for household contents as presented here are supposed to be more transferable than vulnerability curves for household contents. The models presented here might be linked with existing, often locally valid vulnerability curves for building structure loss. Those functions and models created by fitting flow parameters (and structural characteristics) to empirical loss data implicitly contain information about the susceptibility of building structure and therefore also to household contents (e.g., resistant structures might prevent contents from strong exposition). Compared to the classical model, the indirect model type presented here and in Carisi et al. (2018) can also be used to complete loss estimations when higher accessible loss data on structure is known, for instance to provide total loss estimations during flood events. As the models are depending on either vulnerability functions for building structure generating the degree of loss (or monetary loss) or on the loss data of building structure themselves, the limitations of these dependencies are as well transferred to models presented. In addition, the restrictions mentioned have to be considered as well.

2.5 Conclusions

Based on reliable data and established literature, we showed that household content loss is a relevant factor in the estimation of flood losses and should be considered in future loss

predictions or flood risk assessments. In relation to the average total loss of a building including content and structure loss, losses of household content contributes from 21% to 32% based on our data, whereas contributions of up to 36% are found in the literature. The results indicate that especially when low degrees of loss or monetary losses are caused by floods, the vulnerability of contents is clearly higher than the vulnerability of the corresponding building structure. Thus, assuming that generally high flood intensities lead to high losses, it has to be considered that the share of household contents on the total building loss is decreasing relatively in regions with comparatively high losses or degrees of loss.

We present two models, deduced from loss claims on residential buildings with maximum three apartments, which allow to predict the degree of loss or the monetary loss for household contents based only on corresponding losses on the building structure. Moreover, we tested and compared the models in terms of robustness, transferability and predictive power. Both models generate appropriate results with a comparative advantage of the relative over the monetary loss model. They meet the statistical requirements of normally distributed residuals with constant variance which is the basis for a robust model. As shown by random cross-validation, the absolute bias and standard deviation is generally low for both, but lower for the relative loss model. As well, the relative loss model is favourable being more transferable to new regions, as assessed by a non-random cross-validation. As important as that, flow parameters, preparedness and building characteristics-the most relevant parameters to generate direct vulnerability curves - can be neglected here because contents and structure are not only located at the same position, but also owned by the same person. The functions created here are supposed to be linked with locally validated vulnerability curves for building structures or structure loss data to complete total loss estimations. Nevertheless, attention should be paid when applying the functions in regions where the major part of degrees of loss or monetary losses is expected to scatter around the upper or lower range of our data set or just a very small number of data is available. In this case, we presented a method that quantifies uncertainties and supports the interpretation of the model accuracy.

The Box-Cox method is characterised by not insisting on a certain transformation. Instead, it takes into account a multiple set of power transformations (including the log-transformation) to reach normality and homoscedasticity of the residuals and suggests an appropriate λ-parameter based on the quantitative and reproducible maximum likelihood method. By applying tests to the residual distribution, we showed that this transformation method works well for general right-skewed loss data, and meets model assumptions of a Gaussian linear regression. For both, the degree of loss and monetary loss model, as the original data are strongly heteroscedastic, the uncertainties are rising with increasing values of exposed assets and losses. We recommend to consider data transformation, as it is providing a statistically correct estimation of the regression parameters and uncertainties.

Supplementary material

The Code and the data used in this paper are available at https://zenodo.org/record/1443238 or as git-repository at

https://bitbucket.org/MarMos90/houco_lossmodel/src/master/.

Author contributions

Conceptualization, M.M. and A.Z.; Methodology, M.M. and L.F.; Validation and Formal Analysis, L.F. and M.M.; Investigation, M.M., L.F. and A.Z.; Data Curation, M.M.; Writing—Original Draft Preparation, M.M.; Writing—Review & Editing, all; Visualization, M.M., L.F.; Supervision, A.Z., M.K., R.W.

Funding

This research was funded by the Mobiliar Lab for Natural Risks.

Acknowledgments

The authors thank *Swiss Mobiliar Insurance Company* for providing the data and especially Luzius Thomi and Rouven Sturny for advice on the interpretation of the data.

Conflicts of interest

The founding sponsors had no role in the design of the study; in the collection, analyses, or interpretation of data; in the writing of the manuscript, and in the decision to publish the results.

Abbreviations

The following abbreviations are used in this manuscript:

BP	Breusch-Pagan (test)
CI	Confidence Interval
DoL	Degree of Loss
FOEN	Federal Office of Environment
FOWG	Federal Office of Water and Geology
PSL	Pound Sterling Live
PTBS	Pseudo-Transform-Both-Sides
PTBS.seplam	Pseudo-Transform-Both-Sides with separate transformation parameters λ for x and y
SW	Shapiro-Wilks (test)
TBS	Transform-Both-Sides

Appendix

2.A Diagnostic plots

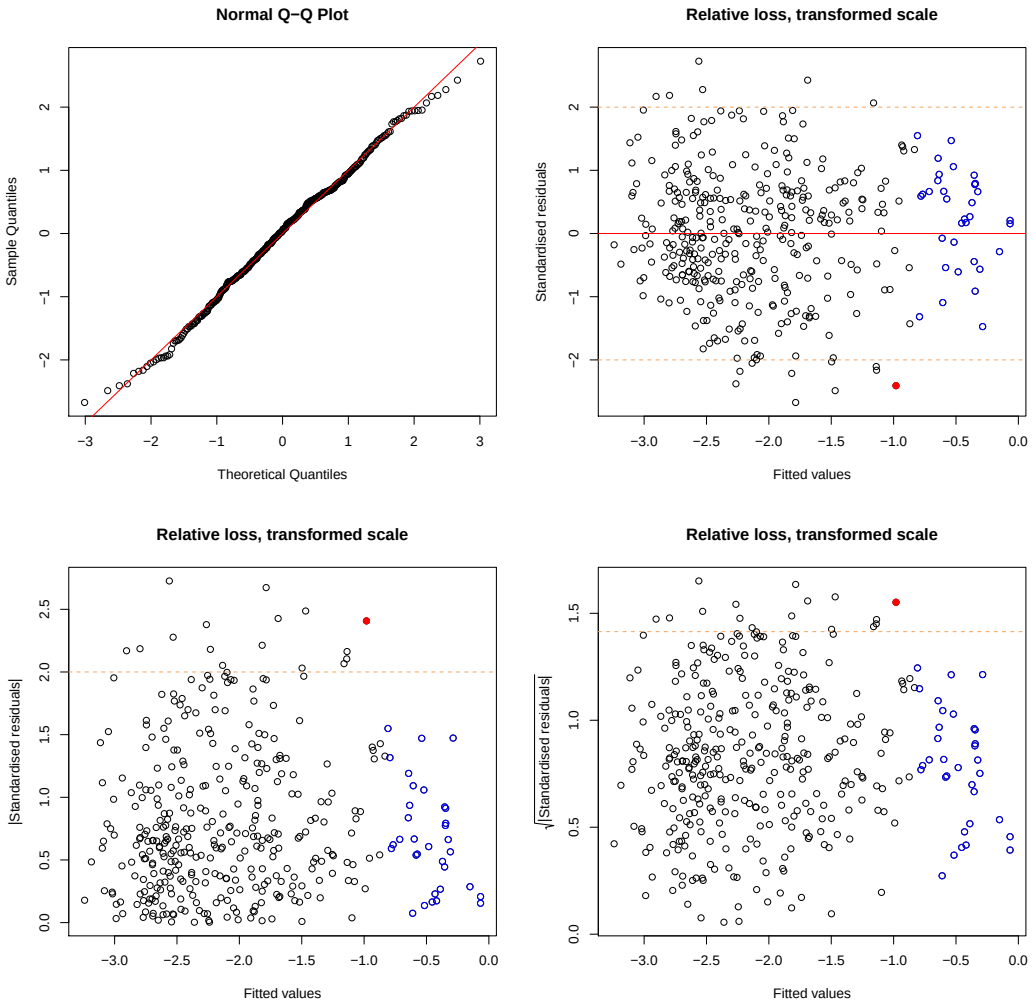

Fig. 2.5: Diagnostic plots for the residuals (transformed degrees of loss) shown by Figure 2.3a. (**Top left**) Normal-Q-Q-plot, points along diagonal line don't reject normality (SW: normality with a p-value = 0.385). All other figures show the fitted values on X-axis against the standardised residuals on the Y-axis as normal (**top right**), absolute (**bottom left**) and the square root (**bottom right**) of the absolute values. Blue borders indicate high leverage points, red filled circles indicate high values for Cook's distance and the orange dashed lines indicate the borders to the definition of large residuals. Heteroscedasticity is not evident. One outlier (Bonferroni outlier test) is not shown in the plot.

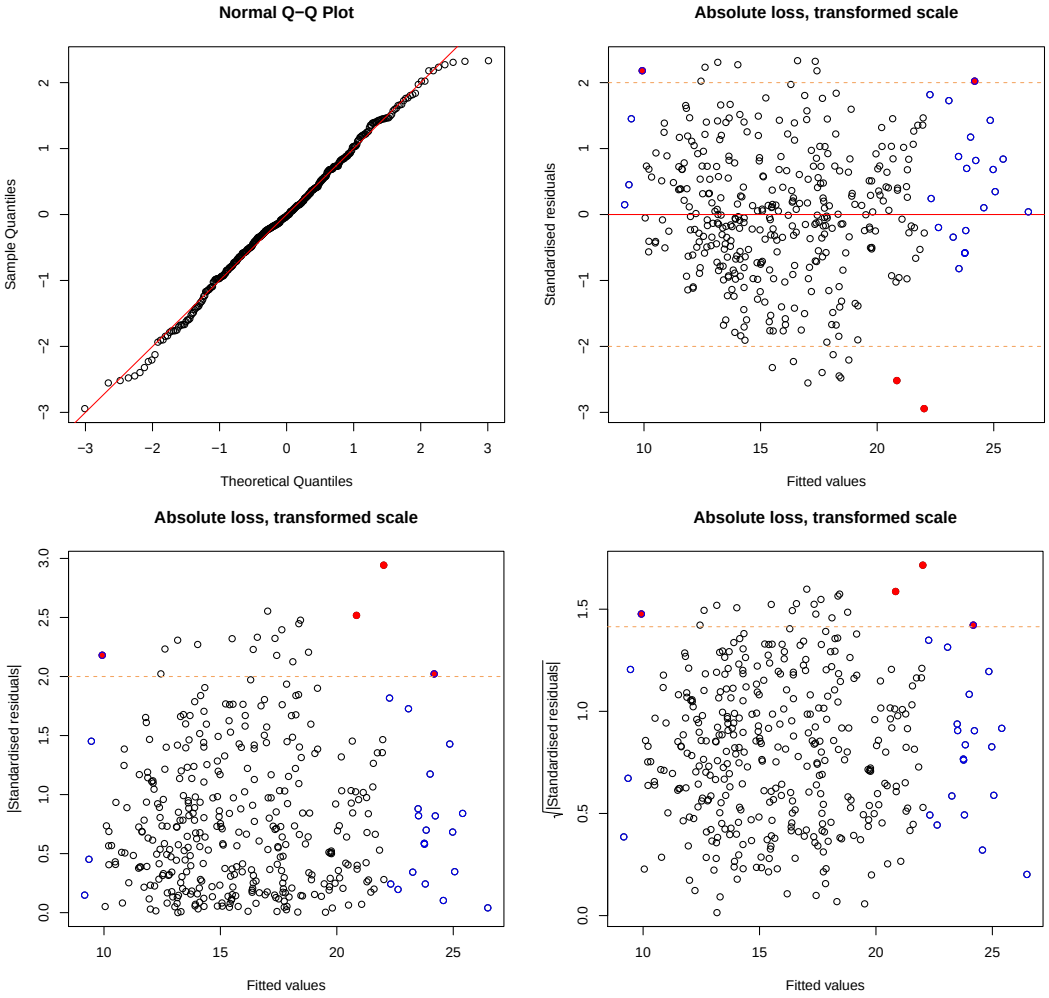

Fig. 2.6: Diagnostic plots for the regression showed in Figure 2.3c. (**Top left**) Normal-Q-Q-plot, points along diagonal line don't reject normality (SW: normality with a p-value = 0.245). All other figures show the fitted values on X-axis against the standardised residuals on the Y-axis as normal (**top right**), absolute (**bottom left**) and the square root (**bottom right**) of the absolute numbers. Blue borders indicate high leverage points, red filled circles indicate high values for Cook's distance and the orange dashed lines indicate the borders to the definition of large residuals. Heteroscedasticity is not evident. One outlier (Bonferroni outlier test) is not shown in the plot.

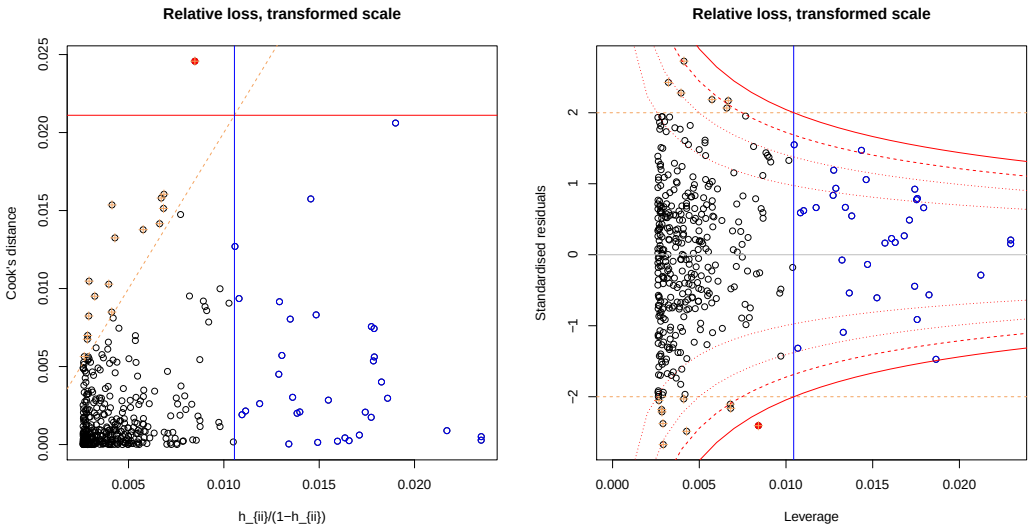

Fig. 2.7: Leverage (X-axis) vs Cook's distance (**left**) and standardised residuals (**right**) for the relative loss model on the vertical axis. Blue borders indicate high leverage points, red filled circles indicate high values for Cook's distance and the orange dashed lines indicate the borders to the definition of large residuals. One outlier (Bonferroni outlier test) is not shown in the plot.

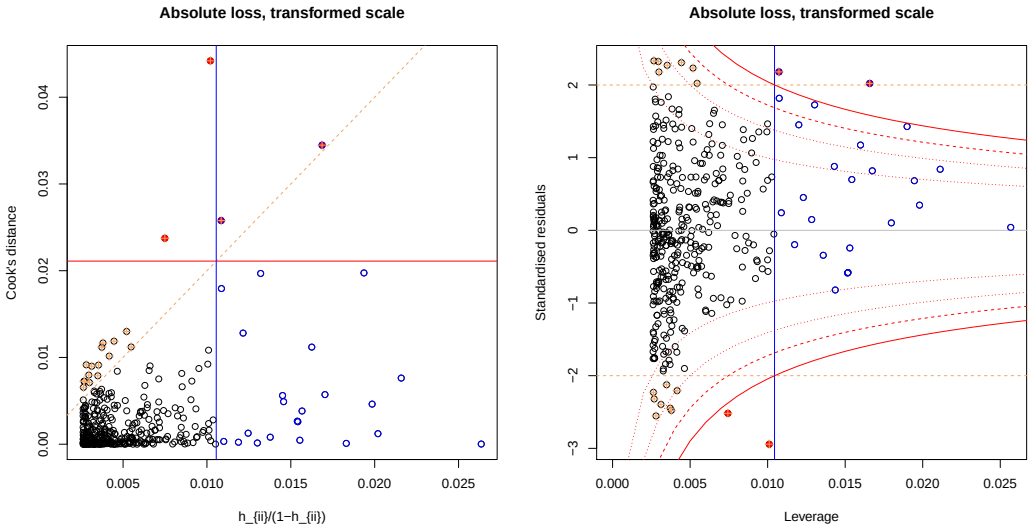

Fig. 2.8: Leverage (X-axis) vs Cook's distance (**left**) and standardised residuals (**right**) of the monetary loss model on the vertical axis. Blue borders indicate high leverage points, red filled circles indicate high values for Cook's distance and the orange dashed lines indicate the borders to the definition of large residuals. The outlier found for the relative loss model (Bonferroni outlier test) is not shown in the plot and was not used during the model fitting procedure.

2.B Cross-validation

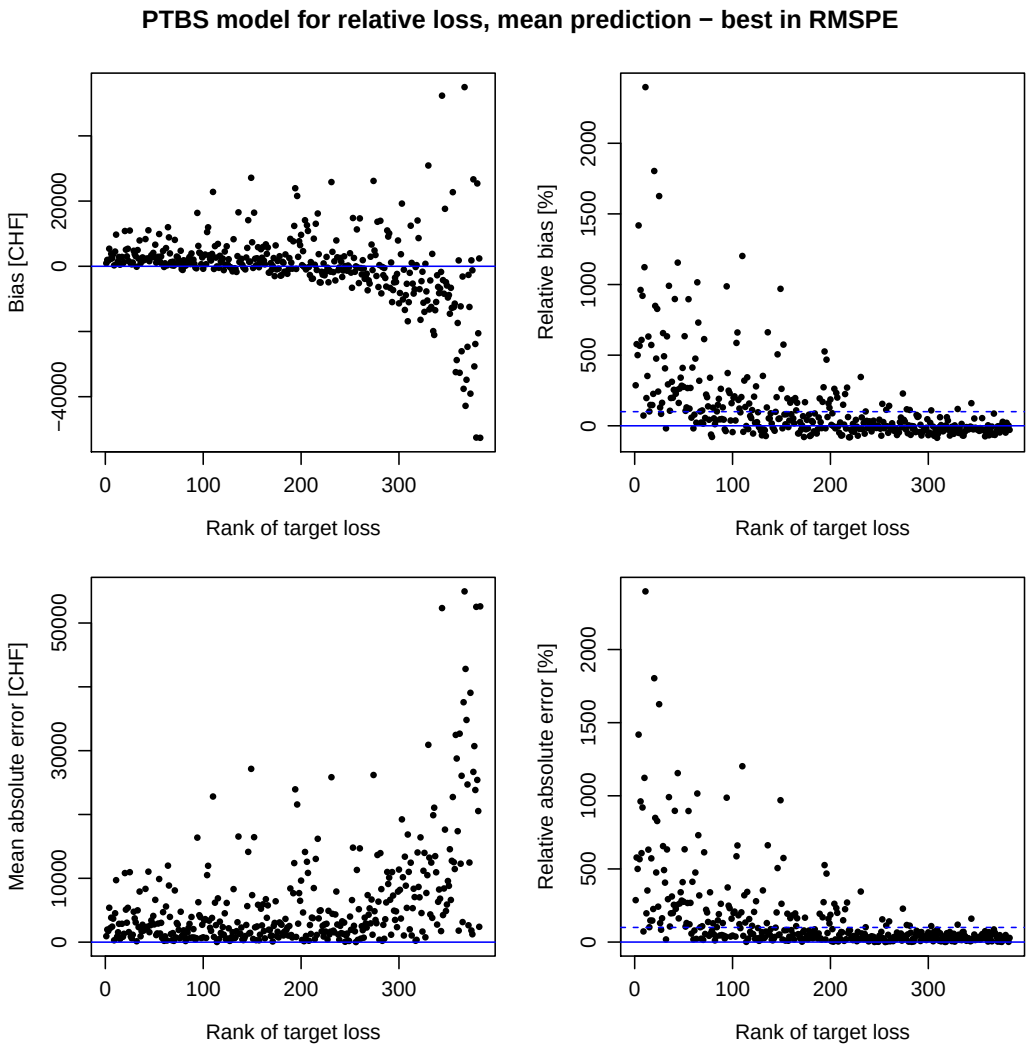

Fig. 2.9: Dependence of single errors on ranking. Absolute errors show high variability in higher ranks of target loss (original scale), whereas relative errors are more variable in lower ranks.

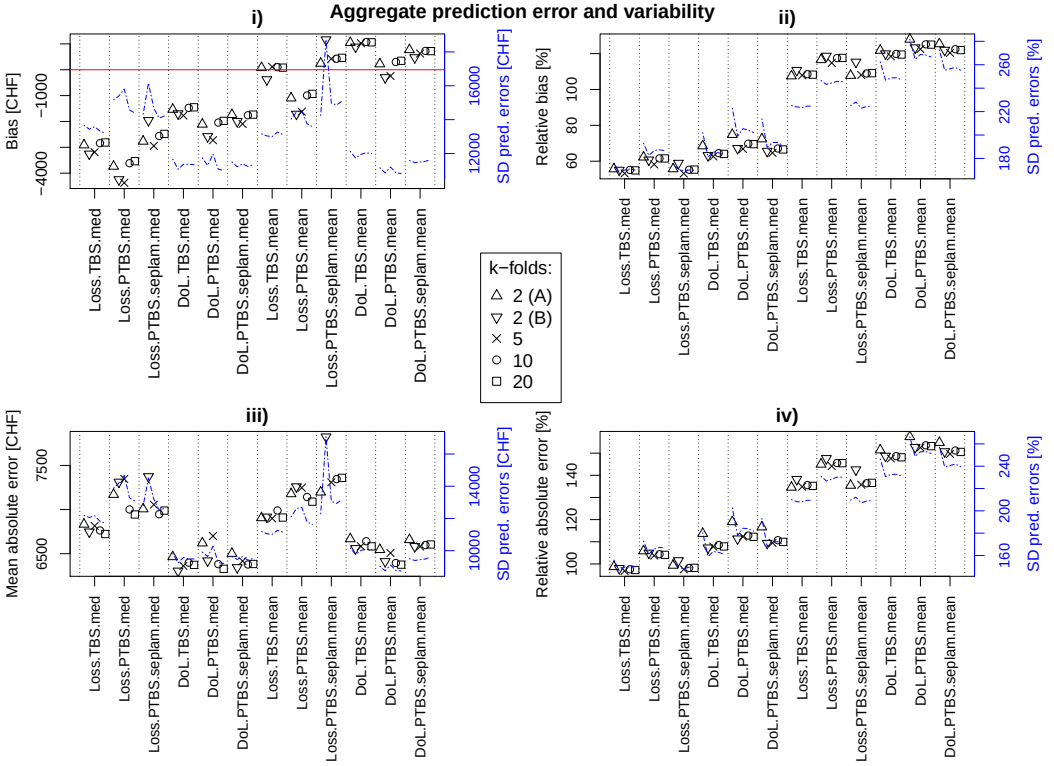

Fig. 2.10: Non-random cross-validation. K-fold = 2, (**A**): Obwalden + Ticino vs. Schwyz + Valais + Uri; (**B**): Obwalden + Schwyz vs. Ticino + Valais + Uri. K-fold = 5: One group per canton. K-Fold = 10/20: Split Obwalden, Ticino, Schwyz and Uri into multiple groups such that all groups have approximately the same size.

2.C Model parameters - best estimates

Table 2.2: Overview of the statistical evaluation and parameters of the two selected models. The estimates of β_0, β_1, λ and σ can be substituted in Equation (2.7) or (2.8) to predict the median or mean of y, respectively. * 95%-confidence interval

	Relative Loss Model	**Monetary Loss Model**
Spearman's ρ	0.746	0.720
Kendall's τ	0.556	0.527
$\hat{\lambda}$ Maximum Likelihood Estimate	0.205	0.131
λ CI *	(0.144, 0.265)	(0.068, 0.193)
$\hat{\sigma}$	0.495	2.745
$\hat{\beta}_0$	-0.098	3.798
β_0 CI *	$(-0.255, 0.060)$	(2.179, 5.416)
$\hat{\beta}_1$	0.817	0.618
β_1 CI *	(0.750, 0.884)	(0.560, 0.676)
adjusted R^2	0.668	0.618
Shapiro-Wilks p-value	0.385	0.245
Breusch-Pagan p-value	0.742	0.221

References

Akbas, S. O., Blahut, J., & Sterlacchini, S. (2009). Critical assessment of existing physical vulnerability estimation approaches for debris flows. *Proceedings of landslide processes: from geomorphologic mapping to dynamic modeling, Strasbourg*, *67*.

Alfieri, L., Cohen, S., Galantowicz, J., Schumann, G. J.-P., Trigg, M. A., Zsoter, E., Prudhomme, C., Kruczkiewicz, A., Coughlan de Perez, E., Flamig, Z., Rudari, R., Wu, H., Adler, R. F., Brakenridge, R. G., Kettner, A., Weerts, A., Matgen, P., Islam, S. A., de Groeve, T., & Salamon, P. (2018). A global network for operational flood risk reduction. *Environmental Science & Policy*, *84*, 149–158. doi:10.1016/j.envsci.2018.03.014.

Amadio, M., Mysiak, J., Carrera, L., & Koks, E. (2016). Improving flood damage assessment models in italy. *Natural Hazards*, *82*, 2075–2088. doi:10.1007/s11069-016-2286-0.

Andres, N., & Badoux, A. (2017). Unwetterschäden in der schweiz im jahr 2016: Rutschungen, murgänge, hochwasser und sturzereignisse. *Wasser, Energie, Luft WEL*, *109*, 97–104. URL: http://www.wsl.ch/fe/gebirgshydrologie/HEX/projekte/schadendatenbank/download/Unwetterschaeden_2016.

Badoux, A., Andres, N., Techel, F., & Hegg, C. (2016). Natural hazard fatalities in switzerland from 1946 to 2015. *Natural Hazards and Earth System Sciences*, *16*, 2747–2768. doi:10.5194/nhess-16-2747-2016.

Box, G. E. P., & Cox, D. R. (1964). An analysis of transformations. *Journal of the Royal Statistical Society. Series B (Methodological)*, *26*, 211–252. URL: http://www.jstor.org/stable/2984418.

Box, G. E. P., & Tidwell, P. W. (1962). Transformation of the independent variables. *Technometrics*, *4*, 531. doi:10.2307/1266288.

Breusch, T. S., & Pagan, A. R. (1979). A simple test for heteroscedasticity and random coefficient variation. *Econometrica*, *47*, 1287. doi:10.2307/1911963.

Cammerer, H., & Thieken, A. H. (2013). Historical development and future outlook of the flood damage potential of residential areas in the alpine lech valley (austria) between 1971 and 2030. *Regional Environmental Change*, *13*, 999–1012. doi:10.1007/s10113-013-0407-9.

Carisi, F., Schröter, K., Domeneghetti, A., Kreibich, H., & Castellarin, A. (2018). Development and assessment of uni- and multivariable flood loss models for emilia-romagna (italy). *Natural Hazards and Earth System Sciences*, *18*, 2057–2079. doi:10.5194/nhess-18-2057-2018.

Carroll, R. J., & Ruppert, D. (1984). Power transformations when fitting theoretical models to data. *Journal of the American Statistical Association*, *79*, 321. doi:10.2307/2288271.

Chinh, D., Dung, N., Gain, A., & Kreibich, H. (2017). Flood loss models and risk analysis for private households in can tho city, vietnam. *Water*, *9*, 313. doi:10.3390/w9050313.

Davino, C., Furno, M., & Vistocco, D. (2014). *Quantile Regression*. Oxford: John Wiley & Sons, Ltd. doi:10.1002/9781118752685.

Davison, A. C., & Hinkley, D. V. (2013). Linear regression. In A. C. Davison, & D. V. Hinkley (Eds.), *Bootstrap Methods and their Application* (pp. 256–325). Cambridge University Press. doi:10.1017/CBO9780511802843.007.

Dottori, F., Figueiredo, R., Martina, M. L. V., Molinari, D., & Scorzini, A. R. (2016). Insyde: A synthetic, probabilistic flood damage model based on explicit cost analysis. *Natural Hazards and Earth System Sciences*, *16*, 2577–2591. doi:10.5194/nhess-16-2577-2016.

Duan, N. (1983). Smearing estimate: A nonparametric retransformation method. *Journal of the American Statistical Association*, *78*, 605. doi:10.2307/2288126.

Dutta, D., Herath, S., & Musiake, K. (2003). A mathematical model for flood loss estimation. *Journal of Hydrology*, *277*, 24–49. doi:10.1016/S0022-1694(03)00084-2.

Ernst, J., Dewals, B. J., Detrembleur, S., Archambeau, P., Erpicum, S., & Pirotton, M. (2010). Micro-scale flood risk analysis based on detailed 2d hydraulic modelling and high resolution geographic data. *Natural Hazards*, *55*, 181–209. doi:10.1007/s11069-010-9520-y.

FOEN (2015). EconoMe 4.0. Wirksamkeit und Wirtschaftlichkeit von Schutzmassnahmen gegen Naturgefahren. Handbuch / Dokumentation. Federal Office for the Environment FOEN.

FOWG (2005). Bericht über die hochwasserereignisse 2005. *Federal Office for Water and Geology*, . URL: http://www.news.admin.ch/NSBSubscriber/message/attachments/1123.pdf.

Fuchs, S., Birkmann, J., & Glade, T. (2012). Vulnerability assessment in natural hazard and risk analysis: current approaches and future challenges. *Natural Hazards*, *64*, 1969–1975. doi:10.1007/s11069-012-0352-9.

Fuchs, S., Keiler, M., & Zischg, A. (2015). A spatiotemporal multi-hazard exposure assessment based on property data. *Natural Hazards and Earth System Science*, *15*, 2127–2142. doi:10.5194/nhess-15-2127-2015.

Fuchs, S., Röthlisberger, V., Thaler, T., Zischg, A., & Keiler, M. (2017). Natural hazard management from a coevolutionary perspective: Exposure and policy response in the european alps. *Annals of the American Association of Geographers*, *107*, 382–392. doi:10.1080/24694452.2016.1235494.

Fuchs, S., & Thaler, T. (Eds.) (2018). *Vulnerability and Resilience to Natural Hazards*. Cambridge University Press.

Gerl, T., Kreibich, H., Franco, G., Marechal, D., & Schroter, K. (2016). A review of flood loss models as basis for harmonization and benchmarking. *PloS one*, *11*, e0159791. doi:10.1371/journal.pone.0159791.

Good, P. I., & Hardin, J. W. (2003). Validation. In *Common Errors in Statistics (and How to Avoid Them)* (pp. 155–162). John Wiley & Sons, Inc. doi:10.1002/0471463760.ch11.

Greene, W. H. (2012). *Econometric analysis*. (7th ed.). Harlow and New York: Pearson Addison Wesley.

Hastie, T., Tibshirani, R., & Friedman, J. (Eds.) (2009). *The Elements of Statistical Learning*. Springer series in statistics. New York, NY: Springer New York. doi:10.1007/978-0-387-84858-7.

Hirabayashi, Y., Mahendran, R., Koirala, S., Konoshima, L., Yamazaki, D., Watanabe, S., Kim, H., & Kanae, S. (2013). Global flood risk under climate change. *Nature Climate Change*, *3*, 816–821. doi:10.1038/nclimate1911.

Hydrotec (2001). Hochwasser-aktionsplan angerbach. teil i: Berichte und anlagen. studie im auftrag desstua düsseldorf, aachen., .

Intergovernmental Panel on Climate Change (2012). *Managing the risks of extreme events and disasters to advance climate change adaptation: Special report of the intergovernmental panel on climate change*. Cambridge: Cambridge University Press.

Jonkman, S. N., Bočkarjova, M., Kok, M., & Bernardini, P. (2008). Integrated hydrodynamic and economic modelling of flood damage in the netherlands. *Ecological Economics*, *66*, 77–90. doi:10.1016/j.ecolecon.2007.12.022.

Kreibich, H., Seifert, I., Merz, B., & Thieken, A. H. (2010). Development of flemocs – a new model for the estimation of flood losses in the commercial sector. *Hydrological Sciences Journal*, *55*, 1302–1314. doi:10.1080/02626667.2010.529815.

Maciejewski, R., Pattath, A., Ko, S., Hafen, R., Cleveland, W. S., & Ebert, D. S. (2013). Automated box-cox transformations for improved visual encoding. *IEEE transactions on visualization and computer graphics*, *19*, 130–140. doi:10.1109/TVCG.2012.64.

Papathoma-Köhle, M. (2016). Vulnerability curves vs. vulnerability indicators: application of an indicator-based methodology for debris-flow hazards. *Natural Hazards and Earth System Science*, *16*, 1771–1790. doi:10.5194/nhess-16-1771-2016.

Papathoma-Köhle, M., Kappes, M., Keiler, M., & Glade, T. (2011). Physical vulnerability assessment for alpine hazards: state of the art and future needs. *Natural Hazards*, *58*, 645–680. doi:10.1007/s11069-010-9632-4.

Papathoma-Köhle, M., Zischg, A., Fuchs, S., Glade, T., & Keiler, M. (2015). Loss estimation for landslides in mountain areas – an integrated toolbox for vulnerability assessment and damage documentation. *Environmental Modelling & Software*, *63*, 156–169. doi:10.1016/j.envsoft.2014.10.003.

Perry, M. B., & Walker, M. L. (2015). A prediction interval estimator for the original response when using box-cox transformations. *Journal of Quality Technology*, *47*, 278–297.

PSL (2018). Euro to swiss franc spot exchange rates for 2005 from the bank of england, . URL: https://www.poundsterlinglive.com/bank-of-england-spot/historical-spot-exchange-rates/eur/EUR-to-CHF-2005.

R Core Team (2016). R: A language and environment for statistical computing. R Foundation for Statistical Computing. URL: https://www.R-project.org/.

Rothery, P. (1988). A cautionary note on data transformation: bias in back-transformed means. *Bird Study*, *35*, 219–221. doi:10.1080/00063658809476992.

Royston, J. P. (1982). An extension of shapiro and wilk's w test for normality to large samples. *Applied Statistics*, *31*, 115. doi:10.2307/2347973.

Ruppert, D., & Matteson, D. S. (2015). *Statistics and Data Analysis for Financial Engineering*. New York, NY: Springer New York. doi:10.1007/978-1-4939-2614-5.

Sakia, R. M. (1990). Retransformation bias: A look at the box-cox transformation to linear balanced mixed anova models. *Metrika*, *37*, 345–351. doi:10.1007/BF02613542.

Sampson, C. C., Smith, A. M., Bates, P. D., Neal, J. C., Alfieri, L., & Freer, J. E. (2015). A high-resolution global flood hazard model. *Water Resources Research*, *51*, 7358–7381. doi:10.1002/2015WR016954.

Sokal, R. R., & Rohlf, F. J. (1969). *Biometry: The principles and practice of statistics in biological research*. (2nd ed.). New York: W.H. Freeman.

Staffler, H., Pollinger, R., Zischg, A., & Mani, P. (2008). Spatial variability and potential impacts of climate change on flood and debris flow hazard zone mapping and implications for risk management. *Natural Hazards and Earth System Science*, *8*, 539–558. doi:10.5194/nhess-8-539-2008.

Swiss Re (2012). Floods in switzerland - an underestimated risk, . URL: http://www.planat.ch/fileadmin/PLANAT/planat_pdf/alle_2012/2011-2015/Swiss_Re__Hg__2012_-_Floods_in_Switzerland.pdf.

Taylor, J. M. G. (1986). The retransformed mean after a fitted power transformation. *Journal of the American Statistical Association*, *81*, 114–118. doi:10.1080/01621459.1986.10478246.

Thieken, A. H., Müller, M., Kreibich, H., & Merz, B. (2005). Flood damage and influencing factors: New insights from the august 2002 flood in germany. *Water Resources Research*, *41*. doi:10.1029/2005WR004177.

Thieken, A. H., Olschewski, A., Kreibich, H., Kobsch, S., & Merz, B. (2008). Development and evaluation of flemops – a new f lood l oss e stimation mo del for the p rivate s ector. In D. Proverbs, C. A. Brebbia, & E. Penning-Rowsell (Eds.), *Flood Recovery, Innovation and Response I* (pp. 315–324). Southampton, UK: WIT Press. doi:10.2495/FRIAR080301.

Totschnig, R., Sedlacek, W., & Fuchs, S. (2011). A quantitative vulnerability function for fluvial sediment transport. *Natural Hazards*, *58*, 681–703. doi:10.1007/s11069-010-9623-5.

UNDRO (1980). Natural disasters and vulnerability analysis. geneva: Office of the united nations disaster relief co-ordinator, .

UNISDR (2015). *Global assessment report on disaster risk reduction (GAR) 2015: Making development sustainable : the future of disaster risk management*. New York: United Nations.

Walther, B. A., & Moore, J. L. (2005). The concepts of bias, precision and accuracy, and their use in testing the performance of species richness estimators, with a literature review of estimator performance. *Ecography*, *28*, 815–829. doi:10.1111/j.2005.0906-7590.04112.x.

Ward, P. J., Jongman, B., Aerts, Jeroen C. J. H., Bates, P. D., Botzen, W. J. W., Diaz Loaiza, A., Hallegatte, S., Kind, J. M., Kwadijk, J., Scussolini, P., & Winsemius, H. C. (2017). A global framework for future costs and benefits of river-flood protection in urban areas. *Nature Climate Change*, *7*, 642 EP –. URL: http://dx.doi.org/10.1038/nclimate3350. doi:10.1038/nclimate3350.

Ward, P. J., Jongman, B., Weiland, F. S., Bouwman, A., van Beek, R., Bierkens, M. F. P., Ligtvoet, W., & Winsemius, H. C. (2013). Assessing flood risk at the global scale: model setup, results, and sensitivity. *Environmental Research Letters*, *8*, 044019. doi:10.1088/1748-9326/8/4/044019.

Weisberg, S. (2005a). Regression diagnostics: Residuals. In *Applied Linear Regression* (pp. 167–193). John Wiley & Sons, Inc. doi:10.1002/0471704091.ch8.

Weisberg, S. (2005b). Scatterplots and regression. In *Applied Linear Regression* (pp. 1–18). John Wiley & Sons, Inc. doi:10.1002/0471704091.ch1.

Weisberg, S. (2005c). Simple linear regression. In *Applied Linear Regression* (pp. 19–46). John Wiley & Sons, Inc. doi:10.1002/0471704091.ch2.

Wenger, S. J., & Olden, J. D. (2012). Assessing transferability of ecological models: An underappreciated aspect of statistical validation. *Methods in Ecology and Evolution*, *3*, 260–267. doi:10.1111/j.2041-210X.2011.00170.x.

Zischg, A., Schober, S., Sereinig, N., Rauter, M., Seymann, C., Goldschmidt, F., Bäk, R., & Schleicher, E. (2013). Monitoring the temporal development of natural hazard risks as a basis indicator for climate change adaptation. *Natural Hazards*, *67*, 1045–1058. doi:10.1007/s11069-011-9927-0.

Zischg, A. P., Hofer, P., Mosimann, M., Röthlisberger, V., Ramirez, J. A., Keiler, M., & Weingartner, R. (2018). Flood risk (d)evolution: Disentangling key drivers of flood risk change with a retro-model experiment. *The Science of the total environment*, *639*, 195–207. doi:10.1016/j.scitotenv.2018.05.056.

3 Evaluation of surrogate flood models for the use in impact-based flood warning systems at national scale

Markus Mosimann[1, 2, 3], Martina Kauzlaric[1, 2, 3], Simon Schick[1, 2, 3], Olivia Martius[1, 2, 3], Andreas Paul Zischg [1, 2, 3]

[1] *Institute of Geography, University of Bern, Hallerstrasse 12, 3012 Bern, Switzerland*

[2] *Mobiliar Lab for Natural Risks, University of Bern, Hallerstrasse 12, 3012 Bern, Switzerland*

[3] *Oeschger Centre for Climate Change Research, University of Bern, Hochschulstrasse 4, 3012, Bern, Switzerland*

Environmental Modelling & Software (Elsevier), 173, 105936, `https://doi.org/10.1016/j.envsoft.2023.105936`
Submitted: 3 March 2023; Accepted: 15 December 2023; Published: 18 January 2024

Abstract

Recent flood events show that gaps in the communication channels from warning services to target groups inhibit mitigation. One approach addressing this issue is impact-based warning. We introduce a library-based surrogate flood model for the use in impact-based warning systems, tested for the main river network of Northern Switzerland. To validate the surrogate model, we compare the impacts to buildings, persons and workplaces with hazard classification, estimated with transient simulations for nine extreme precipitation scenarios. With 78 analyzed model regions, the surrogate approach reaches a Flood Area Index between 0.74 and 0.90 for each scenario (overall 0.84). The Critical Success Index calculated based on exposed persons is 0.77–0.93 (overall 0.89). Our prototype of a library-based flood surrogate model demonstrates the ability of accurately representing a same resolved transient model, bearing the potential to predict flood impacts nationwide in near real-time and the applicability to probabilistic forecasts.

Keywords: Impact-based warning; Impact forecast; Surrogate flood model; Library-based surrogate model; Near real-time warning; Flood warning system

3.1 Introduction

The European floods during summer 2021, the floods in Pakistan 2022 and the floods in California 2023 have once more demonstrated the destructive potential of floods and that they not only lead to high monetary damage but also cost many lives. Fekete & Sandholz (2021) take up the discussions that came up in Germany, after the European Floods 2021 revealed critical issues in disaster management. As one key to bridge communication gaps in future events, they recommend searching for solutions to "decode communication [...] to better understand diverging and ambiguous information and interpretations". Besides the flood event in Germany, there are numerous examples globally where forecasts of upcoming natural hazards resulted in a poor response (World Meteorological Organization, 2015). Considering that extreme weather- and climate-related events are projected to become generally more frequent and intense with climate change (Intergovernmental Panel on Climate Change, 2012), it becomes even more relevant to support decision makers in disaster management with appropriate warnings of natural hazards.

The World Meteorological Organization (WMO) published "Guidelines on Multi-hazard Impact-based Forecast and Warning Services" (World Meteorological Organization, 2015), to support authorities with introducing warning systems that warn users of the possible consequences of a predicted extreme event. This concept is called impact-based warnings (IBWs) and impact forecasts (IFs). Additionally, increasing the availability of and giving access to early warning systems is one of the main targets given by the Sendai Framework for Disaster Risk Reduction 2015–2030 (United Nations, 2015). According to the WMO guidelines, IBWs inform target users about impacts that are expected due to the hazard of a forecasted weather event and known vulnerability, whereas IFs are defined as the "next evolutionary step of warnings" by adding explicit information about exposure on an individual or community level. This information should support their decisions on what mitigation measures to undertake next. Thus, IBWs and IFs aim at optimizing short-term prevention and risk management actions and are therefore issued in a specific way for each target group.

In recent years, the effectiveness of IBWs and IFs has been demonstrated repeatedly. IBWs have a significant effect on the intended response to an extreme event and together with behavioral recommendations they can improve the perception and the understanding of warnings (Weyrich et al., 2018). IBWs demonstrated to improve not only intended response but also risk perception (Potter et al., 2021). Compared to general warnings, IBWs increase the likelihood that protective decisions are taken (Meléndez-Landaverde et al., 2020; Casteel, 2016, 2018). There is a clear need for improvements in collecting and storing flood impact data, as well as for describing or discussing technical standards (Kaltenberger et al., 2020; Potter et al., 2021).

Aiming at providing the highest level of flood warnings by means of highly resolved inundation models that are reliably informing about hazard and impact at a single house level is linked with high computational costs. Conversely, a suitable model for near-real time warnings on a national level needs to simulate predictions with enough lead time and substantially before the upstream element in the model chain gets updated. Therefore, we search for a flood modelling framework applicable as national warning system (Switzerland), optimizing the trade-off between computational efficiency and

high resolution.

As model chains for flood risk assessment do not focus on computational efficiency or a coarse spatial resolution has to be selected, they do not fit the requirements for being implemented in IBW and IF frameworks (van Dyck & Willems, 2013; Ward et al., 2013; Falter et al., 2015; Foudi et al., 2015; Moncoulon et al., 2014; Alfieri et al., 2016; Felder et al., 2018). Recently, the potential for near-real time applications for large regions of highly resolved (10m) raster-based flood models running on GPU was shown (Ming et al., 2020; Apel et al., 2022). Besides that mainly hazard and not impact is in the focus of these studies, the resolution is still too coarse to correctly consider important hydraulic features like dikes, walls or flood defenses in rivers and floodplains. Although sub-grid approaches, or synonymously 1D-2D coupled models, allow to precisely embed river channel geometry into a 2D grid, these approaches show similar resolution-performance trade-offs as the ones used in flood risk assessment (Neal et al., 2011, 2012, 2015; Russo et al., 2015). As an alternative to inundation models running on regular, raster-based computational grids, the resolution of irregular meshes can be adapted for separate regions in the same model. In addition, the representation of hydraulic structures can be enforced when present in the underlying, highly resolved digital elevation model (Horritt & Bates, 2002; Zischg et al., 2018b).

One approach to deal with the trade-off between computational time and spatial resolution are flood surrogate models (Zischg et al., 2018a), or synonymously called « flood libraries » or « flood impact libraries » when combined with exposure and physical vulnerability. These surrogate models are widely known and already applied especially in context of surface water floods (synonymously pluvial floods or flash floods) (Bermúdez et al., 2018; Aldridge et al., 2020; Cox et al.). The term « flood libraries » comes from pre-calculated flood simulations that are stored in a database. In case of a flood forecast, the early warning system searches for the preprocessed flood simulation in the database for which the input hydrograph is similar to the forecasted hydrograph, here in terms of peak discharge. Surrogate modeling aims at developing "cheaper-to-run" surrogates of the original simulation models (Razavi et al., 2012). Surrogate models can be derived from computationally expensive models either by response surface modeling or by developing lower-fidelity models with simplified implementations of the physical equations. Response surface surrogate models and library-based surrogate models are also referred to as metamodels or a model of a model (Razavi et al., 2012). The term surrogate model is also used in the context of deep learning models replacing numerical simulations, an upcoming topic in the field of flood modelling.

To our knowledge, an application of surrogate flood models in IBWs and IFs of fluvial floods on a national scale has not been discussed yet and there is no general architecture or technical specification given defining requirements of a flood model for being a valid application for IBW and IF systems. Based on an analysis of extreme floods in the north alpine part of Switzerland, the goal of this study is to evaluate the potential and limitations of high-resolution flood surrogate models for IBWs or IFs on a national level and to discuss application opportunities, uncertainties and further needs for possible target users.

In this study, we focus on the loss of information when using precomputed flood scenarios (i.e., flood surrogate models) compared to transient simulations. For the model evaluation, we consider flood hazard as well as affected population and buildings.

3.2 Data and Methods

To analyze and discuss the potential of flood surrogate models for an operationalization in impact-based flood warning systems, meteorological and hydrological uncertainties must be decoupled. We use synthetic hydrographs over a range of peaks specific for each floodplain to model flood and impact based on a spatially and temporally highly resolved flood model and store results as flood libraries in a database. The scenarios in the database can be identified by the name of the floodplain and the peak discharge of the used synthetic hydrographs. The nearest neighbor to the peak discharge of the hydrometeorological scenarios is then used as the basis for the prediction of the surrogate model. We use nine extreme hydrometeorological scenarios from reforecast archives as test cases for modelling the flood impacts. The hydrographs of these scenarios serve as input into transient flood models based on the same computational grid of the surrogate flood model. These are our benchmarks against which the surrogate models are compared. We measure the information loss on flood hazard and impact when using the flood surrogate models in comparison to the results of the transient simulation.

3.2.1 Study Area

Figure 3.1 gives an overview of the study area. We consider 24 Swiss rivers together with Lake Lucerne, Lake Thun, Lake Walen and Lake Brienz. The study area covers a relevant part of the main headwater catchments of Northern Switzerland, covering parts of the Swiss Plateau, the Jura mountains, alpine Prealps and the northern Alpine ridge. There are river sections with lakes as upstream boundary conditions: the Aare River downstream of Lake Brienz and Lake Thun, the Reuss River downstream of Lake Lucerne and the Linthkanal downstream of Lake Walen. Although not all of Switzerland is covered by the study area, relevant parts of the Swiss (north alpine) social and environmental characteristics are represented, allowing for a generalization of the results on the applicability of surrogate models at a national scale.

3.2.2 Preprocessing for flood simulation database

In this section, we present the preprocessing steps done to create a database with flood simulation results, following the approach presented in (Zischg et al., 2018a). For the scenarios, we use synthetic hydrographs similar to those created as in their study. Instead of a full 2D-flood model, we rely on semi-automatically generated 1D/2D coupled hydrodynamic models, being more efficient in simulating a high number of simulations. Compared to that study, we expand the impact assessment and the study region significantly to explore the applicability in a nationwide impact-based warning system.

3.2.2.1 Synthetic hydrographs

For the derivation and application of synthetic hydrographs used as upstream boundary conditions for the flood simulations stored in a database, we implement the method proposed by Serinaldi & Grimaldi (2011) and used in Felder et al. (2017); Zischg et al.

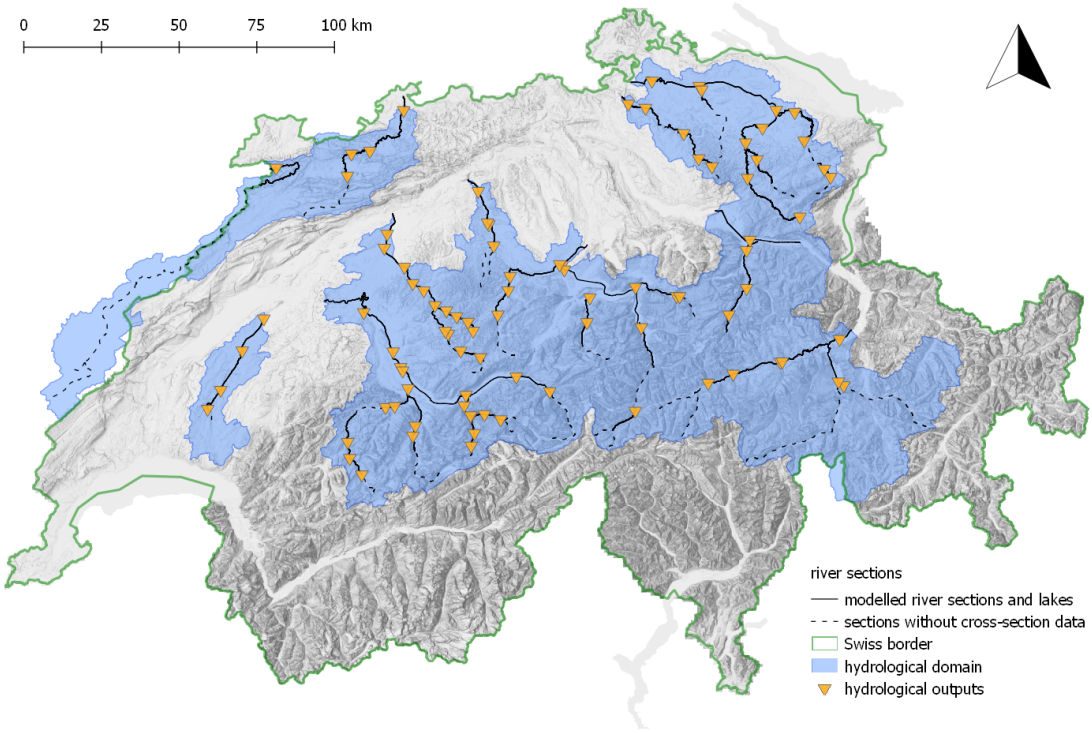

Fig. 3.1: Study area. The blue shaded area indicates the catchment considered in the hydrological model. The lines indicate river sections and lakes used for the hydraulic modelling/impact assessment. Triangles refer to interfaces of hydrological and hydraulic models.

(2018a). For available gauging stations of the Federal Office for the Environment (FOEN, 2021), we manually extract event hydrographs containing only one peak and normalize these in terms of time (setting 0 as the start, and 1 as the end of the event) and discharge (based on the mean discharge over the event). The normalized average of time to peak and normalized average peak discharges of all events at one station are used to fit a two parametric gamma distribution function representing the typical hydrograph shape of the corresponding river or river section (Nadarajah, 2007; Rai et al., 2009). The same event hydrographs extracted are also used to build a linear regression model describing the peak-volume ratio. After the fitted gamma distribution is rescaled to represent a target peak, this regression model is used to further adapt the flood volume of the rescaled hydrograph. The synthetic hydrographs are estimated for every river section individually (locations are indicated by triangles in Figure 3.1) and mimic as such the typical time to peak, peak discharge relative to mean discharge and flood volume. For river sections without gauging stations, synthetic hydrographs derived by stations with similar catchment characteristics (catchment size, specific discharge) are used.

The lower limit of the range of peaks considered for the surrogate model is defined based on the threshold to warning level 3 of 5 given by the FOEN for the main part of their gauging stations (FOEN, 2023). This warning level indicates that local overtopping of river dikes is possible, the threshold is in accordance with roughly a 10- to 30-year flood, adapted based on knowledge of weak spots below this statistical value. The

upper limit of the range of peaks is defined according to the highest discharge/lake level estimated by a hydrological model fed with 157 extreme weather scenarios (further details will follow in sections 3.2.4.1 and 3.2.4.2) and the extreme value statistics given by the FOEN for every gauging station (FOEN, 2021). We simulate lake floodings in 10 cm steps. For rivers, the steps of discharge are set based on the lower limits of the ranges. The flood library consist of between 10 and 30 flood simulations per river section.

3.2.2.2 Hydrodynamic simulations

This study focus on the rivers of national interest in Northern Switzerland, where river cross-section measurements are taken about every 10 years by the Federal Office for the Environment (FOEN, 2022). For the hydraulic simulations, the software BASEMENT (Vetsch et al., 2018) is used. This model provides the functionality to couple 1D and 2D flood models. The cross-section measurements from the FOEN serves as data base for the 1D model, for the 2D model, we derive the topography from high resolution digital terrain models provided by either cantons (Canton of Vaud, 2004; Canton of Aargau, 2014; Canton of Lucerne, 2012; Canton of Solothurn, 2014; Canton of Zug, 2013; Canton of Zurich, 2014; Canton of Bern, 2014), the Federal Office of Topography (Federal Office of Topography, 2013) or the Regierungspräsidium Freiburg/FOEN (Reigierungspräsidium Freiburg, 2015). The 2D model computes the water fluxes in the floodplains based on a triangulated irregular mesh with a configured maximum area of 200 m^2 built with the meshing module BASEmesh (available as plugin for the software QGIS) integrated in BASEMENT. On average, the element size is roughly 130 m^2. To ensure that dikes and hydraulically relevant structures are considered in the 2D flood model, we digitize "breaklines" along these structures manually with the help of a hillshade generated with the high-resolution DEMs. Besides the breaklines, we manually digitize the 2D-perimeter, the 1D-2D coupling interface of the computational grid as lines as well as "flowlines" defining the river sections. This data is stored on a PostgreSQL database with a PostGIS extension also containing the cross-section data (as points and lines). With this data, a major part of the model generation can be automatized: The flowlines serve as basis to select the cross-section data needed and contains tabular information about model parameters like the friction coefficient for a specific river section. The selected cross-sections are transformed into the machine-readable 1D-model file format (BMG). An initial run to provide wet initial conditions in the 1D-model of the coupled model is automatically executed and processed. The 2D-mesh creation occurs independent of the preparation of models for single regions. Here, floodplains are meshed by discretizing all intersecting breaklines, elevation information is attributed to the mesh-nodes. After automatically meshing each floodplain, we transformed the data into the file format for the 2D-model (2DM). The 1D-2D model interfaces are stored as lines in the database, containing additional information about the model region it belongs to and whether the dike crest elevation of the cross-section data or the elevation from the DEM should be considered in the model. In case of rather small structures like walls not detected by the elevation model, it is beneficial to use the dike elevation measured and marked in the cross-section data. The model expects a list with edges defined by two node-ids whose elevation is then compared to the (linearly interpolated) water surface elevation calculated for the closest cross-section (Euclidean distance) of the 1D-model. Within a batch-process initiating the model runs, a python script updates the machine-readable

BASEMENT command files (BMC) concerning simulation runtime, taken from the specific preprocessed synthetic hydrograph. A timestamp in each manually derived data is used to check for necessary updates of the simulation models. Whereas lateral 1D-2D couplings can be derived automatically, the coupling of 1D river sections, for example to consider bifurcations/junctions, must be parametrized manually. After defining 1D-1D couplings for such cases once, the according snippets defining these couplings are stored and can be accessed again in case of an update. This guarantees consistency in the implementation of manually edited parts in the automatic setup of the command file. Due to the modular functionality of the preprocessing, updates or extensions can easily be implemented.

We calibrate the 1D hydraulic model based on stage-discharge relationships given by FOEN (2021), optimizing the friction coefficient to fit the bankfull stage-discharge relation. Additionally, we adapt the friction coefficients in flood models where existing case studies and technical reports are available and discharge capacities are known. A major difference exists for sections where bridges are limiting the discharge capacity, as they are not yet included in our models. We assume dam stability for all our simulation scenarios, meaning that there are no dam breaches considered. A validation of the 2D flood model with the major flood events in 2005 and 2007 is not possible, because flood protection measures as river widenings or levee heightening have been implemented after these events. This makes current cross-section data inappropriate for a validation with suitable past events on regional/national scale. The study Zischg et al. (2018b) serves as a comparison, in which a similar model setup was used.

The computation as a single hydraulic model for Switzerland is currently not feasible. Therefore, regions preferably drained only by a river cross-section and not the floodplain are spatially defined. Hence, flood pathways in the floodplains are not interrupted by the model boundary. Where junctions of large or multiple tributary streams substantially increase the hydrological catchment area, river sections are divided to consider additional discharge downstream of the junction, as there is no further hydrological input other than at the upstream boundary.

3.2.2.3 Impact modelling

The selection of the impact variables is dependent on the targeted user or user group of IBW and IF systems. Here, we address the needs of three potential target group profiles. We want to stress that the definition of target users, their demands and their roles is not in the focus of this study. Nevertheless, to exemplify the validity of the proposed warning system, we define simplified profiles whose requirements were revealed based on a close collaboration and exchange with several stakeholder groups in Switzerland over the last years (Zischg, 2023).

The first and main user group are intervention forces that manage the continuity of social life during flood events. These are disaster risk reduction and civil protection agencies like fire brigades, police or health care providers acting on both a strategic (e.g., resource management) and local emergency level (e.g., evacuations). These groups require information about flooded areas, the number of affected people, the affected infrastructure, i.e., houses, workplaces, hospitals, schools, and nursery homes. In addition, this user group requires a classification and cartographic illustration of the flood hazards,

i.e., they must be informed about the locations of flooded areas that are not accessible anymore and that are critical in terms of risks for life.

The second target user group for which we test the applicability of impact forecasts are insurance companies for buildings. In 19 cantons in Switzerland, insuring of buildings against natural hazards is mandatory and regulated by public insurance companies. The insurance companies are mostly active in the aftermath of an event to make damage estimations to provide financial support. However, insurance companies can warn their customers based on their home locations before the onset of the event and must set up the claim management system within reasonable time after the event. This requires knowing the location of affected customers. With an impact forecast that provides information on flooded houses and flood damages to houses, they can prepare for managing the event by reserving organizational and financial resources. This target group thus needs information on the number of flooded houses and estimates of flood damage in monetary units from an IBW or IF system.

Lastly, we adopt the perspective of a warning service that operates a location-based alert system with the general public as target user group. These private persons ideally use the warnings to avoid dangerous areas and to reduce damage to their building and household content.

We will use these target user profiles to discuss our results in section 4. To provide the required information for the three target groups we selected the following impact variables:

- The flooded area (water depth and hazard class),
- the number and locations of flooded buildings,
- the number and locations of residents of flooded buildings,
- the number and locations of flooded workplaces,
- the number and locations of schools,
- the number and locations of hospitals,
- the number and locations of nursery homes,
- and the estimated monetary damage to flooded buildings.

Exposed objects are defined as objects that intersect computational mesh elements having been wet for at least one timestep during the simulation. We further attribute the maximum flow depth out of all intersecting elements to the exposed object as proposed by (Bermúdez et al., 2018). The estimation of damage is done with a regionally calibrated vulnerability function based on Swiss insurance data (Zischg et al., 2021).

We classify the flooded areas into hazard classes (Table 1 and Fig. 2) following Pregnolato et al. (2017); Arrighi et al. (2019); Costabile et al. (2021). The classification is based on the vulnerability of key elements at risk and indicates hazards for people inside and outside of buildings and for cars. The maximum hazard classes from each precalculated scenario are stored in the database specific for each element, as the hydraulic model outputs the required variables.

Class	Description	Constraints
0	Not exposed to floods	h < 0.01 m
1	Flooded but safe for pedestrians and vehicles	h < 0.3 m AND v < 2.0 m/s AND h*v < 0.3 m^2/s
2	No access for vehicles	h > 0.3 m OR h*v>=0.3 m^2/s
3	Pedestrians and/or vehicles highly vulnerable	h > 0.5 m OR v > 2.0 m/s OR h*v>=0.6 m^2/s
4	Considerable damage to buildings expected	h > 1.5 m

Table 3.1: Classification of hazard classes, where h denotes flood depth and v flow velocity.

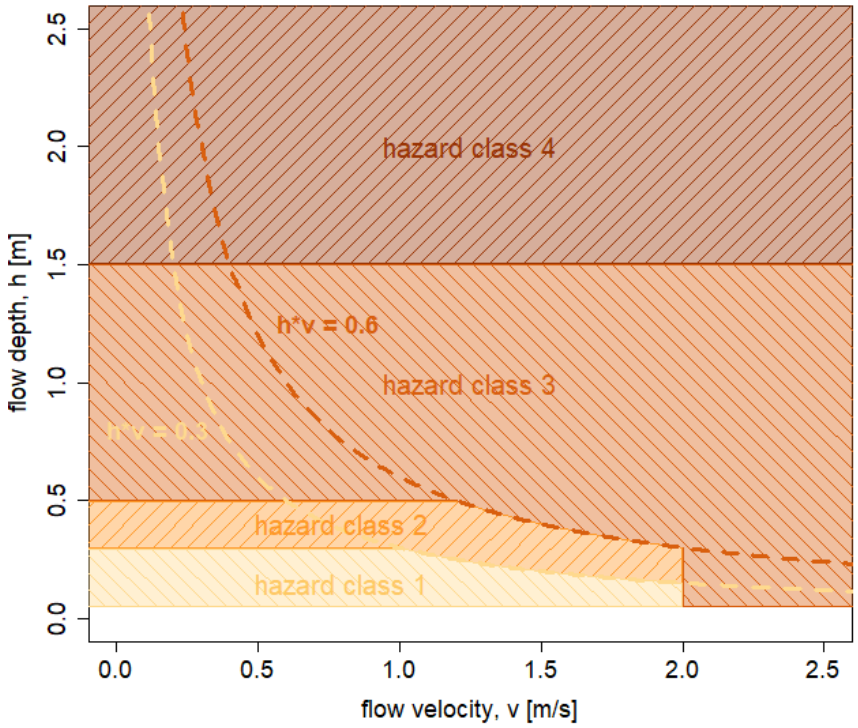

Fig. 3.2: Schematic of hazard classification as defined in Table 3.1

3.2.3 Implementation in early warning systems

The approach as one element of the modelling chain can be coupled to any hydrometeorological forecast. A transient modelling approach with the same spatiotemporal resolution as used to precalculate flood scenarios for the database is not suitable for early warnings, as the simulation time would exceed the lead time of the hydrometeorological forecast.

After the preprocessing described in the previous section, hazard information and the corresponding peak discharge is stored in a database for every mesh element, together with spatial information of exposure data (in our case a PostgreSQL database with a PostGIS extension). To improve performance, we preprocess a matching table of elements from the computational mesh and exposure data. With any given hydrological forecast, the corresponding peak discharges from the predicted hydrographs serve as basis to select the scenario calculated with the peak closest to the predicted peak. Technically,

this corresponds to a k-nearest neighbor analysis with k=1 based on Euclidean distance. After that, the matching table allows to join impact data to the flood surrogate model. This can then be visualized cartographically along with a quantitative summary of the impacts at a desired level of aggregation, even for the entire study area. This can all be achieved in just a matter of minutes. The high performance also allows, e. g., to consider multiple members of an ensemble or to implement a routine considering multiple hydrometeorological forecasts to account for uncertainties. E.g. by setting k=2, the precalculated scenarios with the next higher and lower peak discharges are considered.

In certain cases, a clear separation of rivers is not possible but still necessary, as it is for example the case near junctions, where floods from two joining rivers can affect the same floodplains. The setup of the flood surrogate model for this case is summarized schematically in Figure 3.3, showing that we define a subdomain as one river section with the corresponding floodplain. Here, the surrogate model combines the simulations of the three subdomains (two upstream, one downstream). Every subdomain requires a hydrograph from the hydrological model to select the scenario based on the correct peak discharge. Preparing thorough simulations for a surrogate model at junctions would require simulating multiple combinations of peak discharges in the two upstream rivers. If for example each of the three considered river sections consists of about 20 precalculated scenarios, this would end up in 400 (=20 $\times$ 20) instead of 60 simulations to consider all possible combinations of the two upstream subdomains, assuming that there is no or just minor additional discharge from any other source. To compare a surrogate with a transient model in such a region, the flood predictions of all subdomains (A, B and C in Figure 3.3) in a model region are merged. This means that multiple subdomains might be the source for flooded areas when their floodplains can't be separated topologically. In such cases, the highest magnitude is retained. In a model region with only one river section (= only one subdomain), the procedure is the same, but without the need to merge subdomains. Therefore, impact could directly be derived from "flood magnitude – flood loss" relationships as described in Zischg et al. (2018a). In terms of performance, there is no significant gain of time when doing so, as the join via matching table is already very performant and necessary anyway to provide flood maps. We will present and discuss our results based on the model regions.

3.2.4 Evaluation of the surrogate models

The simplified surrogate model is tested for replacing a time-consuming transient simulation model. This requires measuring the loss of information due to the approximation. For the evaluation of the library-based surrogate flood model, a set of extreme precipitation events is created from hindcast archives leading to floods over a large scale of hydrological Switzerland. After extracting these events from hindcast archives, transient simulations with the hydrological model DECIPHeR and the same hydrodynamic model used for preparing the flood simulation library are applied. For both modeling approaches, the flood impacts are calculated. The results serve as benchmark to measure the accuracy and computational performance of the surrogate flood model to represent the transient simulation.

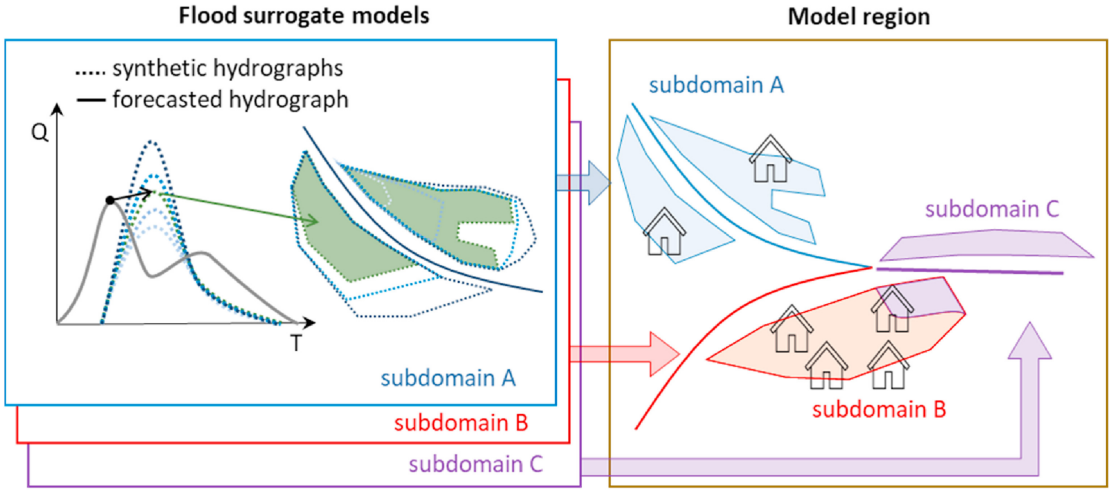

Fig. 3.3: Schematic illustration of the functionality of the flood surrogate model during a forecast, in this illustrated example, consisting of three subdomains A, B and C. Together, the subdomains are defined as one model region (coupled in transient model). Hazard and exposure data is stored on the same database. The spatial relation of every mesh element to the building footprint is preprocessed and stored as a matching table. Flow depth, velocity and the hazard class are stored for every element in an hourly resolution, specifically for each subdomain and each precalculated scenario (based on synthetic hydrographs, dotted lines in discharge (Q) - time (T) diagram). In case of a forecast (straight grey line in Q-T diagram), the scenario with nearest peak is selected (dotted green line and corresponding green area) and combined with exposure information via matching table. This serves as basis to calculate impact. In case of overlapping flood zones of subdomains (here: B + C), the maximum flow depth for each element is used (here: C, illustrated by the filled color)

3.2.4.1 Meteorology

To validate the surrogate modelling approach with precipitation events of high return periods that are hitherto not observed, we apply the reforecast pooling method (UNprecendented Simulated Extreme ENsemble, UNSEEN) as presented in Thompson et al. (2017); Kelder et al. (2020), using the hindcast archive of the European Centre for Medium-Range Weather Forecasts (ECMWF) extended-range forecasts ENSext as well as the seasonal forecasts SEAS5 (Johnson et al., 2019; Stockdale).

To arrive at the spatial and temporal scale of the hydrological model, we:

1. Downscale the hindcast data from a regular 0.4° grid to a spatial resolution of 2 km using quantile mapping (Ivanov & Kotlarski, 2017; CH2018, 2018),
2. and linearly disaggregate the resulting fields from 6-hourly to 1-hourly timesteps.

As reference data to downscale precipitation we use a merged data set consisting of CombiPrecip (Sideris et al., 2014) and Cosmo Rea2 spanning the period 2005–2017. For temperature and evapotranspiration, we use Cosmo Rea6 for the same period. The Cosmo Rea reanalyses (Wahl et al., 2017) include several products, amongst them Cosmo Rea2 and Cosmo Rea6. Both have a temporal resolution of 1 h but differ in the spatial resolution (approximately 2 km vs. 6 km) and period (Cosmo Rea 2 2007–2013 vs. Cosmo Rea6 1995–2017, see also Meteorological Institute of the United Nations (2015)).

To select individual spatially distinct precipitation events with a certain probability of

occurrence, we pool all precipitation events in the hindcast data: First, we compute the 6 hourly time series of running accumulation of area precipitation over the whole hydrological domain of Switzerland, defining this as the feature describing the precipitation events. The time series is then declustered in time such that the precipitation events (and the corresponding accumulation time windows) do not overlap. In order to estimate a return period for the events, we compile the discontinuous hindcasts into pseudo-years, pool both ENSext and SEAS5 together, and fit a GEV distribution (e.g., Coles, 2001) on the resulting yearly blockmaxima.

Finally, we select all events for accumulation periods of 3 and 5 days, which are usually leading to larger discharge peaks, and are the typical durations relevant for the generation of floods in small to mesoscale catchments or catchments with lakes, resulting in a total of 157 events. Each selected event contains nine 1-hourly extra time steps at its start and 10 1-hourly time steps at its end. Note that precipitation in the extra time steps is not considered for the extraction of the events based on the return periods.

3.2.4.2 Hydrological modelling

The hydrological model DECIPHeR is used to infer river discharge from precipitation, temperature and potential evapotranspiration information for the selected extreme weather events (Coxon et al., 2019). To meet the requirements of the complex mountain topography in Switzerland, modules for modelling snow and ice melt need to be added to the original code, similarly to Shannon et al. (2023). We implement a classical temperature-index (TI) melt model, which is solely based on air temperature and linearly relates melt rates to air temperature by a melt factor differing for snow and ice surfaces (Gabbi et al., 2014), where the threshold temperature distinguishing between melt and no melt accounts for the fact that melt is controlled by the energy budget at the surface and can also occur at air temperatures below and above the melting point of snow and ice (Gabbi et al., 2014; Kuhn, 1987). Additionally, routing and storage modules such as regulated lakes and reservoirs are introduced into the hydrological model.

We perform a split-sample calibration-validation for the hydrological model using data between 2005 and 2007 for the calibration and 2008 and 2010 for the validation (see goodness of fit measures in Appendix 3.B). In 2005 and 2007, two of the largest floods impacting a vast area of the Northern Swiss Alps took place, and as such represent a good calibration ground, the main aim of the tool being flood simulations. The period between 2008 and 2010 was chosen considering the inhomogeneity in CombiPrecip, for which in 2011, all three radars it is based on were replaced and the period from 2012 on seems to have a stronger tendency to underestimate precipitation, in particular in the first three years (Panziera et al., 2018). The "dry" biases are present already in the years used for calibration and validation, mainly in Autumn and Winter, when there are less convective storms and the visibility of the radars becomes a major limiting factor. The largest uncertainties are expected close to the national boundaries, where the number of precipitation gauging stations at the ground drops, and in the Eastern part of Switzerland, as well as the Rhone valley (Betschart).

The initial conditions for the hydrological simulations are created using observations from the CombiPrecip dataset of MeteoSwiss (Sideris et al., 2014; MeteoSwiss) with a two years model spin-up. All selected 157 extreme weather scenarios from the hindcast

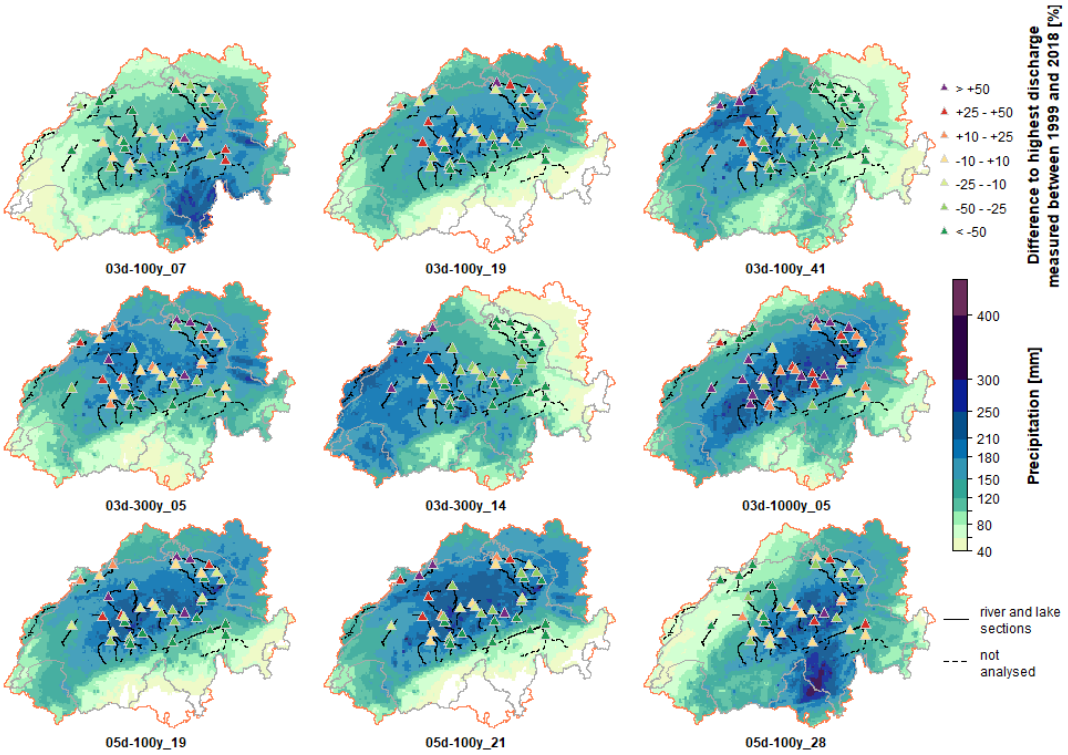

Fig. 3.4: Precipitation sums extracted with UNSEEN method (mm, color shading), together with deviation (%) of the modelled discharge from the highest discharge measured at gauging stations within the study area between 1999 and 2018. The orange outline defines the Swiss hydrological domain, the Swiss boundary is plotted in grey, scenario names are indicated below.

archive are inserted into the year 2010 (a year with average conditions) of CombiPrecip, considering the original season of the hindcast data: winter events (December to February) were inserted on 1 February 2010, spring events (March to May) on 5 April, summer events (June to August) on 15 July and autumn events on 1 November. After inserting the events, the hydrological model is run continuously until the end of the year, this way we ensure that delayed peaks of discharge or maximum levels of lakes reached after the duration of the extracted time window of the weather event are present in the hydrographs.

Finally, out of the 157 extreme precipitation events, nine are selected based on the location of the highest precipitation accumulations and on the temporal evolution of the precipitation events (events with one or two precipitation peaks during three or five days). We consider scenarios with precipitation maxima over western, central as well as eastern Northern Switzerland and scenarios with hotspots over alpine, prealpine and plateau regions. The scenarios cover different return periods, and we choose scenarios that lead to peak discharges exceeding the ones measured during any flood event along the river network (see Figure 3.4).

Note the naming of the scenarios (e. g. 03d-1000y_05) used in subsequent sections: The first part of the scenario name (05d, 03d) indicates the duration in days, the second part (100y, 300y, 1000y) the return period of the precipitation sum averaged over the

hydrological domain of Switzerland, the last part corresponds to the event number (no physical meaning).

3.2.4.3 Transient flood simulations and impact assessment

The simulations in both model setups (transient model/surrogate model) are based on the same irregular mesh with the same elevation information. Differences can be found in multi-domain regions, e. g. with junctions: the subdomains in the transient flood model are directly coupled (1D and 2D), an upstream boundary condition is only defined for the two upstream subdomains, whereas the discharge for the downstream subdomain is calculated hydraulically. There is no difference between the transient model and the surrogate model approach concerning impact assessment.

3.2.4.4 Validation with metrics

To analyze the potential of implementing the flood surrogate models into IBWs and IFs, we assume the nine weather scenarios together with hydrological, hydrodynamic and impact calculations derived with the transient model to be the observation and thus the benchmark against which the surrogate models are compared. This means that the hydrological output is used at the same time also as input to select the surrogates, being this the forecast the surrogate model has to operate with. Thus, we implicitly neglect the uncertainty present in the modeling steps before the application of the flood surrogate model, and only bring into focus the uncertainty in the latter.

For every river section, we extract the peak discharge from the hydrological model and compare the impact of the hindcast event with the outputs of the closest precomputed simulation.

To objectively assess the quality of the surrogate model, we use validation metrics from Bennett et al. (2013), e.g., the Critical Success Index (CSI), also used as Model Fit (F) in Zischg et al. (2018b) when applied for exposed buildings or as Flood Area Index (FAI) in Falter et al. (2013), where flooded area is of interest. In this study, we will use the term *"Model Fit"* independently, e.g., for flood area, flood volume, buildings, people, or workplaces:

$$ModelFit\ (F) = CSI = FAI = \frac{S1T1}{S1T1 + S1T0 + S0T1} \tag{3.1}$$

where *S1T1* denotes the agreement (hits) between transient model approach (T) and the surrogates (S), *S1T0* are, for example, areas defined as wet by the surrogate but dry by the transient model (false alarms) and *S0T1* vice versa (misses).

Additionally, we use the $BIAS$ score as indication whether the surrogate models over- or underestimate hazard and impact compared to the transient model. The $BIAS$ score is calculated as follows:

$$BIAS = \frac{S1T1 + S1T0}{S1T1 + S0T1} \tag{3.2}$$

A $BIAS$ score higher than 1 will therefore indicate an overestimation by the surrogate, whereas values below 1 indicate an underestimation.

3.3 Results

The results of our analysis are structured as follows. First, we compare all synthetic hydrographs from the surrogate models with the hydrographs from the transient simulations (section 3.3.1). After that, we compare the results from the flood simulation (section 3.3.2) followed by an analysis of the impact (section 3.3.3). We follow Zischg et al. (2018b) to define the goodness of fit of the surrogate models matching hazard and impact modelled with the transient approach. Finally, we also bring in the temporal aspect related to the propagation of the flood (section 3.3.4). The results rely on transient simulations done for 78 model regions. To cover all subdomains in these model regions, 1881 flood scenarios in 101 subdomains (= single river sections and its floodplain) had to be precalculated for the flood scenario database used by the surrogate model. With using two cores per simulation, 78 of 101 subdomains simulate with a real-time speed up (rts) of more or equal 10, 14 subdomains with an average rts between 3 and 10, eight subdomains with a rts between 1 and 3 and only one subdomain (lake Lucerne) with a rts below 1 (0.9). The simulations are executable via batch-process and are run in parallel computing on two 10-cores (20 threads) Intel Xeon E5-2660 v3 (2.6 GHz) processor units.

3.3.1 Hydrograph matching

The combination of 78 model regions with nine extreme weather scenarios (=702 transient model runs) results in a total of 310 floods. Figure 3.5 shows the relative difference of the peaks and volumes of the selected synthetic hydrographs and the hydrographs generated in the transient simulation model for all river reaches, excluding lakes and river sections with lake levels as upstream boundary. Here, the difference from the full model to the surrogate can maximally be 5 cm, as lake levels were simulated in 10 cm steps. For most river sections, the difference in peak discharge from synthetic to transient model hydrographs is about ± 5%. The discharge volume is systematically underestimated by synthetic hydrographs. Note that for the volume only timesteps above the minimum calculated peak in the flood library were accounted. According to FOEN (2023), this is the threshold where first river or lake floodings might occur.

Figure 3.6 illustrates one major source of underestimation: Whereas the (main) peak of the hydrograph after two days is well represented by the synthetic hydrograph, the flood relevant volume before two days is not covered. Flood volume driven differences between surrogate and transient model can therefore be expected mostly in floodplains where discharge capacity was exceeded already in the first phase of this event.

3.3.2 Prediction of flood hazard variables

In this section, we focus on the comparison in terms of hazard variables like flooded area, flow depth and flood volume in the floodplains of the model regions. To derive “overall” metrics, we aggregate *S1T0*, *S1T1* and *S0T1* over all model regions and scenarios, meaning that one region is considered multiple times when floods occurred in more than one scenario. We remind the reader that one region can consist of multiple river or lake sections (e.g., at river junctions), when a clear separation of floodplains was not

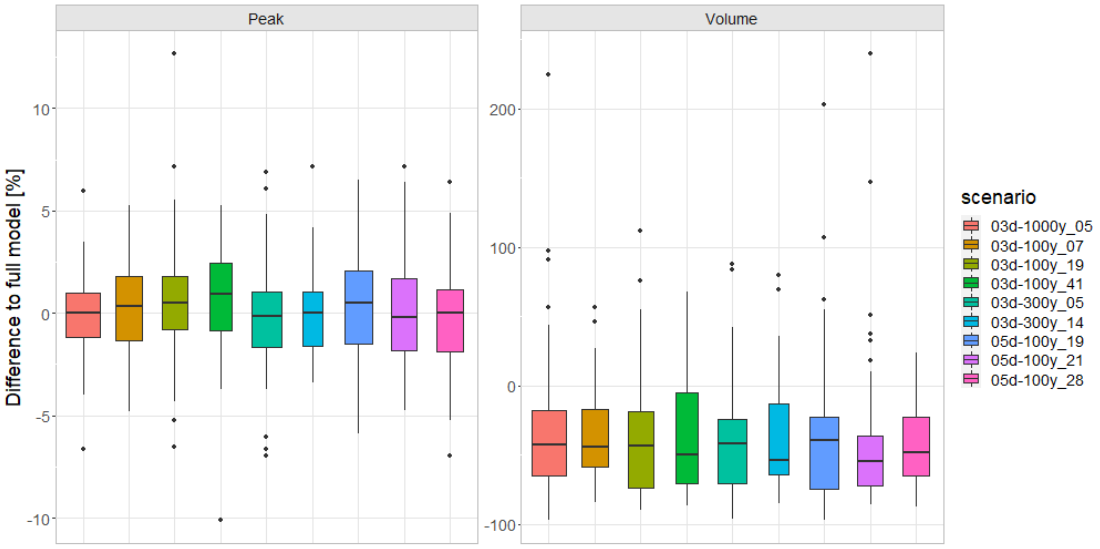

Fig. 3.5: Relative differences in hydrographs for 78 model sections in terms of peak discharge and discharge volume above the smallest simulated peak considered in the libraries. Lake hydrographs are excluded. For the naming of the scenarios, see the last paragraph in section 3.2.4.2

possible (described in section 3.2.2.2). The overall *Model Fit* in terms of flooded areas (*FAI*) for the entire river network is 0.84, the *BIAS* score of 1.014 indicates that over- and underestimation are balanced over the entire study area. As the overall metrics are dominated by model regions with extensive floods, Fig. 7 shows the distributions of calculated *Model Fits* and *BIAS*' for model regions grouped in 10%-quantile ranges of the flooded area in the transient simulation. The area of the river channel (1D model) was not considered to calculate the *Model Fits*.

Although the distributions among the quantiles are not significantly different from each other, there are certain tendencies that can be observed. On the one hand, the more pronounced low *Model Fits* in the first two quantile ranges (1: 0–10%, 2: 10–20%) and their higher variability in the *BIAS*' indicate higher uncertainties in regions where the flooded area is small. On the other hand, there is a slight negative but non-significant tendency in accuracy for the highest quantile range, with a median lower than 0.9 and an underestimation of the flooded area. Although a major part of the *Model Fits* being calculated per scenario and region is higher than calculated overall (0.84), it's mainly the upper two 10%-quantiles that influence this value sharing more than 84% of the total flooded area by the flood model. The regions with flooded areas in the lower five quantiles only share 2% of the total flooded area. Besides flood extent, the intensity of the flood influences the impact. Therefore, we compared calculated flow depths of the transient with the surrogate model based on 2.6 million mesh elements. Table 3.2 shows the quantiles of the flow depth differences calculated by the transient model to the matching simulations of the surrogate model. 80% of all elements show differences less than 20 cm (overall, Q10 – Q90), 5% of the elements show overestimation of more than 46 cm, 5% underestimate flow depth by at least 35 cm. Considering all elements (overall), the zero median together with similar positive and negative values for the quantile ranges (e. g. when comparing Q10 with Q90) indicates a low *BIAS*.

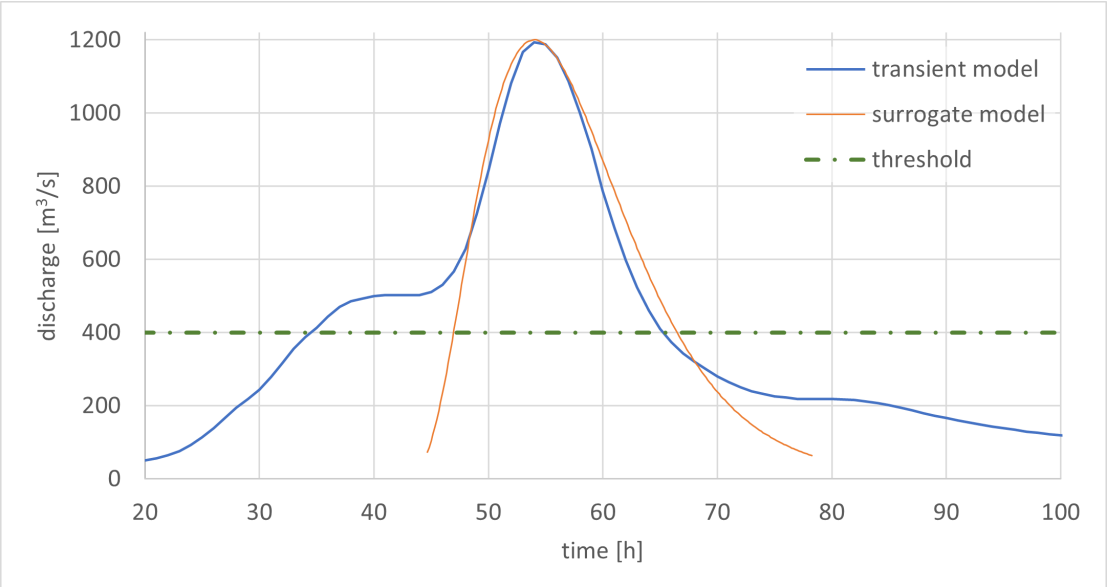

Fig. 3.6: Hydrographs of Emme river near Burgdorf, simulated by the hydrological model (blue, scenario 03d-1000y_05) and derived synthetically (see section 3.2.4.2) for the matching surrogate (orange), fitted by peak discharges. The lowest peak discharge calculated for the Emme river near Burgdorf is 400 m^3/s (=threshold). Even though the volume above this threshold is about 25% higher in the transient model due to the first phase of the event, the visual impression of the synthetic peak fitting the "main peak" of the full hydrograph is good.

Table 3.2: Quantiles of flow depth differences in meters (transient model – surrogate). Negative values indicate overestimation of flow depth by the surrogates, positive values an underestimation. *S1T1* = wet in surrogate and transient model, *S1T0* = wet in surrogate but dry in transient model, *S0T1* vice versa.

	Min	Q5	Q10	Q25	Q50	Q75	Q90	Q95	Max
S0T1	0.01	0.01	0.01	0.03	0.1	0.28	0.71	1.12	4.12
S1T0	-4.67	-1.06	-0.83	-0.52	-0.25	-0.08	-0.02	-0.01	-0.01
S1T1	-3.09	-0.29	-0.08	-0.01	0	0.04	0.15	0.3	2.79
Overall	-4.67	-0.46	-0.2	-0.03	0	0.04	0.17	0.35	4.12

Replacing flooded area with maximum flooded volume in the floodplain (area multiplied with flow depth in equation 3.1) results in slightly but significantly lower overall *Model Fits* (see Appendix 3.A). This can be considered as expected, as the influence of flow depth adds another level of complexity and uncertainty, although the differences in flow depths are not high for most of the elements. The overall *Model Fit* based on flood volume is 0.81, the *BIAS* score 1.000. Besides a generally lower *Model Fit*, there are similar findings as for the flood area.

3.3.3 Prediction of impact

Next, we evaluate the quality of the flood impact estimation by the flood surrogate model. First, we compare exposure of hospitals, schools and nursery homes. Then, we evaluate the simulated hazard classes (as defined in section 3.2.2.3) of the surrogate

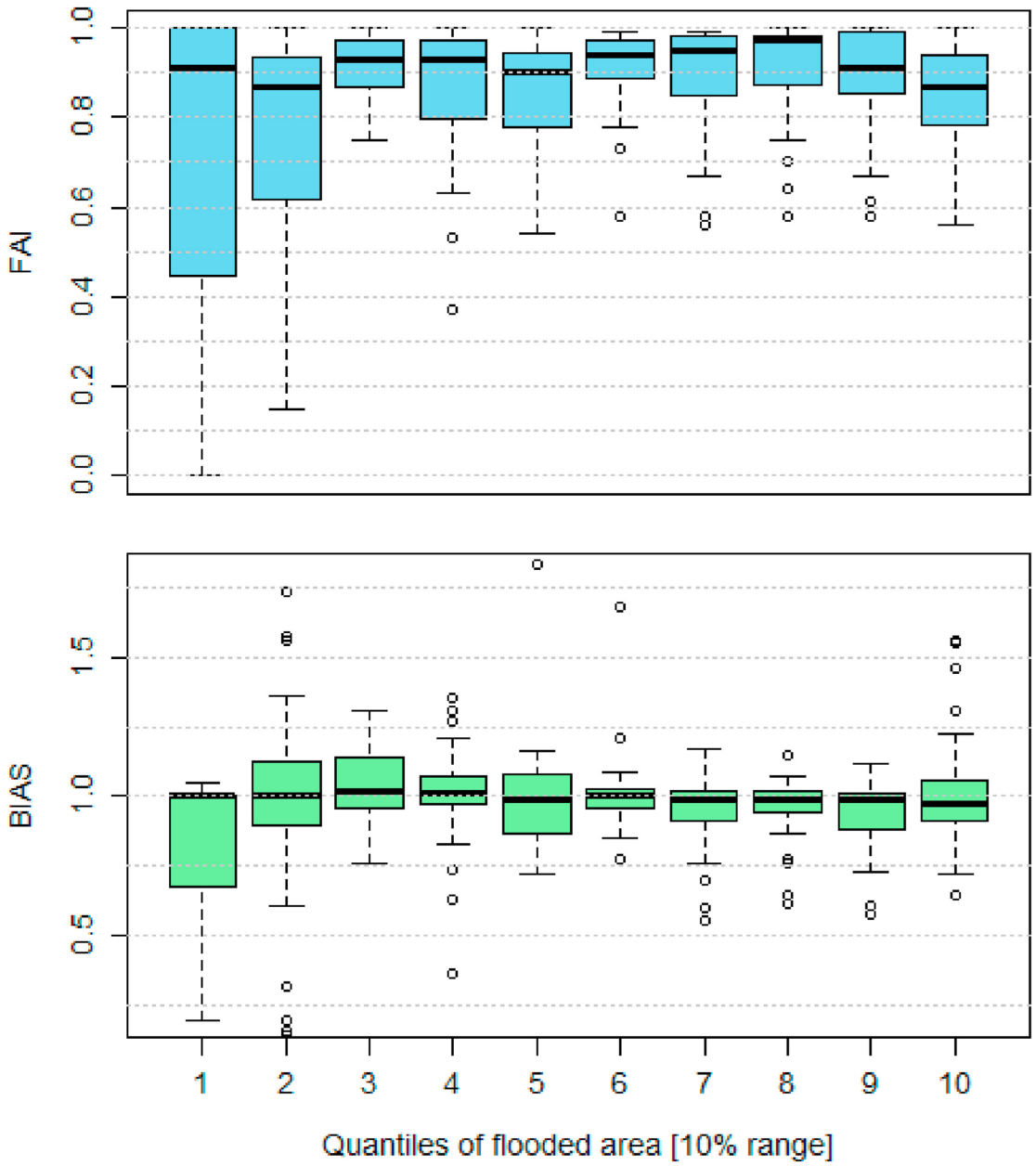

Fig. 3.7: *Flood Area Index* (top) and *BIAS* (bottom), the values used for the boxplots represent indices specific for a combination of model region and scenario (totally 310 floods). The boxplots show the distribution of the indices for each quantile range of flooded area. Depending on the flood area specific for scenarios, a model region can be represented in different quantiles. The 10%-quantile ranges contain regions with following flooded areas (in 10k m2 = hectares): Q1: 0–0.3; Q2: 0.3–1.2; Q3: 1.2–3.1; Q4: 3.1–6.4; Q5: 6.4–16; Q6: 16–33; Q7: 33–57; Q8: 57–87; Q9: 87–241; Q10: 241–2972.

models by comparing them with the hazard classes simulated by the transient model: We compare the hazard classification of area, buildings, persons and workplaces (Figure 3.8). Finally, we compare the flood damage estimation from the transient model and the surrogate approach.

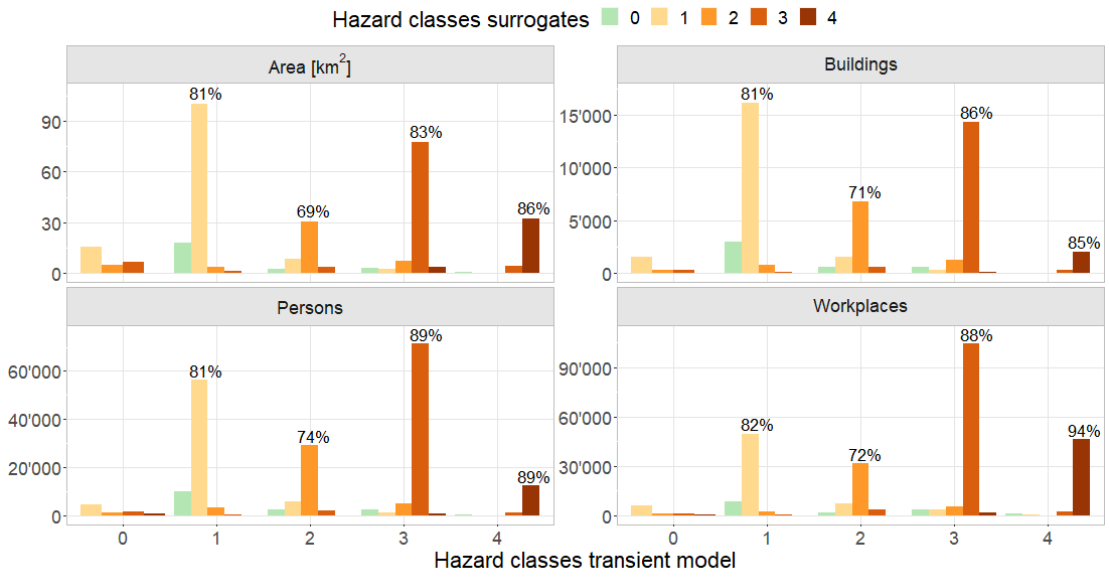

Fig. 3.8: Comparison of hazard classification of area (top left), number of buildings (top right), number of persons (bottom left) and number of workplaces (bottom right) by the transient model and surrogate model. The color of the bars indicates the classification given by the surrogates, the allocation at the x-axis the hazard class given by the transient model. The y-axis shows the numbers related to the title of each facet. The percentages on top of the bars indicate the fraction of the area, buildings, persons and workplaces classified by the transient model that is represented by the surrogates. Workplaces and Persons were allocated to buildings. Green bars represent the misses of the surrogates (*S0T1*), the bars located at the hazard class 0 of the transient model (left most category in each facet) represent false alarms (*S1T0*)

Over all scenarios and regions, 20 nursery home locations are modelled as exposed 62 times in the transient model, five are missed by the surrogate models without any false alarm. In the scenarios 03d-1000y_05 and 05d-100y_28, the model region of the river Muota near Brunnen contains 5 buildings within a hospital area being exposed in both models. In terms of buildings within school areas, 372 (153 unique buildings) are modelled as exposed by the transient model, whereof 49 were modelled as dry by the surrogates (misses). 15 buildings were modelled wet by the surrogate but dry by the transient model (false alarms).

The overall *Model Fits* calculated for buildings (0.88), persons (0.89) and workplaces (0.92) are considerably higher than these for area (0.84) and volume (0.81). This indicates that roughly nine out of 10 buildings, persons or workplaces receive a warning for potential exposure to a flood from the transient as well as from the surrogate model. When additionally penalizing wrong hazard classifications, the Model Fits are reduced to 0.74 for area, 0.78 for buildings, 0.8 for persons and 0.83 for workplaces. This means that e.g., eight out of 10 persons would receive the same warning of the severity of impact (one person out of 10 would be similarly informed about exposure, but different about the consequences). Note that the *Model Fits* for the hazard classes cannot exceed the "general" *Model Fits*. Figure 3.8 gives further details on the quality of hazard classification by the surrogate model.

We see that the second hazard class, showing areas/roads that are no longer passable

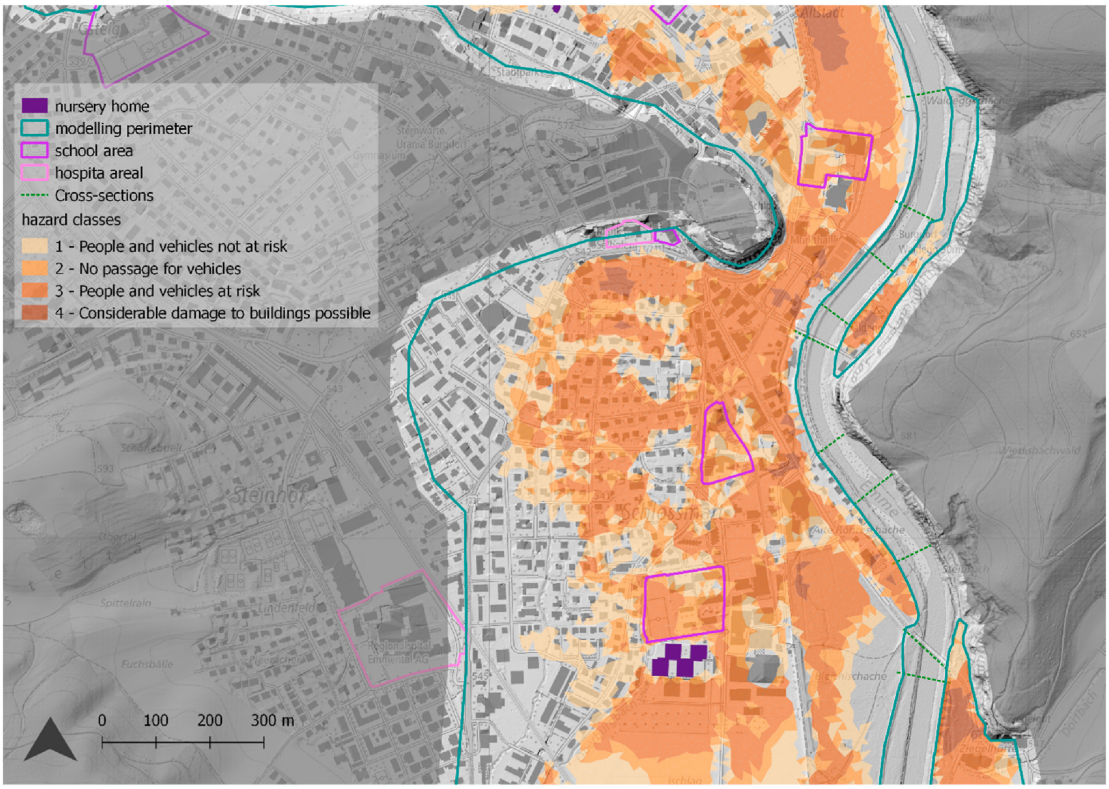

Fig. 3.9: Example of hazard map (from the surrogate model) of the Emme river near Burgdorf to support civil protection indicating predicted impact for people, vehicles and buildings and showing areas and buildings with vulnerable people (background Federal Office of Topography (2013, 2023))

by vehicles, is underrepresented compared to hazard classes 1 and 3. In this hazard class, only 69% of the area modelled by the transient model is also modelled as hazard class 2 by the surrogate model, what is considerably lower as found for class 1 (81%), 3 (83%) and 4 (86%). There are similar findings for buildings, workplaces, and persons. As hazard class 2 is defined for flow depths between 0.3 and 0.5 m and e.g., the *RMSE* of flow depth is 27 cm, the definition of class 2 is probably not suitable for the approach presented. Persons and workplaces have a higher relative exposure in hazard class 3 and 4 compared to area or buildings, these two classes are also better represented by the surrogates independent of the variable. Furthermore, the number of misses in exposure of buildings, persons, and workplaces (green bars) compared to the number of false alarms (colored bars at x = 0) is higher, indicating an underestimation *BIAS*. This is supported by the *BIAS*' in Appendix 3.C, showing that mainly the exposure in scenario 03d-300y_14 is underestimated.

We propose a visualization of the impacts on a map as shown in Figure 3.9. Together with a highly resolved map, information is given about accessibility of certain areas or buildings, regions where people potentially are endangered inside or outside a building and regions with potentially highly vulnerable buildings (school and hospital areas, nursery homes).

Finally, we compare damage estimates from both model set-ups. Table 3.3 gives an overview of the damages calculated using the transient and the surrogate model. In

Table 3.3: Comparison of scenario specific damage estimates based on the full model and surrogate model. For the naming of the scenarios, see the last paragraph in section 3.2.4.2.

Scenario	Damage transient model [CHF million]	Damage surrogate model [CHF million]	Difference [CHF million]	Difference [%]
03d-1000y_05	5460.11	5161.46	-298.65	-5.5
03d-100y_07	598.19	647.07	48.88	8.2
03d-100y_19	919.78	869.95	-49.83	-5.4
03d-100y_41	890.59	753.41	-137.18	-15.4
03d-300y_05	1738.74	1582.91	-155.84	-9
03d-300y_14	1176.06	856.72	-319.35	-27.2
05d-100y_19	1188.33	1098.44	-89.89	-7.6
05d-100y_21	1393.85	1358.49	-35.36	-2.5
05d-100y_28	1590.38	1583.04	-7.35	-0.5
Overall	14956.04	13911.49	-1044.55	-7

two scenarios, 03d-100y_41 and 03d-300y_14, the damage is underestimated by the surrogate model with -15.4% and -27.2%. On average the damage is underestimated by the surrogate approach by -7%. The section of the Emme River from Burgdorf to the junction with the Aare River contributes to this underestimation and is – same as the aggregated damage for each scenario – underestimated in most scenarios. The underestimation of damage in this region amounts to CHF -141 million (-76.1%) in scenario 03d-100y_41 and CHF -303 million (-55.3%) in scenario 03d-300y_14, explaining a major part of the total difference in damage.

As the Emme river floodplain is of major importance and systematically underestimates flood hazard and impact, we tried to assess the reasons:

1) In the first scenario mentioned above 03d-100y_41, one major retention area in the modelled region is not filled to its capacity in the surrogate model, whereas this is the case in the transient model. Therefore, even though the peak discharge is lower in the transient simulation, the outflow out of this retention area hits an industrial area with many large buildings with high values and therefore results in high damage. Something similar happens in scenario 05d-100y_21.

2) In scenario 03d-300y_14, the peak discharge of the transient model is almost in the middle between two synthetic hydrographs but matches best the one with a lower peak. However, the second-best surrogate with a higher peak discharge would lead to an overestimation of the flooded area and therefore most likely of the damage. It can also be observed in scenario 05d-100y_19, 03d-100y_19 (see Figure 3.10, left) and 03d-300y_05 that the impact assessed by the transient model is in between the best surrogate with a lower and the second-best with a higher peak.

3) Similarly, the reasons for the underestimation in scenario 03d-1000y_05 (-13.6% = CHF -223.5 million) might be the missing flood volume above the river capacity before the main event (see Figure 3.6) and the floodplain interactions over multiple subdomains that were modelled separately in the surrogate but together in the transient modelling approach. In general, a Mann-Whitney U test indicates that the Model Fits in regions with floodplains where floods can result from multiple rivers or lakes, and therefore interactions are possible, are significantly lower (median 0.86 compared to 0.94, no significant difference according to Kolmogorov-Smirnof test). In case of a river

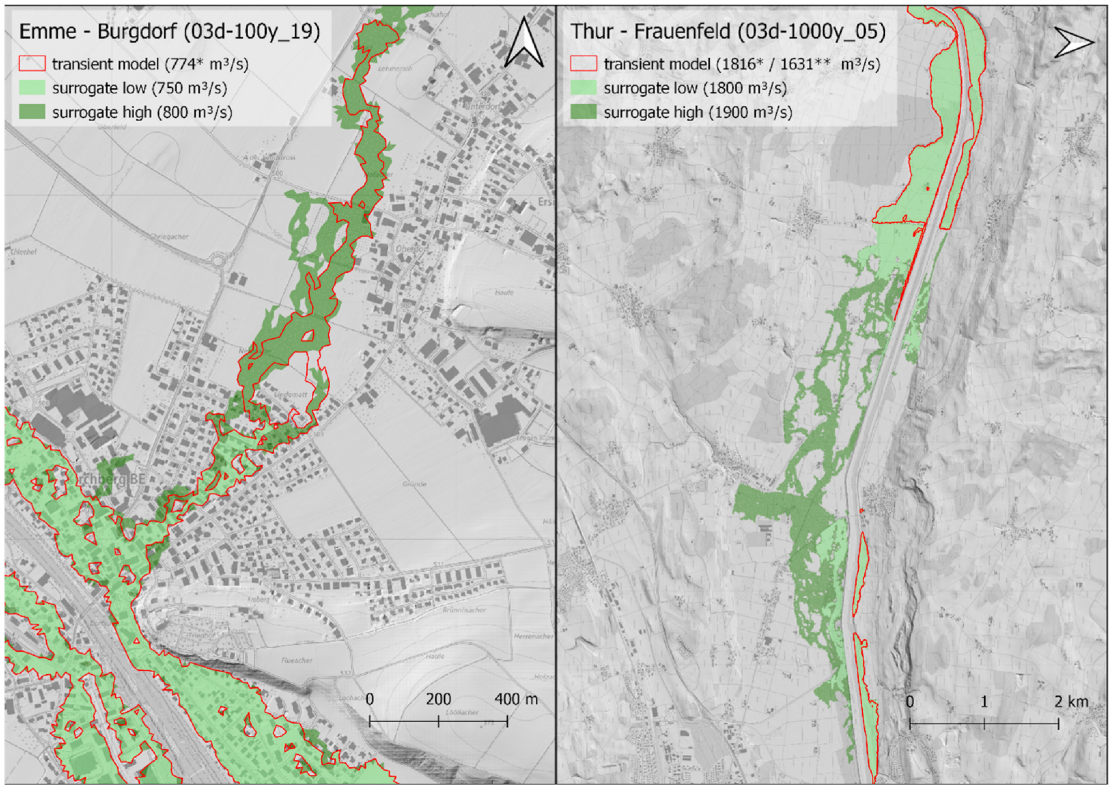

Fig. 3.10: Flood perimeters of the transient model simulation (red polygons) and the two nearest precalcuated scenarios according to peak discharge (light/dark green area). Left: one subdomain of Emme River near Burdgorf (N 47.05866°, E 7.61725°) showing that the surrogate with lower peak underestimates, and the surrogate with higher peak rather overestimates the transient simulation. Right: Downstream subdomain of the Thur River near Frauenfeld (N 47.55885°, E 8.90714°), showing that the surrogate with the higher and the lower peak overestimate the flood perimeter of the transient simulation, as peak attenuation in upstream subdomains and additional tributaries along the river reach of the Thur in this region is not considered. Note that the maps are drawn at different scales and the right map is rotated by 90°. * Discharge calculated by the hydrological model and used to select surrogate ** Hydraulically calculated peak discharge in transient model (lower due to peak attenuation in the upstream subdomain).

junction, the fitting of the scenario for the downstream river section is based on the hydrological output that is not considering peak attenuation. This effect is found in scenario 03d-1000y_05 in the model region enclosing Frauenfeld. In this region, the river Murg flows into the river Thur. The attenuation of the peak discharge in the upstream section of the Thur (from 1600 m^3/s to roughly 1300 m^3/s) is not modelled by the hydrological model and therefore also missing in the surrogate model, leading to an overestimation of the flood in the downstream section (see Figure 3.10, right). This is in agreement with Farrag et al. (2022); Viviroli et al. (2022) who state that retention/attenuation effects should be considered in the modelling chain.

The present analysis is conducted to determine the next-to closest fit (k=2) for the surrogate model. Out of the 310 model regions considered, 51 regions reach a superior *Model Fit* in terms of area (*FAI*). Among these regions, the increase ranges from 0.06 to 0.22 in 22 cases, and from 0.25 to 0.62 in five cases with rather low flooded areas (lower 20% of all simulations). Additionally, the transient model simulated a larger flooded area

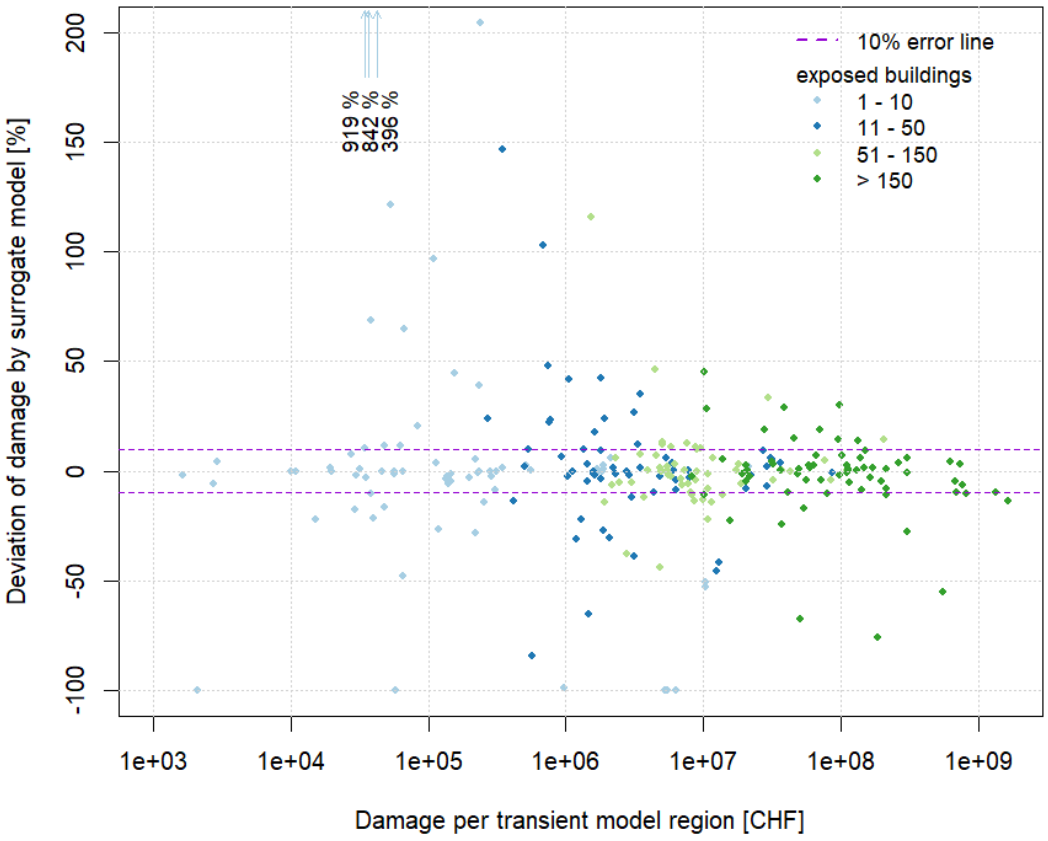

Fig. 3.11: Relative difference of damage between transient approach and approximation with surrogates. The dots represent one full model region.

compared to both nearest neighbors from the surrogate model in 46 out of the 310 cases, while in 18 cases it was smaller. This means that in 246 cases (79.4%), the two closest fits surrounding the peak magnitude are able to estimate the range of the potential flood extend. Specifically aggregated for each scenario, the *Model Fit* can only exceptionally be improved by choosing the next-to closest fits. Compared to the loss in certain cases (up to 0.29), the potential gain (up to 0.06) is small (see Appendix 3.6).

Figure 3.11 shows the relative differences of damage estimates between the transient model and the surrogate model, where every dot represents the damage of one model region in a specific scenario. Note that only in 259 combinations out of 310 flooded model regions (over all scenarios) buildings are exposed and therefore damage estimated. We see that high relative differences in losses occur in regions with low absolute damage. Additionally, we see that in regions with damages above CHF 10 million, there are five cases with positive or negative differences of more than 50% (- > two cases of Emme Burgdorf mentioned above), four model regions with differences from 30 to 50%, 21 regions with differences from 10 to 30% and 68 regions with a difference below 10%.

3.3.4 Temporal aspects

Besides the spatial evolution during an event, the chronology of a flooding is also important. For preparing evacuation measures, for example, the time lag of the peak flow of the predicted hydrograph in the river channel to the peak of flood intensity in the adjacent floodplains might be of interest. Therefore, in this section, we give insights into the ability of the surrogate approach in reproducing the maximum state of a flood event chronologically.

Figure 3.12 shows the expansion of the maximum state of the floods (maximum flow depth within simulation period) over time relative to the time of peak discharge in the modelled hydrographs of the transient model and the synthetic hydrographs of the surrogate model. We see that the evolution of the expansion curve is similar with both approaches, especially for areas that reach maximum state within the first 3h after the peak.

3.4 Discussion

Here we discuss the results presented in the previous section regarding the target user groups. Being aware of national/regional differences in the role certain user groups may play, we assume that the three selected are mostly similar for a large fraction of countries. As mentioned, we inferred the needs of the stakeholders from a close collaboration over recent years and emphasize that the definition of their profiles is not in the focus of this study. Nevertheless, we see it as crucial to consider the perspective of the stakeholder in the development of IBW and IF systems, as these systems aim to bridge the communication gap to the stakeholder by responding to their requirements and competences.

3.4.1 Flood event management of civil protection

Regarding the high responsibility attributed to civil protection (e.g., fire brigades or regionally operating crisis management staffs) during extreme flood events in Switzerland, an adequate warning of this type of stakeholder is of major importance. Warnings triggering wrong action, because, for example, uncertainties are not clearly communicated, might have a major influence in the success of impact mitigation of a flood. We showed that despite only matching peaks of predefined scenarios to hydrographs, surrogate models can represent high resolution transient models with a *Model Fit* of 0.84 for flooded area and 0.89 for exposed people. This means that the loss of information is relatively modest. Areas where rather high impact is expected (hazard classes 3 and 4), are represented accurately. This is important for civil protection to prioritize endangered regions in the planning of their actions. A visualization of the hazard zones and vulnerable regions on a map, e. g., as presented is crucial for civil protection. We recommend providing multiple maps showing a range of impacts. High computational efficiency was shown by extracting flood surrogate models and combining them with exposure data for impact analysis within minutes, supporting a high potential for an implementation into a warning system.

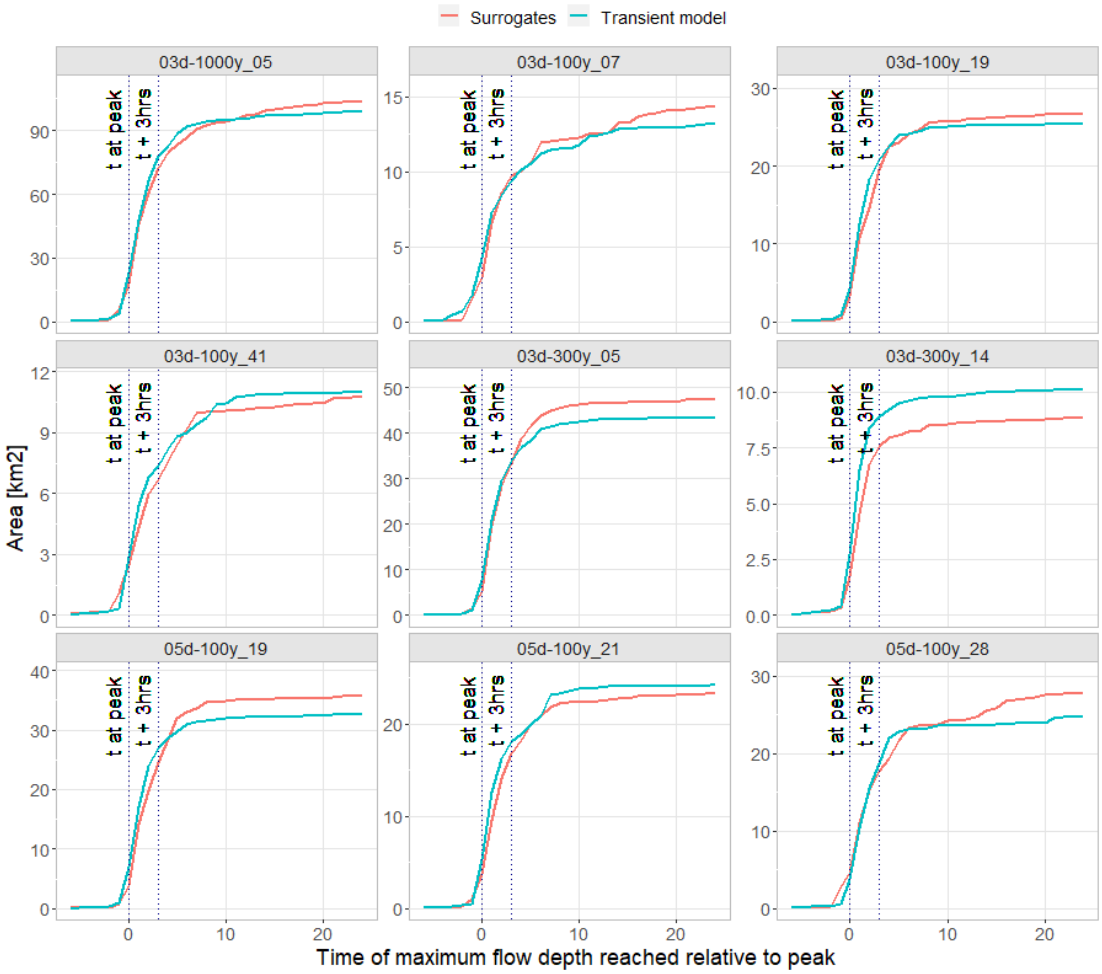

Fig. 3.12: Expansion of maximum state of floods over time across all modelled regions. The X-axis reflects the time difference (in hours) between the time of maximum flow depth at the element-location and the time when peak-discharge is reached in the river channel (time of maximum flow depth in floodplain minus time of peak-discharge in river channel). The Y-axis shows the flooded area in km2 reaching maximum state over the whole study region (note that this Y-axis is scaled differently for each scenario). For the naming of the scenarios, see the last paragraph in section 3.2.4.2. Note that t = 0 is set when the peak discharge is reached (=t at peak), t + 3hrs indicates expansion of the maximum flow depth 3 h after the peak discharge is reached.

We also showed that the surrogate model method even provides a good representation of temporal aspects when it comes to predicting the maximum intensity of an event reached in the first hours. As dikes are well represented in both flood models, it also gives a good overview of the sequence of river capacities overtopped along the river reach. We suggest that forwarding temporal information about such weak points should occur where high-resolution models considering geomorphic characteristics of the river channel and especially its dikes are available. As an alternative, the analysis of the expansion of the wet area instead of the maximum flow depth could be interesting as well. The issue with expansion of the wet area is how to consider events that overtop the river capacity with, e. g., two peaks or consisting of two or more phases with intense precipitation (as shown in Figure 3.6), where for certain areas the time of exposure to the time of maximum

state can be large, which is not covered by the synthetic hydrographs consisting of only one peak. To solve this problem if temporal evolution of wetted area is of interest, the fit of the surrogate should be done also to local maxima of the hydrograph, not only the overall peak.

The surrogate model approach being used to provide hazard maps meets the technical requirements for a web-based solution, but of course also for a locally running system. Storage of the surrogates on a database like PostgreSQL together with PostGIS extension also allows quick cartographical analysis of any precalculated scenario with a GIS.

3.4.2 Preparing insurance companies on cantonal to national scale

Part of flood mitigation is what comes after an event that caused a lot of damage – cleaning up and restore a similar state as before in a reasonable time, bringing back normal life. For this purpose, insurance companies liquidate money within a short time.

Comparing the transient model and the flood library approach, we saw that especially floodplains with low damage and therefore fewer exposed buildings show the highest relative differences, whereas small relative differences in floodplains with high damage can be very meaningful for the overall loss estimation. In seven out of nine scenarios, the overall relative difference was less than 10%. We recommend considering flood volume and/or the next-to-closest fitting surrogate(s) and thereby having a range of possible outcomes of a predicted scenario to account for uncertainties in terms of monetary damage. Based on a check of a sample of the simulated scenarios, we see that for a considerable fraction of the regions in this study, the damage estimated by the transient model between the two closest fits from the flood surrogate model. We also strongly suggest the application of a validated impact model for every region with different typology of cultural heritage and building characteristics (Zischg et al., 2021).

We emphasize that the definition of the model boundary, uncertainties of the underlying digital elevation model, the selection of the vulnerability function, the resolution of the computational mesh, and the specification of topographic breaklines might have an impact on the estimation on building level. Therefore, it is possible that with the method applied here, in certain cases with single or just a few buildings affected, depending on the flow depth at the building and the size of the footprint, a difference in the damage estimation can result.

3.4.3 Alerting private persons by warning services

If we look at the number of persons that a warning based on flood surrogate model compared to a transient model is issued, more than 187'500 would receive a warning in both cases, whereas 16'000 would not receive any warning, 8'000 people would be warned without being exposed to the flood. Although the numbers of misses and false alarms seem to be high in absolute terms, the *Model Fit* (0.89) putting them into perspective to the number of hits implies that the accuracy is still good.

The third hazard class represents flood intensities where people outside of buildings (as pedestrians or drivers of a car) are endangered, whereas the fourth hazard class identifies regions/buildings with such intensities that even high damage is expected and probably also a failure of building structures must be assumed to occur. We show that

85–89% of the buildings and persons that are classified with hazard level 3 or 4 by the transient model are attributed with the same hazard level by the surrogate.

These numbers indicate a potential for an implementation of behavioral recommendations in flood warnings. As this was not part of this study, this must be evaluated in further studies. We also highlight that there is a need for studies looking at consequences of false alarms and misses (relative to hits), trying to answer the question of what accuracy is acceptable or even perceived or reputed as good by society, such that there would be no discussions about missed responsibilities (rather in case of missed warnings) and the reliability of warnings would remain high (despite false alarms). Or in other words: how can people be sensitized for uncertainties in modelled forecasts of impacts.

3.4.4 Limitations, transferability and outlook

In this section, we discuss the limitations of our study, as well as the transferability of our findings to other locations, and provide an outlook for future research. We focus on the results derived by the hydrodynamic (surrogate) flood models.

3.4.4.1 Limitations

As stated in section 3.2.2.2, the possibilities to calibrate and validate the hydrodynamic model are limited: The topography from the time of the last large-scale floods in 2005 and 2007, the most recent relevant events for this purpose, is not reflected in our data, as protective measures were implemented on almost all affected rivers between the floods and the measurements for the cross-profiles and digital elevation models. Nevertheless, we checked the plausibility by comparing the model outcomes of all model regions with the official hazard maps and with technical reports on river hydraulics. Zischg et al. (2018b) show that even uncalibrated hydrodynamic models can reach good validation metrics if the river morphology is well represented in the hydraulic models. To some extent, we see our results as not fully dependent on the model validity, as we focus only on the loss of information when replacing a transient model with a surrogate model. The fact that a surrogate flood model better represents a transient model that was calibrated/validated must be further investigated.

Besides this, there are some technical limitations of the flood model in the study presented. 1) Bridges crossing the rivers of the 1D flood model are not considered hydraulically. At locations where they are limiting the river capacity, significant differences to a potential real event might occur. 2) Besides this, we see missing culverts in the 2D flood model as the most important lacking structures, making the surrogate model as presented a prototype rather than a “ready-to-use” model. By considering these two points, it could serve as supporting tool to test impact-based warning systems. In that regard, we also want to stress that the role of log jam of culverts and collapse of bridges in extreme events as modelled in this study is not clear. 3) The cross-profiles of the rivers are measured approximately every 100m, meaning that sills/small weirs are often not directly considered, resulting in steeper slopes of the riverbed for certain short river sections than it is the case in reality. 4) The 1D model does not consider superelevation occurring, for example, in river bends. In a right turn for example, the water surface elevation at the left embankment might be underestimated by our models

and underestimated at the right embankment. 5) Morphological changes of the river channel due to erosion and sedimentation are neglected. These processes are very likely during extreme events and alter the conveyance capacity.

3.4.4.2 Transferability

The elements of the model chain used to make transient simulations are replaceable by any other method. Our hindcast events can be replaced by any other measurements or forecast meeting the requirements of the successive hydrological model, which is replaceable itself. The coupled 1D-2D hydraulic model can be exchanged with any other hydraulic model.The advantage of the 1D-2D coupled flood model from BASEMENT is that a major part of the preprocessing steps can be automated just based on cross-section point data, 2D model perimeters, breaklines defining relevant hydraulic structures like dams in the floodplain and lines defining the coupling interface of the 1D and 2D model. In addition, the model runs can be initiated via batch process and allow for parallel computing. The framework of the surrogate flood model is transferable to any location where appropriate data is available.

3.4.4.3 Outlook

Besides overcoming the major limitations mentioned above by including bridges and culverts into the hydrodynamic model, solving the systematic underestimation of the flood volume is required to transfer the prototype to operationalization. Besides the issue that a hydrograph with multiple peaks cannot be mapped by synthetic hydrographs with one peak, and the issue of general differences between volume in synthetic and modelled/forecasted hydrographs based on meteorological data, there is another reason for the underestimation of the volume. The simulation time during the recession phase of the hydrograph determines the flooded area. In diffluent, large floodplains (e. g., Burgdorf) the flood water is covering a larger area the longer the simulation time is. The statistical background of the methodology used to create synthetic hydrographs allows to create alternative scenarios with more/less flood volume with the same peak discharge. Hence, alternative flood peak-flood volume relationships should be implemented in the precalculated scenarios. To solve the volume issues, machine learning techniques as presented by Bentivoglio et al. (2022) could improve the quality of the surrogate model, and probably reduce over- and underestimation issues. Simulations as used in our study could serve as basis to train such a model that might especially be beneficial in model regions with large floodplains, where the preprocessing of scenarios with different flood volumes is costly. Nevertheless, existing studies on local and regional level show issues in generalizing ML-based flood models across different case studies and regions (Bentivoglio et al., 2022).

Due to the good performance of the surrogate model approach, we also see the potential that hydrometeorological uncertainties might be considered by either analyzing multiple members or the range of peaks from the ensemble. Alternatively, increasing k in the k-nearest neighbor analysis could also be used to account for such uncertainties. Here, k could be chosen by the difference of peak discharge from one precalculated scenario to another together with the width of the uncertainty band of a hydrological forecast. Our

analyses based on the next-to closest fit shows that the nearest neighbor is generally the better choice, but its consideration can also be beneficial in certain cases. Similar to the volume issue mentioned above, machine learning approaches could help to interpolate between hydrodynamic simulations.

Finally, the issue discussed with the example of the Thur River near Frauenfeld could also be solved by the surrogate model itself: The attenuation effect along a river could be derived in the preprocessing step by documenting the attenuation effect. Additional to the input peak discharge of a synthetic hydrograph, the output peak discharge at the downstream boundary could be measured and entered into the database as well. By applying the surrogate in a downstream direction, the attenuation of the upstream model region could be transmitted to subsequent river reaches and the forecast of the hydrological model could be reduced accordingly.

3.5 Conclusions

The aim of this study was to evaluate whether computationally fast flood surrogate models can replace computationally heavy transient high-resolution models for near real-time warning applications. For this we compared damage simulations run with flood surrogate models with transient high-resolution models for nine extreme weather scenarios in the north alpine part of Switzerland. We evaluated the following variables: flooded area, flood volume, number of exposed buildings, persons, and workplaces.

Over all scenarios and 78 model regions, the *Model Fits* range from 0.81 (flood volume) to 0.92 (workplaces). The surrogates underestimate monetary damage on average by 7%, showing the potential to warn e. g., (re-) insurance companies of losses.

Flood surrogate models can support intervention forces during an event: 89% of exposed persons in the transient model are similarly classified by the surrogate model. There is also a satisfying representation of the temporal evolution of the maximum flow depth by the surrogates. Hazard maps derived from the surrogates indicate regions where people might be exposed to a high risk of life. By using the surrogate model approach, multiple scenarios can be efficiently analyzed (and mapped) to account for uncertainties.

However, we compare two models at magnitudes where very limited observational validation is possible. We used synthetic hydrographs with single peaks to create scenarios for the flood surrogate models. If the discharge volume above river capacity substantially differs from a forecasted hydrograph, the expansion of floods in diffluent floodplains or the magnitude reached in retention areas in the surrogate should be considered with caution.

Nevertheless, we conclude that flood surrogate models is a valid method to be considered for an application in IBW- and IF-systems, as it optimizes the trade-off between high spatial resolution and computational efficiency: The spatial resolution of the transient model is preserved in the surrogate models and the precalculated flood scenarios, together with exposure data, can be derived, processed and aggregated to stakeholder specific needs for multiple scenarios quasi real-time.

Software & data availability

The transient simulations can be viewed and interactively queried at `https://flooddynamics.floodrisk.ch`. The original source code of hydrological model "DECIPHeR Dynamic fluxEs and ConnectIvity for Predictions of HydRology" is freely available at `https://github.com/uob-hydrology/DECIPHeR`; the code version applied in this study is available upon request (please contact M. Kauzlaric by writing to martina.kauzlaric@unibe.ch). The hydrodynamic model BASEMENT-ETHZ is available at `https://basement.ethz.ch/`. The exposure data can be viewed in an aggregated form at `https://schadenpotenzial.hochwasserrisiko.ch`. We used a PostgreSQL-database (`https://www.postgresql.org/`, v. 10.17) with PostGIS extension (`https://postgis.net/`, v. 2.4.4) together with the free software environment of R (`https://www.r-project.org/`) for accessing and storing data. We do not provide the data used for the flood surrogate model as it is stored on a complex relational database. Due to confidential reasons, we're not allowed to share data of persons and workplaces. The building footprints used in this study can be accessed via the website of the Federal Office of Topography swisstopo (SwissTLM3D, `https://www.swisstopo.admin.ch/en/geodata/landscape/tlm3d.html`, v. 1.9)

CRediT authorship contribution statement

Markus Mosimann: Conceptualization, Data curation, Formal analysis, Methodology, Software, Validation, Visualization, Writing – original draft, Writing – review & editing. **Martina Kauzlaric**: Data curation, Formal analysis, Methodology, Validation, Writing – original draft, Writing – review & editing. **Simon Schick**: Data curation, Formal analysis, Methodology, Validation, Writing – original draft, Writing – review & editing. **Olivia Martius**: Project administration, Supervision, Writing – original draft, Writing – review & editing. **Andreas Paul Zischg**: Conceptualization, Methodology, Project administration, Supervision, Writing – original draft, Writing – review & editing.

Declaration of competing interest

The authors declare that they have no known competing financial interests or personal relationships that could have appeared to influence the work reported in this paper.

Data availability

I have shared the information about data and software availability in the manuscript

Appendix

3.A Densities of Model Fits for area (top) and volume (bottom) per region

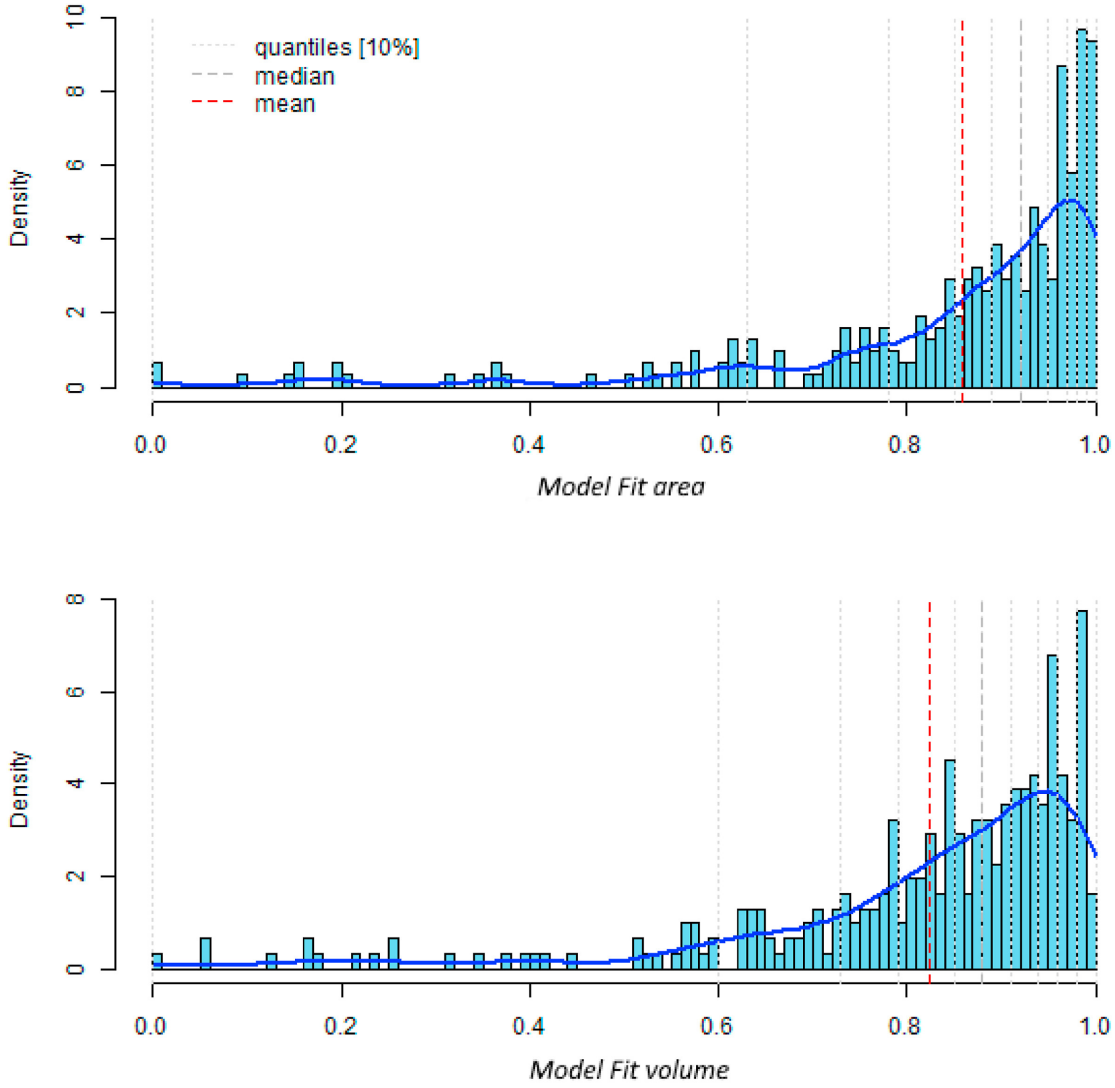

Fig. 3.13: Density distribution of Model Fits for area (top) and volume (bottom) for all regions and scenarios. 10% quantile locations are indicated by the dotted grey lines, the dashed grey line indicates the location of the median (area: 0.92, volume: 0.88), the red line shows the location of the mean (area: 0.86, volume: 0.82).

3.B Goodness of fit for calibration and validation of the hydrological model

Table 3.4: Goodness of fit for calibration and validation of the hydrological model. Hydrological measurements are provided by the Federal Office for the Environment

		cal 2005-2007					val 2008-2010				
River	Location	NSE	KGE2009	PBIAS	biasSFMS	biasFDChigh	NSE	KGE2009	PBIAS	biasSFMS	biasFDChigh
Rhein	Domat/Ems	0.058	0.486	-33.955	-0.280	-0.222	0.247	0.522	-41.431	-0.248	-0.260
Aare	Thun	0.862	0.909	-3.132	-0.013	0.044	0.795	0.877	-7.421	0.011	-0.005
Reuss	Luzern	0.903	0.948	-1.652	-0.044	0.013	0.890	0.942	0.041	0.034	0.017
Thur	Andelfinden	0.751	0.861	2.305	-0.021	-0.022	0.665	0.818	8.144	-0.040	0.018
Linth	Weesen	0.803	0.866	-8.942	-0.014	-0.046	0.888	0.875	0.304	0.076	0.063
Emme	Wiler	0.665	0.727	21.058	0.107	0.184	0.522	0.712	10.794	0.169	0.035
Birs	Muenchenstein	0.733	0.848	7.571	-0.014	0.021	0.434	0.675	0.166	-0.160	-0.111
Kleine Emme	Emmen	0.786	0.858	8.707	0.023	0.048	0.688	0.783	14.841	0.288	0.127
Wigger	Zofingen	0.523	0.585	37.535	0.308	0.246	0.382	0.619	29.868	0.027	0.109
Toess	Neftenbach	0.672	0.827	6.363	0.003	0.058	0.674	0.784	0.739	-0.087	-0.067
Doubs	Ocourt	0.376	0.616	-18.945	-0.147	-0.125	0.028	0.456	-25.189	-0.330	-0.187
Broye	Vully-les-Lacs	0.545	0.704	-10.730	-0.110	-0.162	0.388	0.345	-30.798	-0.329	-0.393

3.C Signals and calculated metrics per scenario

Table 3.5: Signals and calculated metrics per scenario and exposure variable. *BIAS* and *Model Fit* are both optimized at 1 (highlighted with green color).

		03d-1000y_05	03d-100y_07	03d-100y_19	03d-100y_41	03d-300y_05	03d-300y_14	05d-100y_19	05d-100y_21	05d-100y_28	OVERALL
Hits	*Area [km^2]*	98.514	13.539	22.337	10.456	41.77	8.749	30.217	22.484	26.52	**274.586**
	Volume [mio m^3]	62.329	7.742	16.557	6.447	27.53	6.585	20.568	13.505	15.128	**176.391**
	Buildings	17'413	2'117	2'705	2'281	5'223	1'952	3'728	3'995	4'926	**44'340**
	Persons	74'831	8'553	10'682	9'891	20'742	9'420	14'292	16'567	23'861	**188'839**
	Employees	93'617	21'206	8'880	14'961	29'347	8'689	12'698	22'086	46'367	**257'851**
False Alarms	*Area [km^2]*	6.184	1.094	4.425	0.326	6.644	0.111	5.727	0.815	2.27	**27.596**
	Volume [mio m^3]	3.566	0.978	3.127	0.243	5.202	0.263	4.051	1.204	1.907	**20.541**
	Buildings	862	185	115	136	201	24	129	109	238	**1'999**
	Persons	3'022	1'885	247	511	355	58	132	473	911	**7'594**
	Employees	2'268	1'135	696	1'126	232	437	573	284	1'285	**8'036**
Misses	*Area [km^2]*	5.956	1.039	3.464	0.81	3.294	1.688	3.557	2.171	1.546	**23.525**
	Volume [mio m^3]	7.08	0.657	2.374	0.502	3.387	0.576	2.884	1.627	1.51	**20.597**
	Buildings	1'061	54	360	163	604	742	707	254	262	**4'207**
	Persons	3'617	60	1'480	179	2'721	2'763	2'730	898	735	**15'183**
	Employees	4'265	96	927	919	3'976	1'615	1'473	436	565	**14'272**
FAI	*Area*	0.89	0.86	0.74	0.90	0.81	0.83	0.76	0.88	0.87	**0.84**
	Volume	0.85	0.83	0.75	0.90	0.76	0.89	0.75	0.83	0.82	**0.81**
	Buildings	0.90	0.90	0.85	0.88	0.87	0.72	0.82	0.92	0.91	**0.88**
	Persons	0.92	0.81	0.86	0.93	0.87	0.77	0.83	0.92	0.94	**0.89**
	Employees	0.93	0.95	0.85	0.88	0.87	0.81	0.86	0.97	0.96	**0.92**
BIAS	*Area*	1.002	1.004	1.037	0.957	1.074	0.849	1.064	0.945	1.026	**1.014**
	Volume	0.949	1.038	1.040	0.963	1.059	0.956	1.050	0.972	1.024	**1.000**
	Buildings	0.989	1.060	0.920	0.989	0.931	0.733	0.870	0.966	0.995	**0.955**
	Persons	0.992	1.212	0.899	1.033	0.899	0.778	0.847	0.976	1.007	**0.963**
	Employees	0.980	1.049	0.976	1.013	0.888	0.886	0.936	0.993	1.015	**0.977**

3.D Scenario specific differences in Model Fits between the two nearest neighbors

Table 3.6: Difference between scenario-specific Model Fits when using the nearest neighbor (k = 1) and the next-to closest fit (k = 2). Differences are calculated by subtracting the Model Fits based on k = 1 from the Model Fits based on k = 2. Hence, negative (blueish) values indicate that the nearest neighbor better represents the transient flood simulation than the next-to closest fit, positive (reddish) values show that for the specific scenario, the selection of the next-to closest fit would have been the better choice.

	DELTA *Model Fit* (*Model Fit* K2 - *Model Fit* K1)			
Scenario	Area	Buildings	Persons	Workplaces
03d-1000y_05	-0.03	-0.01	-0.01	-0.01
03d-100y_07	-0.05	-0.09	0.02	-0.11
03d-100y_19	0.05	-0.04	-0.03	-0.19
03d-100y_41	-0.07	-0.08	-0.12	-0.03
03d-300y_05	-0.05	-0.03	-0.02	0.03
03d-300y_14	-0.02	0.06	0.04	-0.01
05d-100y_19	-0.05	-0.03	-0.04	-0.17
05d-100y_21	-0.10	-0.08	-0.08	-0.28
05d-100y_28	0.01	-0.03	-0.05	-0.04

References

Aldridge, T., Gunawan, O., Moore, R. J., Cole, S. J., Boyce, G., & Cowling, R. (2020). Developing an impact library for forecasting surface water flood risk. *Journal of Flood Risk Management*, *13*. doi:10.1111/jfr3.12641.

Alfieri, L., Feyen, L., Salamon, P., Thielen, J., Bianchi, A., Dottori, F., & Burek, P. (2016). Modelling the socio-economic impact of river floods in europe. *Natural Hazards and Earth System Science*, *16*, 1401–1411. doi:10.5194/nhess-16-1401-2016.

Apel, H., Vorogushyn, S., & Merz, B. (2022). Brief communication: Impact forecasting could substantially improve the emergency management of deadly floods: case study july 2021 floods in germany. *Natural Hazards and Earth System Science*, *22*, 3005–3014. doi:10.5194/nhess-22-3005-2022.

Arrighi, C., Pregnolato, M., Dawson, R. J., & Castelli, F. (2019). Preparedness against mobility disruption by floods. *The Science of the total environment*, *654*, 1010–1022. doi:10.1016/j.scitotenv.2018.11.191.

Bennett, N. D., Croke, B. F., Guariso, G., Guillaume, J. H., Hamilton, S. H., Jakeman, A. J., Marsili-Libelli, S., Newham, L. T., Norton, J. P., Perrin, C., Pierce, S. A., Robson, B., Seppelt, R., Voinov, A. A., Fath, B. D., & Andreassian, V. (2013). Characterising performance of environmental models. *Environmental Modelling & Software*, *40*, 1–20. doi:10.1016/j.envsoft.2012.09.011.

Bentivoglio, R., Isufi, E., Jonkman, S. N., & Taormina, R. (2022). *Deep Learning Methods for Flood Mapping: A Review of Existing Applications and Future Research Directions*. doi:10.5194/hess-2022-83.

Bermúdez, M., Ntegeka, V., Wolfs, V., & Willems, P. (2018). Development and comparison of two fast surrogate models for urban pluvial flood simulations. *Water Resources Management*, *32*, 2801–2815. doi:10.1007/s11269-018-1959-8.

Betschart, M. (). A study of convective events in switzerland with radar and a high-resolution nwp mode. URL: https://www.meteoswiss.admin.ch/services-and-publications/publications/scientific-publications/2012/a-study-of-convective-events-in-switzerland-with-radar-and-a-high-resolution-nwp-model.html.

Canton of Aargau (2014). DTM 0.5-Meter Raster. Canton of Aargau, Abteilung Wald. URL: https://www.geocat.ch/geonetwork/srv/api/records/e8f0247a-f139-4535-97f6-0d4b6cad302f-6571?language=all. Last accessed: 04.04.2024.

Canton of Bern (2014). Digitales Terrainmodell LIDAR 50cm. Canton of Bern, Amt für Wald KAWA. URL: https://www.agi.dij.be.ch/de/start/geoportal/geodaten/detail.html?type=geoproduct&code=LDTM50CM. Last accessed: 04.04.2024.

Canton of Lucerne (2012). Digitales Terrainmodell (DTM) 2012, 0.5m-Raster. Canton of Lucern, Dienststelle Raum und Wirtschaft, Abteilung Geoinformation. URL: https://daten.geo.lu.ch/produkt/dtm1205m_ds_v1. Last accessed: 04.04.2024.

Canton of Solothurn (2014). Digitales Terrainmodell (DTM) 2014. Canton of Solothurn, Amt für Geoinformation. URL: https://data.geo.so.ch/?filter=ch.so.agi.lidar_2014.dtm. Last accessed: 04.04.2024.

Canton of Vaud (2004). Modèles altimétriques lidar. Canton of Vaud. URL: https://www.vd.ch/themes/territoire-et-construction/cadastre-et-geoinformation/geodonnees/altimetrie-lidar/technologie-lidar/lidar-2001-2006. Last accessed: 04.04.2024.

Canton of Zug (2013). Höhenmodell der amtlichen Vermessung 2013 auf Basis "LIDAR". Canton of Zug, Amt für Grundbuch und Geoinformation, Abteilung Vermessung. URL: https://zg.ch/de/planen-bauen/geoinformation/amtliche-vermessung. Last accessed: 04.04.2024.

Canton of Zurich (2014). Digitales Terrainmodell (DTM) - 2014. Canton of Zurich, Amt für Raumentwicklung - Geoinformation. URL: https://www.stadt-zuerich.ch/geodaten/download/298. Last accessed: 04.04.2024.

Casteel, M. A. (2016). Communicating increased risk: An empirical investigation of the national weather service's impact-based warnings. *Weather, Climate, and Society*, *8*, 219–232. doi:10.1175/WCAS-D-15-0044.1.

Casteel, M. A. (2018). An empirical assessment of impact based tornado warnings on shelter in place decisions. *International Journal of Disaster Risk Reduction*, *30*, 25–33. doi:10.1016/j.ijdrr.2018.01.036.

CH2018 (2018). Ch2018 - climate scenarios for switzerland, technical report. National Centre for Climate Services. URL: https://www.nccs.admin.ch/nccs/en/home/data-and-media-library/data/ch2018---climate-scenarios-for-switzerland.html.

Coles, S. (2001). *An Introduction to Statistical Modeling of Extreme Values*. London: Springer London. doi:10.1007/978-1-4471-3675-0.

Costabile, P., Costanzo, C., de Lorenzo, G., de Santis, R., Penna, N., & Macchione, F. (2021). Terrestrial and airborne laser scanning and 2-d modelling for 3-d flood hazard maps in urban areas: new opportunities and perspectives. *Environmental Modelling & Software*, *135*, 104889. doi:10.1016/j.envsoft.2020.104889.

Cox, T., Hampson, R., Hooper, R., Hunter, N., Porter, I.-H., Revilla-Romero, B., Stroud, R., & Wylde, R. (). Real-time flood impacts mapping: Technical report. Environment Agency. URL: https://assets.publishing.service.gov.uk/media/6037956ae90e070563e5a6da/Real-time_flood_impacts_mapping_-_report__1_.pdf.

Coxon, G., Freer, J., Lane, R., Dunne, T., Knoben, W. J. M., Howden, N. J. K., Quinn, N., Wagener, T., & Woods, R. (2019). Decipher v1: Dynamic fluxes and connectivity for predictions of hydrology. *Geoscientific Model Development*, *12*, 2285–2306. doi:10.5194/gmd-12-2285-2019.

Falter, D., Schröter, K., Dung, N. V., Vorogushyn, S., Kreibich, H., Hundecha, Y., Apel, H., & Merz, B. (2015). Spatially coherent flood risk assessment based on long-term continuous simulation with a coupled model chain. *Journal of Hydrology*, *524*, 182–193. doi:10.1016/j.jhydrol.2015.02.021.

Falter, D., Vorogushyn, S., Lhomme, J., Apel, H., Gouldby, B., & Merz, B. (2013). Hydraulic model evaluation for large-scale flood risk assessments. *Hydrological Processes*, *27*, 1331–1340. URL: https://onlinelibrary.wiley.com/doi/full/10.1002/hyp.9553. doi:10.1002/hyp.9553.

Farrag, M., Brill, F., Dung, N. V., Sairam, N., Schröter, K., Kreibich, H., Merz, B., de Bruijn, K. M., & Vorogushyn, S. (2022). On the role of floodplain storage and hydrodynamic interactions in flood risk estimation. *Hydrological Sciences Journal*, *67*, 508–534. doi:10.1080/02626667.2022.2030058.

Fekete, A., & Sandholz, S. (2021). Here comes the flood, but not failure? lessons to learn after the heavy rain and pluvial floods in germany 2021. *Water*, *13*, 3016. doi:10.3390/w13213016.

Felder, G., Gómez-Navarro, J. J., Zischg, A. P., Raible, C. C., Röthlisberger, V., Bozhinova, D., Martius, O., & Weingartner, R. (2018). From global circulation to local flood loss: Coupling models across the scales. *The Science of the total environment*, *635*, 1225–1239. doi:10.1016/j.scitotenv.2018.04.170.

Felder, G., Zischg, A., & Weingartner, R. (2017). The effect of coupling hydrologic and hydrodynamic models on probable maximum flood estimation. *Journal of Hydrology*, *550*, 157–165. doi:10.1016/j.jhydrol.2017.04.052.

FOEN (2021). Stations and data. Federal Office for the Environment FOEN. URL: https://www.hydrodaten.admin.ch/en/stations-and-data.html. Last Accessed: 04.04.2024.

FOEN (2022). Naturgefahren: Flussvermessung. Federal Office for the Environment FOEN. URL: https://www.bafu.admin.ch/bafu/de/home/themen/naturgefahren/fachinformationen/naturgefahrensituation-und-raumnutzung/gefahrengrundlagen/naturgefahren--flussvermessung.html. Last accessed: 04.04.2024.

FOEN (2023). Flood alert map for rivers and lakes of national interest. Federal Office for the Environment FOEN. URL: https://www.hydrodaten.admin.ch/en/warnkarte_national.html.

Foudi, S., Osés-Eraso, N., & Tamayo, I. (2015). Integrated spatial flood risk assessment: The case of zaragoza. *Land Use Policy*, *42*, 278–292. doi:10.1016/j.landusepol.2014.08.002.

Gabbi, J., Carenzo, M., Pellicciotti, F., Bauder, A., & Funk, M. (2014). A comparison of empirical and physically based glacier surface melt models for long-term simulations of glacier response. *Journal of Glaciology*, *60*, 1140–1154. doi:10.3189/2014JoG14J011.

Horritt, M. S., & Bates, P. D. (2002). Evaluation of 1d and 2d numerical models for predicting river flood inundation. *Journal of Hydrology*, *268*, 87–99. doi:10.1016/S0022-1694(02)00121-X.

Intergovernmental Panel on Climate Change (2012). *Managing the risks of extreme events and disasters to advance climate change adaptation: Special report of the intergovernmental panel on climate change*. Cambridge: Cambridge University Press.

Ivanov, M. A., & Kotlarski, S. (2017). Assessing distribution-based climate model bias correction methods over an alpine domain: added value and limitations. *International Journal of Climatology*, *37*, 2633–2653. doi:10.1002/joc.4870.

Johnson, S. J., Stockdale, T. N., Ferranti, L., Balmaseda, M. A., Molteni, F., Magnusson, L., Tietsche, S., Decremer, D., Weisheimer, A., Balsamo, G., Keeley, S. P. E., Mogensen, K., Zuo, H., & Monge-Sanz, B. M. (2019). Seas5: the new ecmwf seasonal forecast system. *Geoscientific Model Development*, *12*, 1087–1117. doi:10.5194/gmd-12-1087-2019.

Kaltenberger, R., Schaffhauser, A., & Staudinger, M. (2020). "what the weather will do" – results of a survey on impact-oriented and impact-based warnings in european nmhss. *Advances in Science and Research*, *17*, 29–38. doi:10.5194/asr-17-29-2020.

Kelder, T., Müller, M., Slater, L. J., Marjoribanks, T. I., Wilby, R. L., Prudhomme, C., Bohlinger, P., Ferranti, L., & Nipen, T. (2020). Using unseen trends to detect decadal changes in 100-year precipitation extremes. *npj Climate and Atmospheric Science*, *3*. doi:10.1038/s41612-020-00149-4.

Kuhn, M. (1987). Micro-meteorological conditions for snow melt. *Journal of Glaciology*, *33*, 24–26. doi:10.3189/S002214300000530X.

Meléndez-Landaverde, E. R., Werner, M., & Verkade, J. (2020). Exploring protective decision–making in the context of impact–based flood warnings. *Journal of Flood Risk Management*, *13*. doi:10.1111/jfr3.12587.

MeteoSwiss (). Hourly precipitation estimation through rain-gauge and radar: Combiprecip. Federal Office of Meteorology and Climatology Meteo Swiss. URL: file:///C:/Users/mmosimann/Downloads/ProdDoc_CPC.pdf.

Ming, X., Liang, Q., Xia, X., Li, D., & Fowler, H. J. (2020). Real–time flood forecasting based on a high–performance 2–d hydrodynamic model and numerical weather predictions. *Water Resources Research*, *56*. doi:10.1029/2019WR025583.

Moncoulon, D., Labat, D., Ardon, J., Leblois, E., Onfroy, T., Poulard, C., Aji, S., Rémy, A., & Quantin, A. (2014). Analysis of the french insurance market exposure to floods: a stochastic model

combining river overflow and surface runoff. *Natural Hazards and Earth System Science*, *14*, 2469–2485. doi:10.5194/nhess-14-2469-2014.

Nadarajah, S. (2007). Probability models for unit hydrograph derivation. *Journal of Hydrology*, *344*, 185–189. doi:10.1016/j.jhydrol.2007.07.004.

Neal, J., Schumann, G., & Bates, P. (2012). A subgrid channel model for simulating river hydraulics and floodplain inundation over large and data sparse areas. *Water Resources Research*, *48*, 619. doi:10.1029/2012WR012514.

Neal, J., Schumann, G., Fewtrell, T., Budimir, M., Bates, P., & Mason, D. (2011). Evaluating a new lisflood-fp formulation with data from the summer 2007 floods in tewkesbury, uk. *Journal of Flood Risk Management*, *4*, 88–95. doi:10.1111/j.1753-318X.2011.01093.x.

Neal, J. C., Odoni, N. A., Trigg, M. A., Freer, J. E., Garcia-Pintado, J., Mason, D. C., Wood, M., & Bates, P. D. (2015). Efficient incorporation of channel cross-section geometry uncertainty into regional and global scale flood inundation models. *Journal of Hydrology*, *529*, 169–183. doi:10.1016/j.jhydrol.2015.07.026.

Panziera, L., Gabella, M., Germann, U., & Martius, O. (2018). A 12-year radar-based climatology of daily and sub-daily extreme precipitation over the swiss alps. *International Journal of Climatology*, *38*, 3749–3769. doi:10.1002/joc.5528.

Potter, S., Harrison, S., & Kreft, P. (2021). The benefits and challenges of implementing impact-based severe weather warning systems: Perspectives of weather, flood, and emergency management personnel. *Weather, Climate, and Society*, *13*, 303–314. doi:10.1175/WCAS-D-20-0110.1.

Pregnolato, M., Ford, A., Wilkinson, S. M., & Dawson, R. J. (2017). The impact of flooding on road transport: A depth-disruption function. *Transportation Research Part D: Transport and Environment*, *55*, 67–81. doi:10.1016/j.trd.2017.06.020.

Rai, R. K., Sarkar, S., & Singh, V. P. (2009). Evaluation of the adequacy of statistical distribution functions for deriving unit hydrograph. *Water Resources Management*, *23*, 899–929. doi:10.1007/s11269-008-9306-0.

Razavi, S., Tolson, B. A., & Burn, D. H. (2012). Review of surrogate modeling in water resources. *Water Resources Research*, *48*. doi:10.1029/2011WR011527.

Reigierungspräsidium Freiburg (2015). Hydraulische berechnungen hochrhein. Reigierungspräsidium Freiburg.

Russo, B., Sunyer, D., Velasco, M., & Djordjević, S. (2015). Analysis of extreme flooding events through a calibrated 1d/2d coupled model: the case of barcelona (spain). *Journal of Hydroinformatics*, *17*, 473–491. doi:10.2166/hydro.2014.063.

Serinaldi, F., & Grimaldi, S. (2011). Synthetic design hydrographs based on distribution functions with finite support. *Journal of Hydrologic Engineering*, *16*, 434–446. doi:10.1061/(ASCE)HE.1943-5584.0000339.

Shannon, S., Payne, A., Freer, J., Coxon, G., Kauzlaric, M., Kriegel, D., & Harrison, S. (2023). A snow and glacier hydrological model for large catchments – case study for the naryn river, central asia. *Hydrology and Earth System Sciences*, *27*, 453–480. doi:10.5194/hess-27-453-2023.

Sideris, I. V., Gabella, M., Erdin, R., & Germann, U. (2014). Real-time radar-rain-gauge merging using spatio-temporal co-kriging with external drift in the alpine terrain of switzerland. *Quarterly Journal of the Royal Meteorological Society*, *140*, 1097–1111. doi:10.1002/qj.2188.

Stockdale, T. (). Seas5 user guide. European Centre for Medium-Range Weather Forecasts. doi:10.21957/2y67999y.

Thompson, V., Dunstone, N. J., Scaife, A. A., Smith, D. M., Slingo, J. M., Brown, S., & Belcher, S. E. (2017). High risk of unprecedented uk rainfall in the current climate. *Nature communications*, *8*, 107. doi:10.1038/s41467-017-00275-3.

Federal Office of Topography, s. (2013). swissALTI3D. Federal Office of Topography, swisstopo.

Federal Office of Topography, s. (2023). National map 1:10 000. Federal Office of Topography, swisstopo.

United Nations (2015). Sendai framework for disaster risk reduction 2015-2030. URL: SendaiFrameworkforDisasterRiskReduction2015-2030.

van Dyck, J., & Willems, P. (2013). Probabilistic flood risk assessment over large geographical regions. *Water Resources Research*, *49*, 3330–3344. doi:10.1002/wrcr.20149.

Vetsch, D., Siviglia, A., Caponi, F., Ehrbar, D., Gerke, E., Kammerer, S., Koch, A., Peter, S., Vanzo, D., Vonwiller, L., Facchini, M., Gerber, M., Volz, C., Farshi, D., Mueller, R., Rousselot, P., Veprek, R., & Faeh, R. (2018). Basement - basic simulation environment for computation of environmental flow and natural hazard simulation..

Viviroli, D., Sikorska-Senoner, A. E., Evin, G., Staudinger, M., Kauzlaric, M., Chardon, J., Favre, A.-C., Hingray, B., Nicolet, G., Raynaud, D., Seibert, J., Weingartner, R., & Whealton, C. (2022). Comprehensive space–time hydrometeorological simulations for estimating very rare floods at multiple sites in a large river basin. *Natural Hazards and Earth System Science*, *22*, 2891–2920. doi:10.5194/nhess-22-2891-2022.

Wahl, S., Bollmeyer, C., Crewell, S., Figura, C., Friederichs, P., Hense, A., Keller, J. D., & Ohlwein, C. (2017). A novel convective-scale regional reanalysis cosmo-rea2: Improving the representation of precipitation. *Meteorologische Zeitschrift*, *26*, 345–361. doi:10.1127/metz/2017/0824.

Ward, P. J., Jongman, B., Weiland, F. S., Bouwman, A., van Beek, R., Bierkens, M. F. P., Ligtvoet, W., & Winsemius, H. C. (2013). Assessing flood risk at the global scale: model setup, results, and sensitivity. *Environmental Research Letters*, *8*, 044019. doi:10.1088/1748-9326/8/4/044019.

Weyrich, P., Scolobig, A., Bresch, D. N., & Patt, A. (2018). Effects of impact-based warnings and behavioral recommendations for extreme weather events. *Weather, Climate, and Society*, *10*, 781–796. doi:10.1175/WCAS-D-18-0038.1.

World Meteorological Organization (2015). Wmo guidelines on multi-hazard impact-based forecast and warning services, . URL: https://library.wmo.int/doc_num.php?explnum_id=7901.

Zischg, A. P. (2023). Modeling spatiotemporal dynamics of flood risk change. In A. Zischg (Ed.), *Flood risk change* (pp. 187–271). Amsterdam: Elsevier. doi:10.1016/B978-0-12-822011-5.00003-X.

Zischg, A. P., Felder, G., Mosimann, M., Röthlisberger, V., & Weingartner, R. (2018a). Extending coupled hydrological-hydraulic model chains with a surrogate model for the estimation of flood losses. *Environmental Modelling & Software*, *108*, 174–185. doi:10.1016/j.envsoft.2018.08.009.

Zischg, A. P., Mosimann, M., Bernet, D. B., & Röthlisberger, V. (2018b). Validation of 2d flood models with insurance claims. *Journal of Hydrology*, *557*, 350–361. doi:10.1016/j.jhydrol.2017.12.042.

Zischg, A. P., Röthlisberger, V., Mosimann, M., Profico-Kaltenrieder, R., Bresch, D., Fuchs, S., Kauzlaric, M., & Keiler, M. (2021). Evaluating targeted heuristics for vulnerability assessment in flood impact model chains. *Journal of Flood Risk Management*, *5*, 171. doi:10.1111/jfr3.12736.

4 Two sides of the same coin? Hydrometeorological uncertainties in impact-based flood warning systems and climate change sensitivity of floodplains

Markus Mosimann[1, 2, 3], Olivia Martius[1, 2, 3], Andreas Paul Zischg [1, 2, 3]

[1] *Institute of Geography, University of Bern, Hallerstrasse 12, 3012 Bern, Switzerland*

[2] *Mobiliar Lab for Natural Risks, University of Bern, Hallerstrasse 12, 3012 Bern, Switzerland*

[3] *Oeschger Centre for Climate Change Research, University of Bern, Hochschulstrasse 4, 3012, Bern, Switzerland*

Weather and Climate Extremes (Elsevier)
Submitted: 05 April 2024

Abstract

The sensitivity of floodplains to floods of various magnitudes is strongly influenced by the relationship between the hydrogeomorphology and the built environment. To provide a nuanced measure of impact sensitivity to changes in flood magnitude, we introduce a novel floodplain sensitivity index (FSI) that integrates slope and curvature metrics derived from the magnitude–impact curve. We apply the method to 179 floodplains in Switzerland. Our analysis reveals that higher flood magnitudes might substantially amplify impacts, given that many of the most sensitive magnitude thresholds have not yet been exceeded. However, we do not find coherent patterns in the FSI across geographic or topographic regions or along entire rivers. The shape of the impact curves and thus the impact sensitivity is specific not only to the floodplain but also to the type of impact. The FSI contributes to flood risk management by providing a method to identify the critical flood magnitude thresholds that lead to severe impacts if exceeded. The FSI helps in assessing the effects of uncertainties in hydrometeorological forecasts on impact-based warnings and of uncertainties in climate change projections for long-term flood risk management strategies.

Keywords: Impact-based warning; impact-based forecast and warning services; impact sensitivity; climate change sensitivity; hydrometeorological uncertainties; flood risk as-

sessment

4.1 Introduction

Floods are among the most devastating natural hazards and affect millions of people every year. To mitigate flood impacts, many countries have implemented systems for flood warning and response. Among these, impact-based forecast and warning services (IBFWS) have gained popularity, because they provide information on potential impacts that is more readily interpreted by authorities (World Meteorological Organization, 2021). However, the accuracy and reliability of such systems depends on the quality and reliability of the modelling framework and the forecasts.

Hydrometeorological uncertainties in the forecasting chain limit their value to decision makers during an event (Weyrich et al., 2018; Potter et al., 2018; Meléndez-Landaverde et al., 2020; Casteel, 2016; Kaltenberger et al., 2020). Probabilistic ensemble forecasts offer one option for addressing the challenges of these uncertainties by modelling hazard and impacts top-down from the forecast ensemble members and probabilities (Merwade et al., 2008; Cloke & Pappenberger, 2009; Bhola et al., 2020; Contreras et al., 2020; Keller et al., 2019; Mülchi, R., Rössler, O., Schwanbeck, J., Weingartner, R., Martius, O.). However, these approaches are often tested at local and regional scales that are unsuited to IBFWS at a national scale because they are limited by the trade-off between the computational efficiency and spatial resolution of flood models (see also Savage et al., 2016). Mosimann et al. (2023) present one approach to optimizing this trade-off by the development of flood library-based surrogate models that support IBFWS.

The impacts of climate change on floods have become more evident in recent years (e.g., Clarke et al., 2022; Faranda et al., 2022). According to the Intergovernmental Panel on Climate Change (Intergovernmental Panel on Climate Change, 2021), intense river flood events will occur more frequently in future both in western and central Europe and across most of the globe. The resilience of human–environment systems needs to be enhanced to adapt to new flood regimes. Consequently, the sensitivity of rivers and their floodplains to climatic change, *climate sensitivity* , needs to be assessed and understood. Recent studies have sought to quantify the impact of climate change on flood risk by coupling hydrometeorological scenarios of climate change to flood and impact (e.g., Cloke et al., 2013; Alfieri et al., 2015; Arnell & Gosling, 2016; Xu et al., 2019; Kelder et al., 2022). Similar to IBFWS, these approaches follow a top-down direction. Conway et al. (2019) call for bottom-up assessments of climate risks to complement top-down approaches and state that "integrating [such assessments'] results is a much-needed step towards developing relevant information to address the needs of immediate adaptation decisions."

Zischg & Bermúdez (2020) and Devitt et al. (2023) conducted global bottom-up analyses to assess the sensitivity of floodplains and population exposure to varying flood event magnitudes. Devitt et al. (2023) highlight that populations residing in floodplains most sensitive to lower-magnitude events are at significant risk from increases in hazard magnitudes due to climate change. Zischg & Bermúdez (2020) highlight the need for national assessments and for assessments of other types of impact than exposure

of population. Both studies use collections of flood simulation outputs to establish magnitude–impact relationships, an approach that is analogous to the methods employed in library-based surrogate models for flood risk assessment (Zischg et al., 2018) and in IBFWS (Mosimann et al., 2023). In these, magnitude–impact relationships are typically visualized as risk curves. This approach reveals new potential for flood risk assessment, and interesting findings emerge from the global view. However, the strong generalization and coarse resolution of flood models may not be applicable to regional and national applications. Furthermore, comparing hazards across floodplains with return periods presents challenges. Assessing climate change sensitivity solely from return periods derived from historical data is questionable and could lead to misleading assumptions, because future frequency distributions are unknown. In addition, variations in such changes cannot be assumed to be consistent on a global scale (Intergovernmental Panel on Climate Change, 2021).

Subsequently, we discuss our hypothesis with the relationship between discharge and exposed population and flooded area for the floodplain of the Emme River near Burgdorf (Figure 4.1). Such magnitude–impact relationships are often called "flood risk" or "impact" curves. In Figure 4.1, every point corresponds to an independent flood simulation that was overlaid with exposure data. The value on the Y-axis of the point describes the impact, in this example the number of exposed people (black dots) or the flooded area in km^2(red triangles) given the magnitude, here discharge, indicated on the X-axis. Therefore, each point or triangle along the curve corresponds to a single flood scenario with a specific peak discharge. The slope of the line connecting two points denotes the increase in impact with the increase in flood magnitude. Steep slopes in the impact curve indicate sensitivity to hydrometeorological uncertainties and changes to magnitude due to climate change, similar to those presented in other studies (Devitt et al., 2023; Zischg et al., 2018). To exemplify this, we consider two ranges with a difference of 100 m^3/s peak discharge in Figure 4.1 (A = 600-700 m^3/s, green; B = 800-900 m^3/s, blue). This could be independent forecasts with the same ensemble forecast from a hydrological model, increases of discharge that are expected in a future climate, or an uncertainty range from climate projections for a certain future flood event. Even though the range of discharge does not differ in absolute terms, the increase in exposed population in range A is significantly larger than that in range B.

For an ensemble forecast with range B, the influence of the hydrometeorological uncertainty (blue band) plays a minor role as the impacts expressed as the numbers of exposed people are similar across the forecast range. This reduces the uncertainties of the entire model chain. The magnitude–impact curve within range A has a steeper slope with a potential exposure of people ranging from close to zero to up to 3,000. Sensitivity is therefore higher in range A.

The same is valid for sensitivity to climate change, where the ranges A and B may stand for a hypothetical increase of peak discharges or the uncertainty of an estimate of discharge with a certain frequency.

Moreover, Figure 4.1 shows that sensitivity may vary between different types of impacts as in this example: the slopes of the blue (people) and red (flooded area) line are similar in range B but not in range A. The visual examination of these relationships underpins the need for a more comprehensive analysis and the importance of considering the heterogeneity of the slopes within the entire range of plausible flood events.

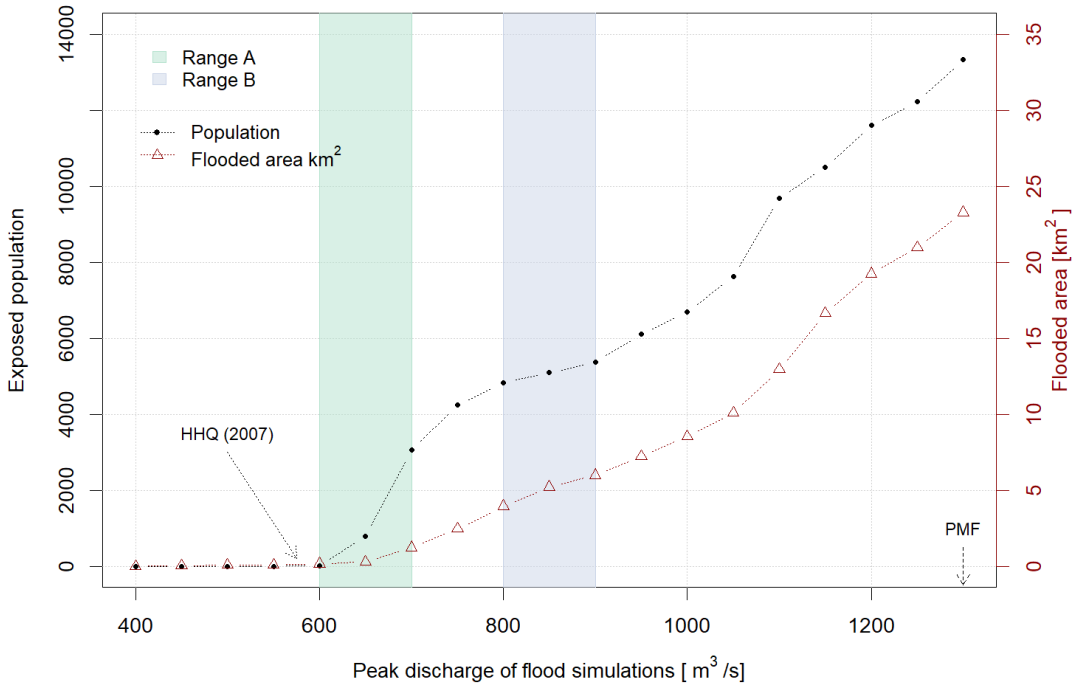

Fig. 4.1: Discharge–impact diagram derived from surrogate models for the section of Emme River near Burgdorf (exposed people are shown in black; flooded area is shown in red). HHQ indicates a rough estimation of the maximum discharge from 100 years of measurements of a downstream (662 m^3/s) and upstream (485 m^3/s) gauging station. The catchment size at the hydraulic upstream boundary condition of this floodplain is roughly in the center of the catchment area of these gauging stations. The probable maximum flood (PMF, 1300 m^3/s) was set according to Felder et al. (2019) and defines the upper limit of the magnitude spectrum. Windows A and B indicate hypothetical forecast ensembles or discharge projection ranges.

Hence, our proposition underscores the significance of identifying these locations through a comprehensive analysis of the curve, offering key insights for both IBFWS and the assessment of climate change impact. This approach remains scenario-neutral and bottom-up, indicating the magnitudes for which the uncertainties from hydrometeorological or climate scenarios are reduced or exacerbated. Furthermore, it specifies crucial thresholds that would yield substantial, moderate, or minimal alterations to the flood's impact on the floodplain when exceeded. Although interpretations may differ across time horizons, the identification of thresholds remains essential and is similar for both approaches, making them to two sides of the same coin. Therefore, this paper aims to analyze and discuss the co-benefits of magnitude–impact relationships as a multipurpose tool applied in a bottom-up approach to improve uncertainty assessment for IBFWS in short-term flood risk management on one side of the coin and, to detect and quantify climate sensitivity in rivers and floodplains in the long term on the other.

4.2 Data and Methods

The main objective of this study is to analyze magnitude–impact relationships to assess floodplain sensitivity. We hypothesize that such an analysis can be beneficially used in IBFWS and for climate change risk assessment. The methods for flood and impact modelling follow Mosimann et al. (2023). They developed surrogate flood models using preprocessed flood simulations stored in a comprehensive database, often referred to as a flood library. These models are designed for integration into a national IBFWS. The database contains not only flood data but also exposure information, such as building footprints augmented with population and workplace statistics, and an assessment of structural building value. Our enhancement of this database includes incorporating damage assessments for household contents. We conduct an analysis of the correlation between flood intensity and resulting impacts across 44 rivers and 11 lakes within Switzerland's primary river network, segmented into 179 distinct floodplains (Figure 4.2). Further details follow in sections 4.2.1 and 4.2.2.

We use the term "magnitude" to refer to the two types of input to our flood models: peak discharge and maximum lake level. We adopt the term "magnitude spectrum" to encapsulate the entire scope of our flood simulations, defined by the lower and upper limits of flood magnitudes within the floodplain. For discussions of specific intervals within this spectrum, we use the term "magnitude range." To simplify matters, we categorize the modelled river sections and lakes collectively as "floodplains." We use "impact" as a broad term for the various consequences of a simulated flood scenario, such as the flooded area and volume, exposure to buildings, population, and workplaces, and damage to building structure and household contents. Magnitude–impact diagrams, subsequently termed "impact curves," display the relationship between these variables and thus provide a framework for evaluating the susceptibility of floodplains to increases in magnitude and uncertainties stemming from climate change or from uncertainties associated with hydrometeorological forecasts.

4.2.1 Hydrodynamic modelling

Impact curves are derived from flood simulations. We use an extended version of the precalculated hydrodynamic simulations presented in Mosimann et al. (2023). Figure 4.2 provides an overview of the modelled river and lake network. We use surveyed river cross-sections from the Federal Office for the Environment FOEN (FOEN, 2022), categorized as "rivers and lakes of Swiss national interest." We use the data to calculate the flow in river channels with the BASEMENT 1D hydrodynamic model (Vetsch et al., 2018). The 1D model is coupled to a 2D model, with which highly resolved digital terrain models provided by various sources are used to derive the topography (Canton of Vaud, 2006; Canton of Lucerne, 2012; Canton of Zug, 2013; Canton of Aargau, 2014; Canton of Solothurn, 2014; Canton of Zurich, 2014; Canton of Bern, 2014; swisstopo, 2013; RPF, 2015). The 2D flood module of BASEMENT consists of an unstructured, irregular mesh of triangled elements. An element is defined as wet when the flow depth exceeds 0.01m. We define flood extent as the area including all elements that have been wet for at least one modelled timestep and flooded volume as the sum of the areas multiplied by the maximum flow depths of elements.

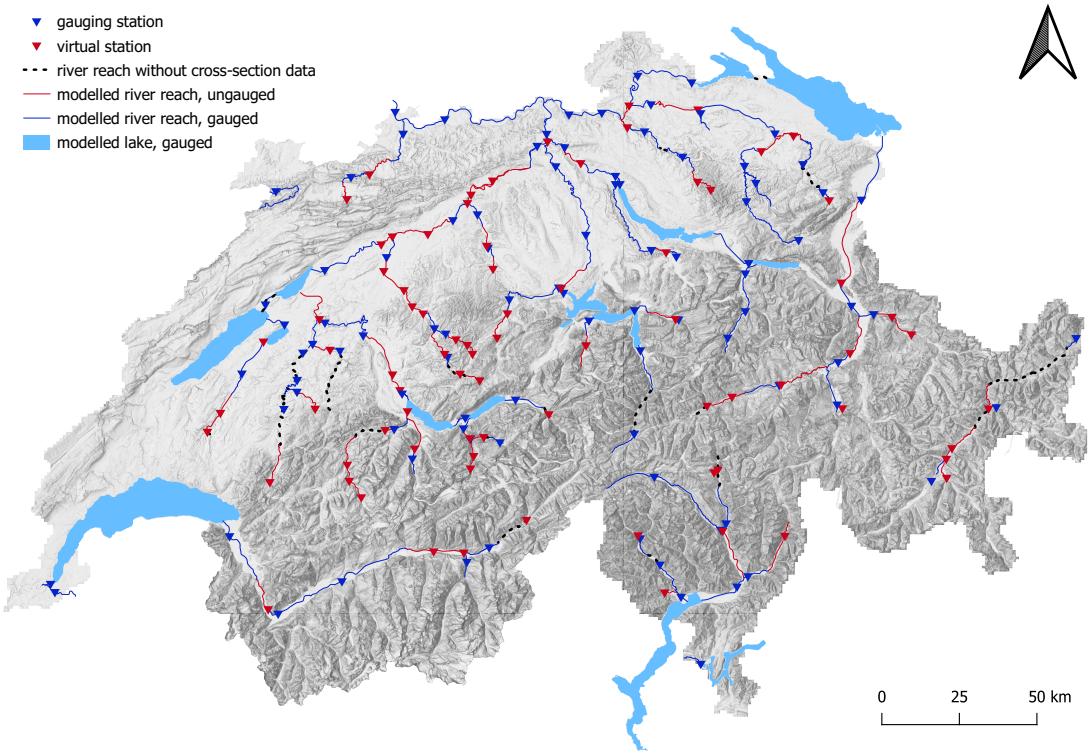

Fig. 4.2: Study area. The lines indicate river sections and the light blue areas lakes, both categorized as floodplains for the hydraulic modelling and impact assessment. Triangles indicate the locations where synthetic hydrographs were used as the upper boundary conditions of the hydrodynamic model. Red triangles and lines indicate river sections without gauging stations, and a reference station was used to produce synthetic hydrographs (see Section 4.2.1). Blue triangles and lines indicate river sections with data available from gauging stations from the Federal Office for the Environment (FOEN, 2024b). Note that certain gauging stations are not located at the upstream boundary condition of the hydraulic model to optimally represent the hydrological conditions for the entire section. All lakes shown are gauged and modelled with a 24-hour steady-state lake level.

To create a series of realistic river flood scenarios from which to derive the impact curve, synthetic hydrographs are created from observed hydrographs (FOEN, 2021); these serve as the upstream boundary conditions for the hydraulic model presented in Mosimann et al. (2023). The synthetic hydrographs are rescalable to any desired peak discharge and mimic the typical time to peak, peak discharge relative to mean discharge, and flood volume of a river section. To simulate lake floods, we use a steady-state approach and maintain a specific lake level for a duration of 24 hours.

We need to choose lower and upper limits to define the magnitude spectrum in a floodplain. The lower limit of peak magnitudes corresponds to the threshold of danger level 3 set by the FOEN (FOEN, 2024a) with an average return period of 10 to 30 years. Danger level 3 is the first level, at which according to the FOEN, flooding can occur locally. The upper limit ideally corresponds to the probable maximum flood (PMF). We considered the maximum estimated from multiple sources to define this value specifically for each floodplain: (i) extreme value statistics provided by the FOEN for every gauging station (FOEN, 2024b), (ii) maximum discharges derived with a hydrological model

from hindcasted extreme precipitation scenarios Mosimann et al. (2023), and (iii) PMFs derived in other studies (Felder et al., 2017, 2019). In Figure 4.2, river sections with direct derivation of synthetic hydrographs from gauging stations (FOEN, 2024b) are colored in blue. River reaches without gauging stations are shown in red. Here, synthetic hydrographs are derived from stations with similar catchment sizes and specific discharges. All lakes considered are monitored by the FOEN (FOEN, 2021) and modelled with peak lake levels in increments of 10cm. We conducted between 10 and 31 simulations for each of the 179 floodplains (Lake Geneva and Lake Maggiore with 36 simulations and Lake Zurich with 46). Discrepancies in simulation count arise from variations in the magnitude spectrum. In cases where lower and upper limit values exhibit narrower ranges, fewer simulations were conducted. In total, we simulated 3278 independent flood scenarios from synthetic hydrographs.

4.2.2 Impact assessment

Beside flooded area and volume described in the previous section, we analyze exposure of buildings, population, and workplaces. The large-scale topographic landscape model of Switzerland swissTLM3D provided the building footprints (swisstopo, 2023). The Federal Statistical Office (FSO) provided the Buildings and Dwellings Statistics (FSO, 2021) and Enterprise Statistics (FSO, 2020) datasets. These are merged with building footprints as described by Röthlisberger et al. (2016). Exposure values are subsequently aggregated to the intersecting building footprints.

To quantify the monetary damage to buildings, we first estimate the building values following the M4 approach by Röthlisberger et al. (2018): average values per building volume differentiated by land use category and building purpose. We use updated versions of the building zones provided by the Federal Office for Spatial Development (ARE) (ARE, 2022), the building footprints *swissTLM3D* and the Buildings and Dwellings Statistics datasets to differentiate land use category and building purpose. We multiply the average price per cubic meter with the building volume. As proposed by Bermúdez et al. (2018), we identify the maximum flow depth reached across the exposed building footprints. We use a regionally calibrated, one-parametric flow depth vulnerability function (Zischg et al., 2021).

$$dod = \begin{cases} 0 & \text{if } fd = 0, \\ (0.18846 + 0.17152 \times fd)^2 & \text{otherwise.} \end{cases} \tag{4.1}$$

where dod denotes the degree of damage and fd is the maximum flow depth across the building footprint. Monetary damage for the building is

$$d_{building} = building\ value \times dod, \tag{4.2}$$

where $d_{buildings}$ is the structural damage estimated for a building. For residential buildings, we calculate damage to household contents with the damage function by Mosimann

et al. (2018). This function expects transformed monetary damage on buildings as input ($d^{(\lambda)}_{building}$). Therefore, the exponent λ of the Box-Cox transformation,

$$d^{(\lambda)}_{building} = \frac{d^{\lambda}_{building} - 1}{\lambda}, \tag{4.3}$$

is set to 0.131. To derive monetary damage to household contents with the conditional mean estimate, as proposed by the authors, we use the following function:

$$d_{content} = (1 + \lambda\beta_0 + \lambda\beta_1 * d^{(\lambda)}_{building})^{\frac{1}{\lambda}} \times \left(1 + \frac{\sigma^2(1-\lambda)}{2(1 + \lambda\beta_0 + \lambda\beta_1 * d^{(\lambda)}_{building})^2}\right) \tag{4.4}$$

Here, additional to λ used to back-transform damage into CHF, β_0 (=3.798) and β_1 (=0.618) are estimates from the linear regression on the transformed scale, whereas σ denotes the standard deviation used to derive the conditional mean estimate. Appendix 4.A gives some more insights into the functionality of the vulnerability and damage functions used and described in this section.

4.2.3 Sensitivity analysis

We assess the sensitivity of floodplains to increasing flood magnitudes by calculating the slope (Section 4.2.3.1) and curvature (Section 4.2.3.2) of the impact curve across all impact types. In Section 4.2.3.3, we define and explain the purpose of a combined index for floodplain sensitivity (floodplain sensitivity index FSI) that accounts for both slope and curvature.

The selection of discrete magnitude steps between two scenarios involves a degree of subjective judgment or expert knowledge (see 4.2.1). Consequently, we investigate the sensitivity of slope, curvature, and the FSI using moving windows spanning two, three, and four simulations. Analyzing different moving window sizes facilitates an understanding of the significance of the interval selection between scenarios of varying peak magnitudes. Additionally, a moving window can also be used to smooth sensitivity estimates. In practice, the range of uncertainty in, for instance, a forecast may provide a basis for determining the size of a moving window. We denote the number of simulations encompassed by a moving window as mw in equations and explanations.

4.2.3.1 Slope as indicator

To calculate the slope of the impact curve, we calculate the increase of impact as absolute value dy_{abs}, the relative increase of impact dy_{rel} as the ratio of dy_{abs} to the impact derived with the magnitude at the upper limit of the magnitude spectrum y_{Xmax}, and we derive the normalized increase in magnitude dx_{rel} at every simulation i as follows:

$$dy_{abs,i} = y_{i+(mw-1)} - y_i, \tag{4.5}$$

$$dy_{rel,i} = \frac{dy_{abs,i}}{y_{Xmax}} \tag{4.6}$$

$$dx_{rel} = \frac{mw - 1}{nScenarios - 1} \tag{4.7}$$

In this context, $mw - 1$ represents the incremental increase in magnitude starting from simulation i, and $i + (mw - 1)$ indicates the impact at the next higher simulated peak discharge as determined by the width of the moving window. We prefer the increase in magnitude on normalized discharge dx_{rel} over an absolute increase because the magnitude scales are not comparable across river sections. Moreover, the interpretation of units in slope, such as people per m^3/s, can be misleading due to varying discharge levels between river sections. For instance, consider the Rhine at Basel (danger level 3 = 3050 m^3/s) and the Emme at Wiler (danger level 3 = 430 m^3/s): Because discharge in Basel is significantly higher, the interval must also be correspondingly larger (Rhine River: 100 m^3/s); Emme: 50 m^3/s)). Consequently, even if both scenarios resulted in an increase of 100 exposed people, the Emme River's value would appear higher due to its smaller interval, despite both intervals being tailored to specific river characteristics. Therefore, we use the normalized increase of magnitude according to the number of simulations ($= nScenarios$). We use $nScenarios - 1$ because the normalized X-value of the first simulation is 0. For instance, 11 simulations would provide 10 intervals of 0.1.

Similarly, dy_{rel} is rescaled from 0 (no impact) to 1 (maximum impact). We also perform a normalization for impact, as the meaning of this is region specific. The number of people, buildings, and workplaces to protect depends on the resources available. Even though the absolute numbers for impact are relevant and indeed crucial to prioritizing flood mitigation, the purpose of our study is to detect the highest sensitivities independent of impact.

By rescaling both magnitude and impact to a range from 0 to 1, and given that the definition of lower and upper limits is consistent across all floodplains when using the same methodology, comparability is warranted at the national scale. Normalization facilitates a straightforward interpretation of the slope: Values exceeding 1 indicate a stronger than average increase of impact with change in magnitude and therefore a higher sensitivity. Conversely, values below 1 indicate below-average increase.

The normalized values d_yrel and d_xrel provide a basis for calculating the slope S of the impact curve:

$$S_i = \frac{dy_{rel,i}}{dx_{rel}}. \tag{4.8}$$

4.2.3.2 Curvature as indicator

It is of interest to know where the slope of the impact curve changes. These points indicate critical magnitude thresholds at which significant changes in impact occur and

thus are important to identify for short- and long-term interventions. To determine such thresholds, we calculate curvature C for every simulation i as follows:

$$C_i = (dS_i) = S_i - S_{i-(mw-1)}. \tag{4.9}$$

In contrast to the mathematical second derivative of the magnitude–impact curve, we neglect the difference along the X-axis by setting this to 1 because we simulate discreet peak magnitude steps with a constant increase. Therefore, curvature as formulated in Equation 4.9 is the difference between the slope of the impact curve subsequent (S_i) and prior ($S_{i-(mw-1)}$) to simulation i, depending on the width of the moving window. The advantage of this formulation is the straightforward interpretation of the values of C_i: Positive values characterize convex ranges of the curve with an increasing subsequent slope, and negative values characterize concave ranges with a decreasing subsequent slope. For example, $C_i = 2$ indicates that when exceeding the peak magnitude at simulation i, the slope increases by twice the mean slope of the curve. If $C_i = -1$, the slope decreases by the average slope of the curve, and $C_i = 0$ indicates that the slope remains the same.

4.2.3.3 Floodplain Sensitivity Index

By focusing only on S or C to describe the sensitivity of impact to changes in magnitude, some major issues arise for flood risk management. Steep slopes in the impact curves indicate expansion of the flooded areas, particularly in densely populated and industrial zones. Additionally, due to retention effects, steep slopes can correspond to higher flow depths in the floodplain, leading to increased monetary damage. High curvature values indicate new sources of impact, such as the inundation of previously unaffected settlements and sectors within settlements. This may result from various factors, including a general expansion of the flood, the emergence of new weak spots in river channels near settlements, and the exceeding of capacity in retention basins. Because a steep slope does not necessarily imply strong curvature, and vice versa, it is imperative to consider both parameters to describe floodplain sensitivity accurately. Thus, we introduce the floodplain sensitivity index (FSI) to account for both:

$$Floodplain\ Sensitivity\ Index = FSI_i = \left(\frac{S_i}{max(S)} + \frac{C_i}{max(C)}\right) \times 0.5. \tag{4.10}$$

The normalization of slope and curvature with the maximum value specific to each floodplain is conducted to mitigate the influence of the modifiable areal unit problem (MAUP), as outlined, for instance, by Rothlisberger et al. (2017). Otherwise, the slope and curvature in river sections with relatively small model perimeters, and consequently usually smaller impacts, may exhibit disproportionately higher values. Normalization with the maximum value allows a more robust interpretation of relative differences in slope and curvature, which facilitates comparisons between various river sections independent of their spatial discretization. Furthermore, maximum normalization ensures equal weighting of curvature and slope. Given that slope values increase monotonically, their maximum is consistently higher than that of curvature. By normalizing from the

maximum, we prevent slope from exerting undue influence on the final estimation of FSI. We opt against weighting the parameters, no clear rationale suggests that one parameter holds greater significance than the other.

4.3 Results

4.3.1 Sensitivity assessment based on impact curves

Impact curves as presented in Figure 4.1, slope as defined in Equation 4.8, curvature as defined in Equation 4.9 and the combined floodplain sensitivity index FSI as defined in Equation 4.10 are applied to all 179 floodplains, separate for each impact type (flooded area and volume, exposure of buildings, people and workplaces, damage to building structure and household content).

Figure 4.3 shows the normalized slope and curvature for the floodplain of the Emme River at Burgdorf (region discussed in Section 4.1 and Figure 4.1) when using window widths of two (top), three (middle), and four (bottom) simulations for the calculation of the indices with the number of affected people as impact measure. The most critical threshold, at which FSI is maximized, is illustrated as the magnitude in the center of the windows considered to calculate slope subsequent (blue area) and prior (red area) to this threshold. The curve derived from FSI calculations provides a comprehensive overview of the crucial thresholds in the impact curve. It highlights areas in which an increase in magnitude would result in substantial changes of impact— and where such changes are less pronounced, which is equally vital. Although a discrepancy occurs when defining the most critical threshold, with allocations ranging from 600 to 650 m^3/s, the overlapping of the moving windows (green areas) leads us to interpret this difference as insignificant. Similarly, the second threshold, denoted by the peak of the FSI curve at 1050 m^3/s when using a window width of two simulations and 1000 m^3/s for windows spanning three or four simulations, exhibits a similar pattern of overlapping and minor variation. The use of moving windows spanning three and four simulations results in a smoother curve, providing a clearer visual signal of sensitivity and lower maximum slopes and curvatures (as indicated at the bottom right of the figures). Because we employ maximum normalization to derive FSI, the sensitivity curves remain comparable. The same procedure is followed for every floodplain and every impact type.

4.3.2 Allocation of sensitivity maxima in Swiss rivers and lakes

Figure 4.4 displays the impact curves for exposed buildings (left, n = 158) and exposed population (right, n = 150) derived with the FSI using a window width of three simulatons. This indicates whether the maximum sensitivity is situated in the lower (= A), middle (= B), or upper (= C) third of the magnitude spectrum, highlighted in green. The distribution of regions across specific magnitude ranges (Buildings: A = 44, B = 52, C = 62; Population: A = 36, B = 45, C = 69) indicates a highly heterogeneous shape of the impact curves. For the magnitude spectrum analyzed in 179 floodplains, no flooding occurs in 10, in 21 floodplains there is no impact on buildings, and in 29 floodplains there is no impact on population. Among 79 floodplains with gauging stations, the distribution of the highest recorded flood magnitudes varies: 29 floodplains

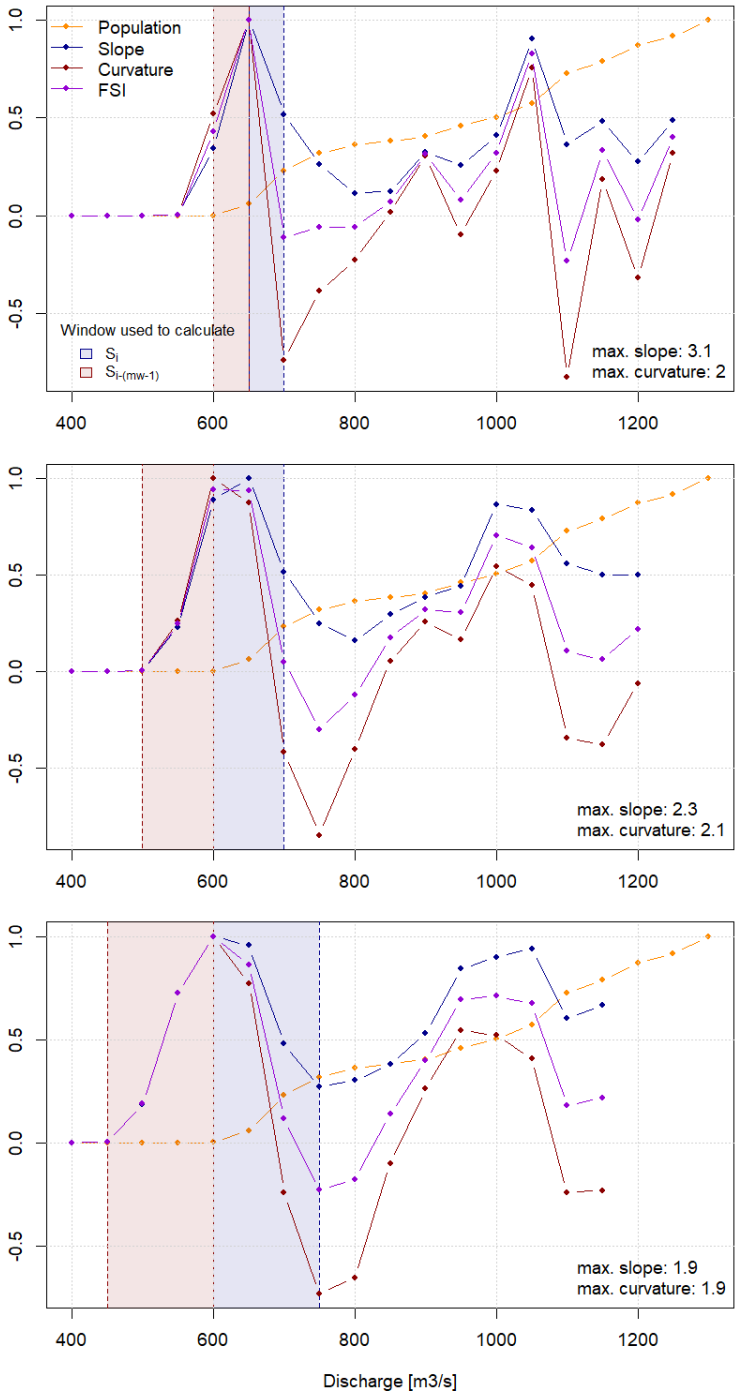

Fig. 4.3: Sensitivity indices when using a moving window width of two (top), three (middle), and four (bottom) simulations. The blue highlighted areas indicate the window that was considered to calculate the slope after the most sensitive threshold (S_i at simulation i where $FSI_i = max(FSI)$), following Equation 4.8. The red highlighted areas indicate the window used to calculate the slope before this threshold, to be used as input in Equation 4.9 ($S_{i-(mw-1)}$, and mw denotes the number of simulations the moving window is spanning). The results from these two equations are then used to calculate FSI following 4.10. If the FSI reaches 1.0, curvature and slope are maximized at the same magnitude.

experienced their highest magnitudes in the lower (A), 37 in the middle (B), and 16 in the upper third (C) of the magnitude spectrum.

The purple lines represent the median, interquartile range, and 10–90% quantile values for normalized impact at normalized magnitudes. Comparing these lines derived for buildings and population (or workplaces, see Appendix 4.B, Figure 4.11), we observe a shift towards higher magnitudes with more pronounced critical thresholds, indicated by sharper bends at higher magnitudes and steeper slopes thereafter.

This shift is particularly noticeable for the purple lines summarized in the middle ranges (B), and for the 10, 25, and 50% quantile lines in the lower and upper thirds (A, C). The shift can also be attributed to the higher number of lines for exposed population located in range C.

Across all model regions, the same pattern is evident when comparing flooded area and volume (Appendix 4.B, Figure 4.9). Notably, there is no significant difference between the impact curves for structural and contents damage to buildings (Appendix 4.B, Figure 4.10).

4.3.3 The roles of moving window size and impact type

To acquire information about the sensitivity of the FSI to the width of the moving window, and therefore the definition of increases in magnitude defined to simulate the floods, and to test whether the sensitivities of different impact types in the same floodplain correlate with each other, we conduct a Spearman correlation analysis of the location of maximum FSI values over all impact types and window widths analyzed. We use the magnitude with maximum FSI as input for the correlation analysis. This provides information about whether the sensitivity is calculated differently across various impact types and whether the analysis is sensitive to the incremental increase of magnitude between two simulations. Figure 4.5 summarizes the results visually and quantitatively, illustrating the correlation coefficients calculated. Because a general positive correlation is to be expected, we categorize the correlation coefficients as follows:

- very weak: 0–0.2
- weak: 0.2–0.4
- moderate: 0.4–0.6
- strong: 0.6–0.8
- very strong: 0.8–1

In all cases, the correlations within the same impact type but with different sizes of moving window are mostly very strong, except for flooded area, where a strong correlation can be observed. There are few strong correlations between different impact types. In most cases, the correlation is weak to moderate, but it is still significant in every case. Furthermore, Figure 4.5 shows how the correlation between the hazard variables, flooded area and flooded volume, and impact is weak. We also tested whether the number of simulations is correlated with the magnitudes with maximum FSI of any impact type. At a significance level of 5%, there is no correlation.

Table 4.1 shows the frequency of shifts in the most sensitive magnitude across floodplains and impact types when the width of the moving window is increased from two to three or four incremental steps and from three to four. Negative numbers in the

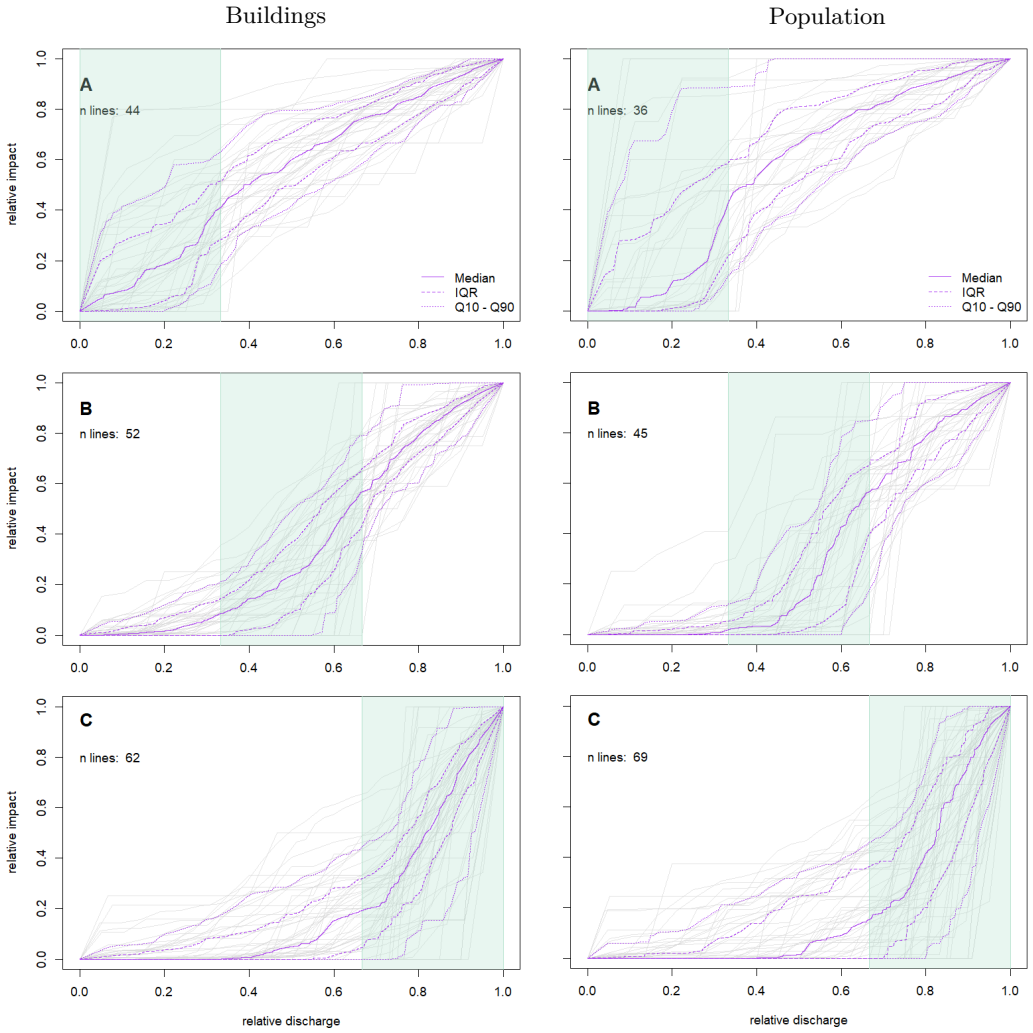

Fig. 4.4: Impact curves for buildings (left, n = 158) and people (right, n = 150). Purple lines indicate median (straight), interquartile range (dashed) and range from 10th to 90th quantile. A: Maximum floodplain sensitivity (Equation 4.10 based on window widths spanning three simulations) located in first third (green) of the magnitude spectrum. B: Maximum sensitivity located in second third of magnitude spectrum. C: Maximum sensitivity located in upper third of the magnitude spectrum.

column headers right of the vertical line indicate shifts towards lower magnitudes by n incremental steps. "0" indicates no change in magnitude, and a positive number indicates a shift towards higher magnitudes. The most important effect of increasing the moving window is a shift towards mainly lower magnitudes. The increase in the width often corresponds to the shift in incremental steps. In many cases, the increase in the moving window width from two to four incremental steps also leads to a high number of critical magnitudes being shifted by two incremental steps towards lower magnitudes (-2). The consistency of the most sensitive magnitudes with increasing window width varies between 30.6% (Slope, "2 to 4") and 53.4% (Curvature, "2 to 3"). The FSI counts generally fall between those for curvature and slope, which aligns with expectations

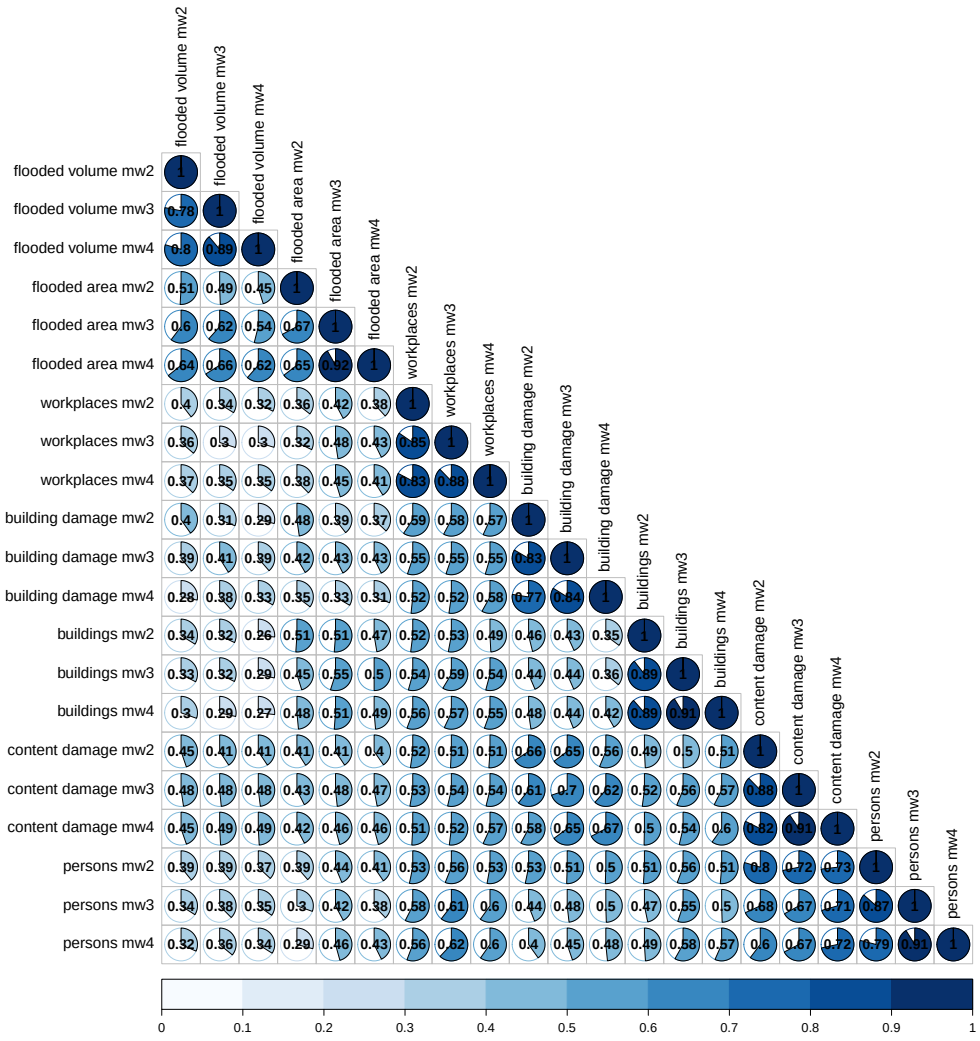

Fig. 4.5: Spearman correlation of the magnitude with maximum FSI across all impact types and moving window sizes ($mw2$ = moving window over two simulations, $mw3$ = three simulations, $mw4$ = four simulations). Besides the number, colors, and pies indicate the correlation coefficient.

because the index integrates both metrics.

In addition to exploring the effect of varying moving window widths, our analysis also looks at instances where the magnitude of the most sensitive range remains consistent across all sensitivity parameters: slope, curvature, and the floodplain sensitivity index (FSI). Depending on the width of the moving window, in 30.6% to 36% of cases, the most sensitive thresholds identified using the FSI do not align with either slope or curvature assessments (Table 4.2).

	Increase of moving window width from	Shift of most sensitive magnitude by n incremental steps						
		n ≤ -3	-2	-1	0	1	2	≥ 3
Slope	2 to 3	45	0	496	502	0	7	43
	2 to 4	35	382	264	335	0	5	72
	3 to 4	11	37	536	411	51	0	47
Curvature	2 to 3	116	10	308	584	10	2	63
	2 to 4	137	234	191	445	13	12	61
	3 to 4	70	22	346	538	70	8	39
Floodplain Sensitivity Index	2 to 3	106	9	362	551	8	4	53
	2 to 4	98	286	224	416	1	12	56
	3 to 4	40	30	408	508	71	3	33
	simulations							

Table 4.1: Shift of most sensitive magnitude due to the increase of the moving window width. Analysis of the frequency of shifts in the most sensitive magnitude across impacts and floodplains (n = 1093) when the width of the moving window is expanded from two to three or four incremental steps, and from three to four. In the column headers right of the vertical line, negative values denote a shift to lower magnitudes, "0" means no change in magnitude, and positive numbers indicate a shift to higher magnitudes.

Moving window	FSI = Slope FSI ≠ Curv.	FSI ≠ Slope FSI = Curv.	FSI ≠ Slope FSI ≠ Curv.	Total
2 scenarios	103	202	29	334
3 scenarios	101	221	36	358
4 scenarios	112	234	48	394

Table 4.2: Number of cases out of 1093 in which the magnitude with the highest value of slope (Equation 4.8), curvature (Equation 4.9), or either do not agree with the magnitude with the highest value of the floodplain sensitivity index FSI (Equation 4.10).

4.3.4 Spatial distribution of floodplain sensitivity

Figure 4.6 indicates for every floodplain in which third of the magnitude spectrum the FSI, with window width of three simulations, is maximized for affected buildings and people, damage on buildings and flooded volume (see Figure 4.4: A = lower third; B = middle third; C = upper third of the spectrum). There is no clear pattern of regions or rivers with high values in the same part of the magnitude spectrum. In most cases, at least one impact type has maximum sensitivity in a different magnitude range, and results cannot be aggregated for multiple sections of the same river.

Moreover, Figure 4.7 indicates the maximum sensitivity value according to the FSI in every third of the magnitude spectrum. The maps support the findings in Section 4.3.2 that critical thresholds are shifted to the upper range with subsequent strongly increasing impact curves, leading to higher sensitivities as is the case for linear and convex exposure curves.

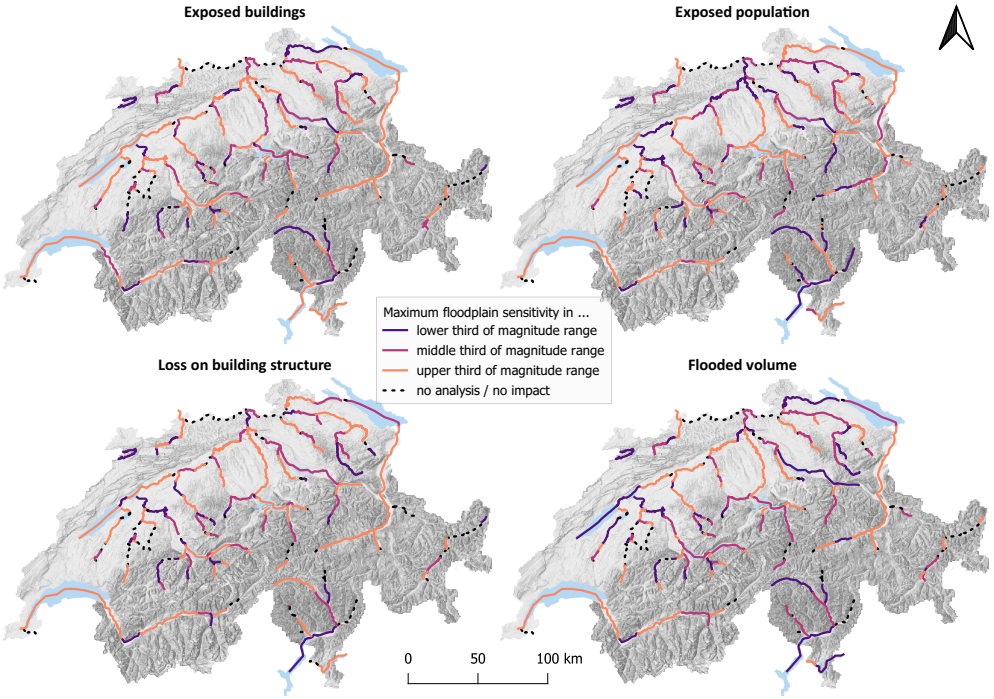

Fig. 4.6: Location of the highest value for FSI (Equation 4.10) based on a moving window spanning three simulations for ranges (lower, medium, upper third) in the magnitude spectrum of the modelled floodplains. For instance, orange lines indicate that the highest sensitivity according to the FSI is in the upper third of the magnitude spectrum.

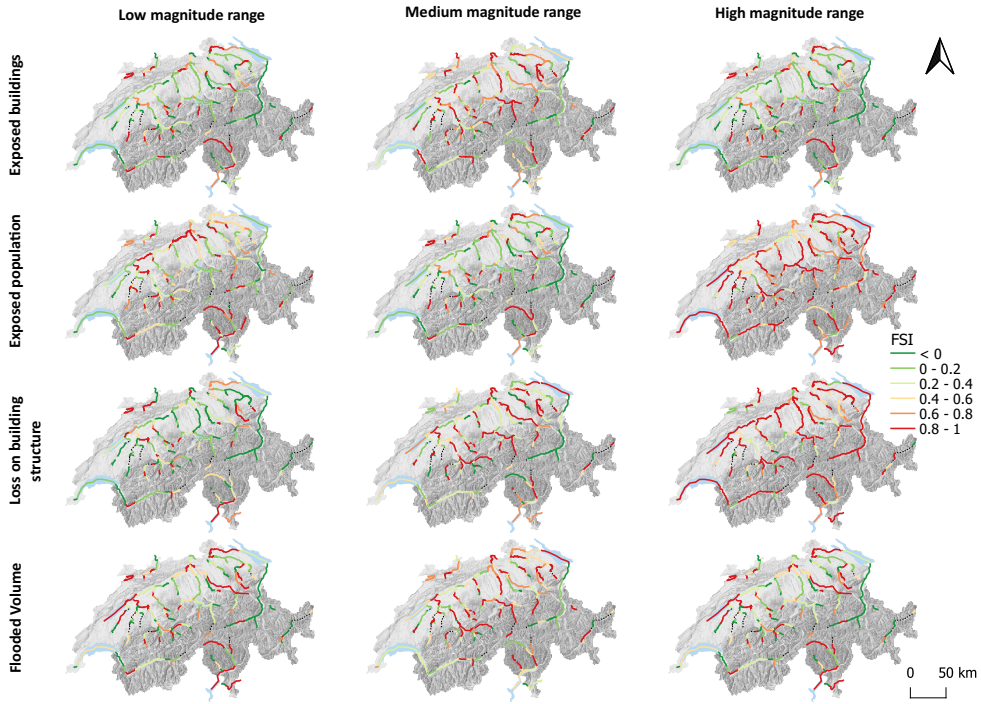

Fig. 4.7: Maximum FSI (Equation 4.10, windows spanning three simulations) values in the lower, medium and upper third (columns) of the magnitude spectrum for each impact type (rows).

4.4 Discussion

The impact curve summarizes the interaction between the hydrogeomorphological characteristics of a floodplain and the built environment. The goal of this study was to find a way to quantitatively locate sensitive ranges on the impact curves for the floodplains of the main rivers and lakes in Switzerland. The solution should help resolve two main issues in flood risk management: hydrometeorological uncertainties in impact-based warnings of floods, such as the magnitude range given by different members in a flood forecast, and increases in the frequency of certain flood magnitudes due to climate change and its uncertainties. We define the floodplain sensitivity index (FSI) by considering slope, representing the rate of change, and curvature, indicating the change in the rate of change. By considering both slope and curvature normalized to the maximum values observed along the impact curve, the FSI offers consolidated information on the floodplain's responsiveness or susceptibility to changes in specific flood magnitude ranges. We analyze the sensitivity of this index to moving windows spanning two, three, and four simulations, and we apply the index to various impact types: flooded area and volume, exposure of buildings, population and workplaces, and damage to household contents and buildings.

4.4.1 Spatial patterns and impact type characteristics

Floodplain sensitivity varies along the major rivers and lakes of Switzerland. No spatial pattern is evident that would enable the characterization of larger regions by the sensitivity of impacts to changes in magnitude. Neither rivers nor any other regional features exhibit consistent sensitivity patterns, either in the occurrence of the most critical threshold in the impact curve (lower, middle and upper third, Figure 4.6) or in high sensitivity levels according to the FSI (Figure 4.7). This is also supported by Figure 4.4 (see also Appendix 4.B). It demonstrates that when dividing the magnitude spectrum into three parts and assigning floodplains to these by the most sensitive threshold, a considerable number of the 179 floodplains analyzed are assigned to each part (A: 17–32%, B: 23–29%, C: 35–47%, no impact: 6-22% of all floodplains, depending on impact type). In the current climate the highest magnitude in 79 river sections with gauging stations was mostly observed in the middle range B (37 = 47%) and the lower range A (26 = 33%). With climate-change, the upper part of the magnitude spectrum (C, 16 observations = 20%) might become more relevant. Even though we attempt to condense the impact curves within each part for all impact types by calculating various quantiles (0.1, 0.25, 0.5, 0.75, 0.9), examples of impact curves, such as the one illustrated for the Emme River at Burgdorf, demonstrate that both convex and concave shapes of the impact curve can be present within one floodplain and differ between impact types. Besides confirming the nonlinearity of impact curves observed in other studies (e. g., Devitt et al., 2023; Zischg & Bermúdez, 2020), the shape of the curves and therefore their interpretation are specific to floodplain and impact type.

Additionally, we analyzed whether the magnitudes with the highest FSI correlate (Spearman Rank Correlation) across all impact types and moving windows spanning two, three, or four flood simulations. The damage to household contents may be inferred from the damage to building structures and the exposure of people, as the magnitude of

the highest FSI is strongly correlated (>0.67). This is not surprising, because damage to contents arises largely from building damage and is only applicable to residential buildings.

Flooded area and volume are moderately to strongly correlated (0.54–0.69). Nevertheless, the meaning of the variables is important. Whereas flooded area indicates the expansion, flooded volume also considers flow depth, which is important in regions with retention areas. There, the expansion of the flooded area stops during retention, while the flood volume, and therefore flow depth, continues to increase. This is important for the interpretation of uncertainties, as vulnerability functions for estimating the degree of damage to a building usually use flow depth as input variable (e.g., Dutta et al., 2003; Jonkman et al., 2008; Fuchs et al., 2019; Zischg et al., 2021) and imply an increase in damage even though the number of directly affected buildings remains the same. Flow depth is also relevant to assessing the accessibility of road networks (Pregnolato et al., 2017; Arrighi et al., 2019).

Affected workplaces can in many cases be estimated by the number of affected buildings, the number of people, and to some extent also by building damage. This is most likely because buildings with a large number of workplaces have larger footprints and a higher volume, which in turn lead to higher building values as estimated by m^3 prices given by Röthlisberger et al. (2018). However, a thorough examination of the impact curve for workplaces may serve as a proxy for indirect damage through disruption of business operations, healthcare costs, and infrastructure damage and restoration. Classifying commercial buildings by their major accident potential and vulnerability to various flow depths, such as determining whether a major accident occurs at flow depths of 10 or only at 100 cm, could provide valuable insights.

4.4.2 Practical application in flood risk management

Steep slopes on the impact curve highlight magnitude ranges in which a general increase of impact occurs with an increase of magnitude. Curvature describes the shape of the curve. Positive values indicate an increase of slope over a certain magnitude threshold, a convex shape, whereas negative values describe ranges in which the slope after a threshold is lower than before, a concave shape. By combining both, the FSI provides a critical tool for identifying specific magnitude ranges and thresholds at which uncertainties stemming either from short-term forecasts or long-term climate projections significantly influence impact assessments. High FSI values indicate magnitude ranges where these uncertainties are relevant to the impact, whereas low FSI values signal ranges where such uncertainties have little effect on the perceived impact. Negative FSI values and values around 0.0 indicate magnitude ranges with reduced increase and generally low increase of impact with increase in magnitude. Values above 0.0 and below 0.2 usually indicate low to average sensitivity, whereas values between 0.2 and 0.5 can indicate strong floodplain sensitivity. Values above 0.5 indicate highly sensitive magnitude ranges. Multiple thresholds can occur within one floodplain. The normalization of slope and curvature with the maximum values in a floodplain poses the challenge that all FSI values are to be interpreted relative to the highest values in the magnitude spectrum. If very strong curvature and slope located in the upper part of the magnitude spectrum lead to a high FSI, increases in the lower part will thus be only moderate, even though their

impact might be substantial in absolute terms, for instance the number of additionally exposed people. Therefore, providing information on absolute numbers and providing a map with potential impacts is indispensable as shown by Mosimann et al. (2023).

There are also positive aspects of this supposed disadvantage: A forecasted magnitude range that predominantly displays low FSI values but demonstrates a significant absolute difference indicates the presence of a critical threshold within the human–environment system beyond the anticipated magnitude range. For instance, Apel et al. (2022) observed that the forecasted water level of the Ahr River (Germany) for the flood event in 2021 was significantly lower than the actual measurement. This discrepancy was likely due to the backwater effects caused by a bridge, a factor that the hydrological model failed to incorporate. Fischer et al. (2021) states that climate-induced extremes "have substantial impacts due to a tendency to adapt to the highest intensities, and no higher, experienced during a lifetime." These examples underscore the importance of considering unforeseen factors in flood forecasting and the potential value of extending our analytical horizon beyond current expectations. Notably, hydrodynamic modelling, and therefore the assessment of hazard, exposure, and damage, is not free from uncertainties (e.g., Mosimann et al., 2023; Neal et al., 2015). Damage estimations in particular can vary depending on the vulnerability function used (e. g., Keller et al., 2019; Zischg et al., 2021). However, flood pathways and river capacities are largely decided by topographical constraints, with the consequence that hazard derivation is more deterministic and robust when using highly resolved elevation models (Horritt & Bates, 2001; Savage et al., 2016).

We tested further alternatives to calculate the FSI. Firstly, instead of using the maximum-normalized values of slope and curvature, the non-normalized values of each derivative can simply be averaged. The issue this approach raised was that it mainly attributed regions with comparably low exposure with very high sensitivities (MAUP): A flood that damages 2 buildings in a small area with 10 buildings impacts 20%. In larger areas with 1000 buildings, 200 need to be damaged to reach the same ratio. Secondly, we tested whether a limitation on the X-axis to the magnitudes that impacted the considered variables would be more meaningful. We decided not to follow this pathway: because the definitions of the limits of magnitude spectrum are different for each floodplain, the flood ranges are no longer comparable. As mentioned, the upper limit is optimally defined by the probable maximum flood, whereas the lower limit should also be defined by a comparable method. The definition of the lower limit by a magnitude with a specific return period can support comparability across floodplains, but we emphasize that it is paradoxical to fully interpret climate change impacts from statistical values that will no longer be valid in a warmer climate, when extreme events will occur more frequently. Additionally, return periods derived from extreme value statistics are not meaningful during warnings because a hydrometeorological forecast is not fully stochastic. Thirdly, we failed to develop a meaningful sensitivity index with absolute values. We tried to calculate slope, for instance for the number of additionally exposed people per m^3/s increase in peak discharge, but as 1 m^3/s has a very different meaning for each river, the interpretation of sensitivity is rather difficult and is no longer comparable across rivers and lakes. A potential improvement to the index might involve subtracting the curvature from the slope, followed by normalization to their maximum values, to create a more comprehensive measure. In this case, 0 would mean that the slope of the impact curve decreases with the same value as increases or that there was a slope of 0 before

and after a magnitude.

4.4.2.1 Impact-based warning

Hydrometeorological forecast uncertainties play a major role in warnings for floods, because they define the range of potential river discharges and lake levels to be expected. Communicating these uncertainties is essential to increase the awareness of false alarms and misses in warnings (Manzey et al., 2014). Frequent false alarms and misses harm public perception and trust in future warnings. Whereas false alarms potentially lead to a disregard of alerts in future (Potter et al., 2021), misses lead to debates on the reliability of forecasting models and missed responsibilities in the decision-making process (Fekete & Sandholz, 2021). Either of them can reduce the credibility of warning systems. To prevent this from happening, incorporating uncertainties into warning systems and communication strategies is crucial to sensitizing decision makers and the general public effectively.

We illustrate a possible application of our method with two hypothetical forecasts depicted as ranges A and B in Figure 4.1. If range A corresponds to the uncertainty band of a hydrometeorological forecast, the FSI close to 1 (see Figure 4.3) indicates that the impacts increase substantially within the forecasted range. This indicates that the forecasted range includes a critical threshold. The high impact uncertainty indicated by a high FSI underscores the need for cautious and thoughtful warnings. In range B, the hydrometeorological forecast covers a low FSI, meaning that the potential impact is not very sensitive to variations in the discharge within the uncertainty limits. However, whichever discharge of the forecast ensemble occurs in range B, it exceeds the threshold shown in range A. As the difference of impact within range B is small, more precise warnings can be formulated to mitigate the specific impact resulting from exceeding the threshold shown in range A.

4.4.2.2 Climate change

Similar to hydrometeorological uncertainties, the FSI aids in contextualizing the uncertainty associated with estimating future flood events. For instance, considering uncertainties of a 100-year flood on current measurements (assumed as range A in Figure 4.1) and on future climate projection (assumed as range B), we observe that today's 100-year flood has a higher uncertainty of impact than does its future counterpart, because impact is less sensitive to increases in discharge (low FSI). This implies that mitigation measures for such a 100-year flood can be defined more precisely, as the potential impacts are less sensitive for the future range of uncertainty. Conversely, large impact sensitivity (high FSI) indicates large uncertainty in the range of projected future magnitudes.

Additionally, the index provides a valuable tool for identifying severe impacts from climate-change-induced magnitude increases. When the best estimate of a 100-year flood today is compared with the future projection, the highest value of the FSI within the range spanned by these two magnitudes offers insights into whether the magnitude increase contains a critical threshold that could trigger significant changes in flood risk.

4.5 Conclusions

This study introduces the floodplain sensitivity index (FSI) derived from flood magnitude–impact relationships (impact curves) and offers a comprehensive bottom-up approach for flood risk assessment. The FSI provides valuable insights for two important applications: (i) assessing climate change sensitivity and (ii) understanding the relevance of hydrometeorological uncertainties in impact-based forecast and warning services (IBFWS). This dual perspective underscores the intrinsic link between short-term flood forecasting uncertainty and uncertainty associated with projects of the long-term shifts in flood magnitudes due to climate change, marking them as two sides of the same coin.

The FSI highlighs critical flood magnitude thresholds, where slight variations in flood magnitude lead to substantial difference in impacts, combining information on the slope and the curvature of the impact curve. We use the FSI to analyze the sensitivity of various impact types across 179 floodplains in Switzerland. We investigate flood magnitudes in a spectrum roughly between the 10 to 30 year return period and estimations of probable maximum floods. When analyzing floodplain sensitivity to the affected population, we find that in 36 floodplains (20.1%), the highest sensitivity is in the lower third of the magnitude spectrum, and in 44 floodplains (24.6%), it is in the middle third. Among the 79 floodplains with gauging stations, the highest observed magnitudes for 37 (47%) are in the middle third, and for 16 (20%), in the upper third. This highlights the varied sensitivity of floodplains and the importance of considering sensitive thresholds in the upper third of the magnitude spectrum, as climate change projections anticipate an increase of flood magnitudes in Switzerland.

The weak to moderate correlation of the most critical magnitude thresholds across impact types (flooded area and volume, number of affected buildings, people and workplaces, damages to buildings and contents) suggests that information of impact sensitivity needs to be tailored to the priorities of the users. Users interested in, for instance, business interruption require information about affected workplaces, as critical thresholds of flooded area, population, and building damage may be defined at other magnitudes.

The absence of consistent spatial patterns of floodplain sensitivity in segmented rivers, and administrative, geographic, and topographic regions emphasize that each floodplain has specific nonlinear shape characteristics of the impact curves. This requires the development of multifaceted flood mitigation strategies designed to minimize both the impacts of flood events through IBFWS, as well as addressing the overarching trends driven by climate change.

The study shows the potential of integrating FSI insights with absolute impact measures to enhance the precision of flood warnings and to inform climate change mitigation efforts effectively. The FSI may become an essential tool to communicate the sensitivity of impacts in flood risk management, capable of supporting policy and decision-making processes towards more resilient and adaptable floodplain management practices.

Appendix

4.A Dependency of damage to building value and flow depth

Figure 4.8 illustrates the flow-depth-dependent damage to four buildings with different building values estimated using the methods described in Section 4.2.2 (left), and the proportion of content damage in the total damage (right). The importance of content damage decreases with increasing flood magnitude and with more valuable buildings. In summary, the role of household contents is less prominent when there is a substantial structural damage to a building. As this relationship is not linear, signals may differ between floodplains when looking at the combination or just on one of each damage type. The largest differences can be expected for floodplains where buildings with comparatively low values are exposed from one scenario to the next, or where the flow depths of newly exposed buildings are rather low. This is exemplified on the right of Figure 4.8: Assume there are two buildings, one with a value of CHF 0.5M and the other with a value of CHF 1.5M, and both are flooded with a flow depth of 0.5 meters. The proportion of total damage due to contents is more than 25% in the building with a lower value, whereas the proportion of total damage due to contents for the more expensive building is less than 20%.

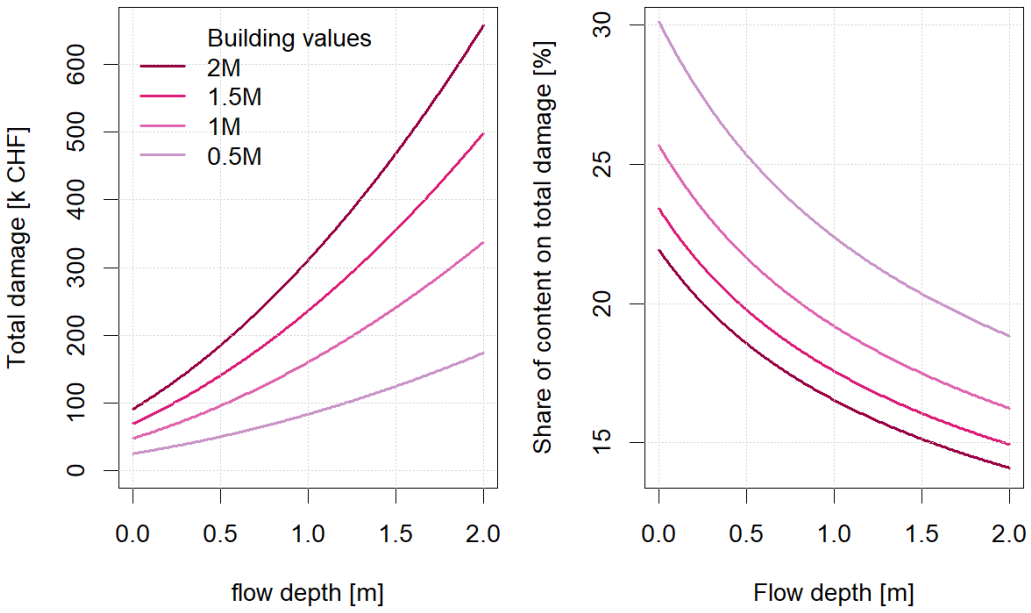

Fig. 4.8: Total building damage (left) including damage to building structure estimated with a regionally calibrated vulnerability function (Zischg et al., 2021) and damage to household contents estimated with a model for building damage (Mosimann et al., 2018), and content damage as a proportion of the total damage to a building (right). The lines represent buildings with different building values (0.5M, 1M, 1.5M and 2M).

4.B Impact curves for structural and content damage on buildings, workplaces, flooded area, and volume

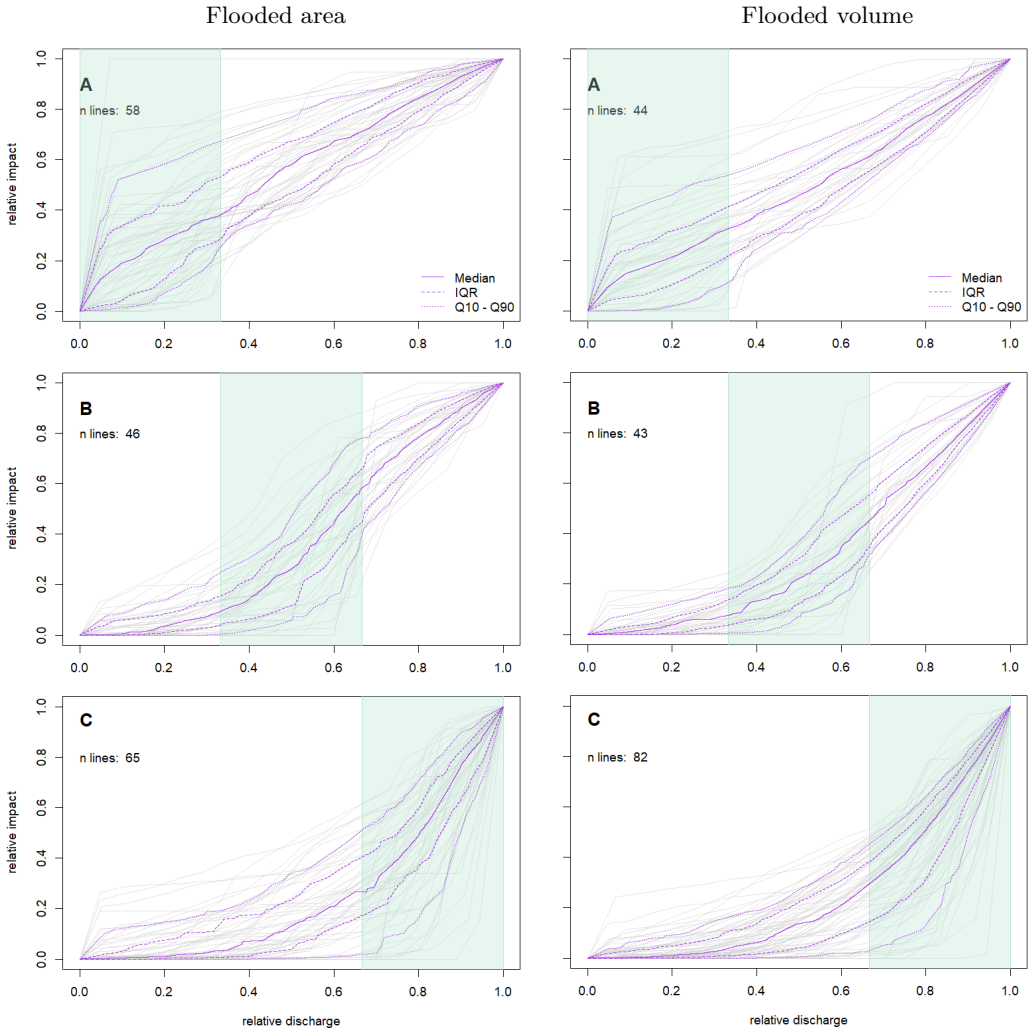

Fig. 4.9: Impact curves for flooded area (left, n = 169) and flooded volume (right, n = 169). Purple lines indicate median (straight), interquartile range (dashed) and range from 10th to 90th quantile. A: Maximum floodplain sensitivity (Equation 4.10, three scenarios considered) located in lower third of the magnitude spectrum. B: Maximum sensitivity located in middle third of the magnitude spectrum. C: Maximum sensitivity located in upper third of the magnitude spectrum.

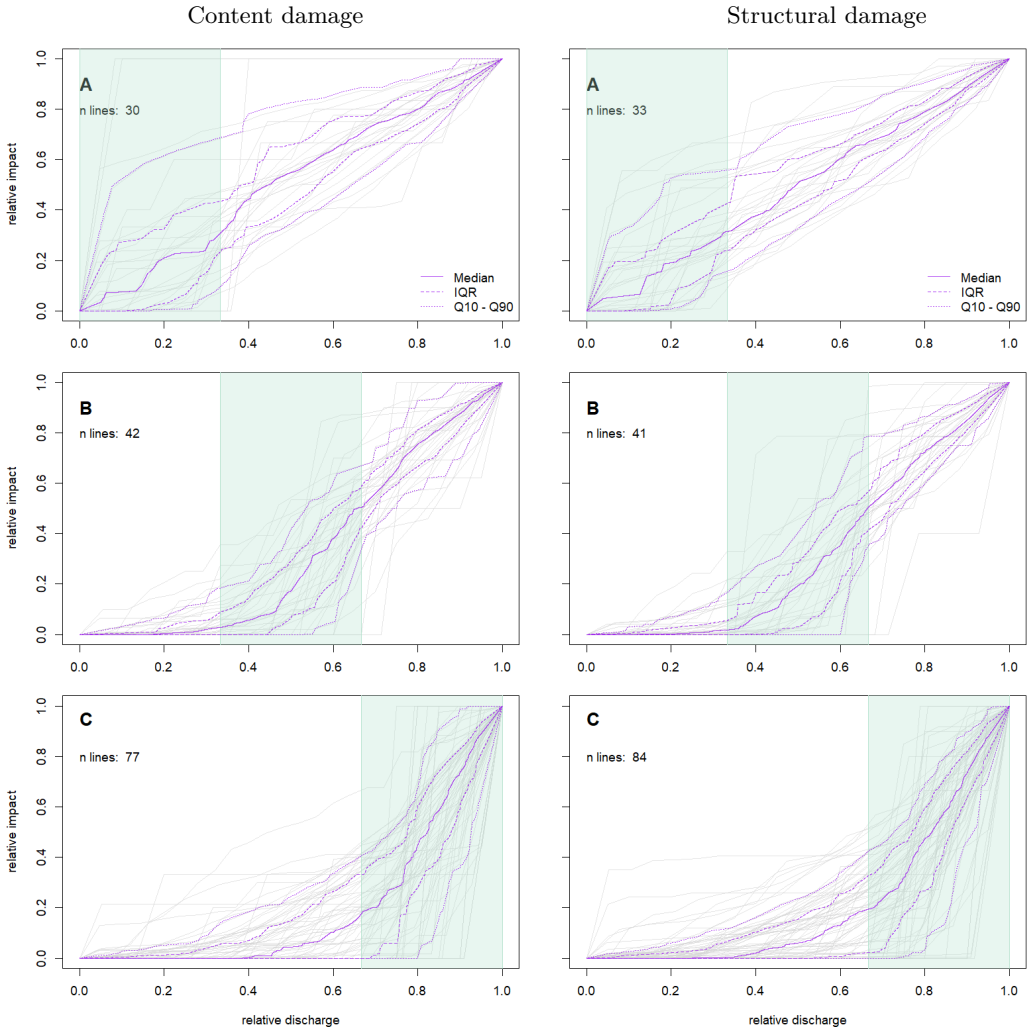

Fig. 4.10: Impact curves for content damage (left, n = 149) and building structure damage (right, n = 158). Purple lines indicate median (straight), interquartile range (dashed) and range from 10th to 90th quantile. A: Maximum floodplain sensitivity (Equation 4.10, three scenarios considered) located in lower third of the magnitude spectrum. B: Maximum sensitivity located in middle third of the magnitude spectrum. C: Maximum sensitivity located in upper third of the magnitude spectrum.

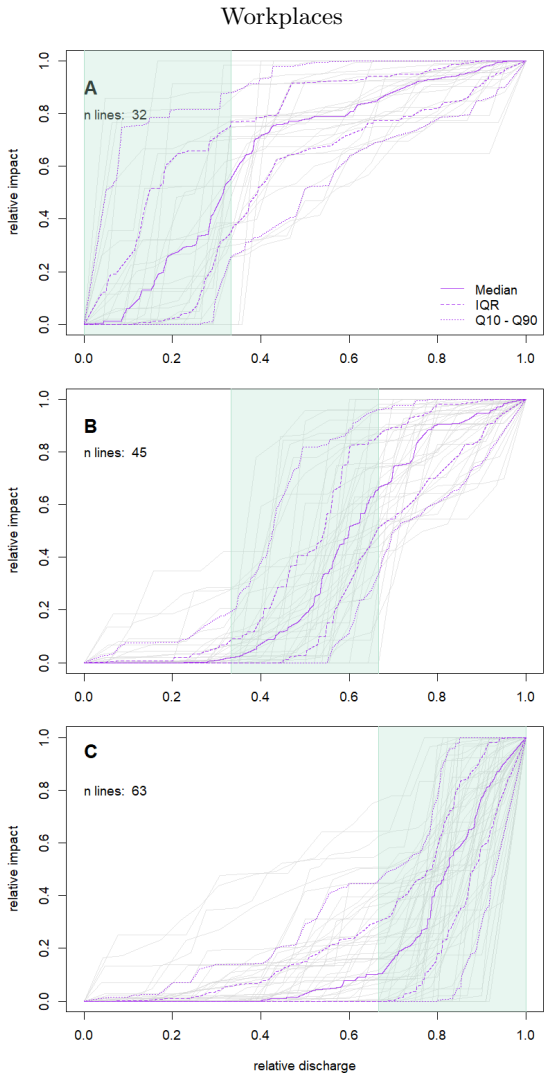

Fig. 4.11: Impact curves for workplaces (n = 140). Purple lines indicate median (straight), interquartile range (dashed) and range from 10th to 90th quantile. A: Maximum floodplain sensitivity (Equation 4.10, three scenarios considered) located in lower third of the magnitude spectrum. B: Maximum sensitivity located in middle third of the magnitude spectrum. C: Maximum sensitivity located in upper third of the magnitude spectrum

References

Alfieri, L., Feyen, L., Dottori, F., & Bianchi, A. (2015). Ensemble flood risk assessment in europe under high end climate scenarios. *Global Environmental Change*, *35*, 199–212. doi:10.1016/j.gloenvcha.2015.09.004.

Apel, H., Vorogushyn, S., & Merz, B. (2022). Brief communication: Impact forecasting could substantially improve the emergency management of deadly floods: case study july 2021 floods in germany. *Natural Hazards and Earth System Science*, *22*, 3005–3014. doi:10.5194/nhess-22-3005-2022.

ARE (2022). Building zones switzerland. Federal Office for Spatial Development ARE. URL: https://www.are.admin.ch/are/de/home/raumentwicklung-und-raumplanung/grundlagen-und-daten/bauzonenstatistik-schweiz.html. Last accessed: 04.04.2024.

Arnell, N. W., & Gosling, S. N. (2016). The impacts of climate change on river flood risk at the global scale. *Climatic Change*, *134*, 387–401. doi:10.1007/s10584-014-1084-5.

Arrighi, C., Pregnolato, M., Dawson, R. J., & Castelli, F. (2019). Preparedness against mobility disruption by floods. *The Science of the total environment*, *654*, 1010–1022. doi:10.1016/j.scitotenv.2018.11.191.

Bermúdez, M., Ntegeka, V., Wolfs, V., & Willems, P. (2018). Development and comparison of two fast surrogate models for urban pluvial flood simulations. *Water Resources Management*, *32*, 2801–2815. doi:10.1007/s11269-018-1959-8.

Bhola, P. K., Leandro, J., & Disse, M. (2020). Building hazard maps with differentiated risk perception for flood impact assessment. *Natural Hazards and Earth System Science*, *20*, 2647–2663. doi:10.5194/nhess-20-2647-2020.

Canton of Aargau (2014). DTM 0.5-Meter Raster. Canton of Aargau, Abteilung Wald. URL: https://www.geocat.ch/geonetwork/srv/api/records/e8f0247a-f139-4535-97f6-0d4b6cad302f-6571?language=all. Last accessed: 04.04.2024.

Canton of Bern (2014). Digitales Terrainmodell LIDAR 50cm. Canton of Bern, Amt für Wald KAWA. URL: https://www.agi.dij.be.ch/de/start/geoportal/geodaten/detail.html?type=geoproduct&code=LDTM50CM. Last accessed: 04.04.2024.

Canton of Lucerne (2012). Digitales Terrainmodell (DTM) 2012, 0.5m-Raster. Canton of Lucern, Dienststelle Raum und Wirtschaft, Abteilung Geoinformation. URL: https://daten.geo.lu.ch/produkt/dtm1205m_ds_v1. Last accessed: 04.04.2024.

Canton of Solothurn (2014). Digitales Terrainmodell (DTM) 2014. Canton of Solothurn, Amt für Geoinformation. URL: https://data.geo.so.ch/?filter=ch.so.agi.lidar_2014.dtm. Last accessed: 04.04.2024.

Canton of Vaud (2006). Modèles altimétriques lidar. Canton of Vaud. URL: https://www.vd.ch/themes/territoire-et-construction/cadastre-et-geoinformation/geodonnees/altimetrie-lidar/technologie-lidar/lidar-2001-2006. Last accessed: 04.04.2024.

Canton of Zug (2013). Höhenmodell der amtlichen Vermessung 2013 auf Basis "LIDAR". Canton of Zug, Amt für Grundbuch und Geoinformation, Abteilung Vermessung. URL: https://zg.ch/de/planen-bauen/geoinformation/amtliche-vermessung. Last accessed: 04.04.2024.

Canton of Zurich (2014). Digitales Terrainmodell (DTM) - 2014. Canton of Zurich, Amt für Raumentwicklung - Geoinformation. URL: https://www.stadt-zuerich.ch/geodaten/download/298. Last accessed: 04.04.2024.

Casteel, M. A. (2016). Communicating increased risk: An empirical investigation of the national weather service's impact-based warnings. *Weather, Climate, and Society*, *8*, 219–232. doi:10.1175/WCAS-D-15-0044.1.

Clarke, B., Otto, F., Stuart-Smith, R., & Harrington, L. (2022). Extreme weather impacts of climate change: an attribution perspective. *Environmental Research: Climate*, *1*, 012001. doi:10.1088/2752-5295/ac6e7d.

Cloke, H. L., & Pappenberger, F. (2009). Ensemble flood forecasting: A review. *Journal of Hydrology*, *375*, 613–626. doi:10.1016/j.jhydrol.2009.06.005.

Cloke, H. L., Wetterhall, F., He, Y., Freer, J. E., & Pappenberger, F. (2013). Modelling climate impact

on floods with ensemble climate projections. *Quarterly Journal of the Royal Meteorological Society*, *139*, 282–297. doi:10.1002/qj.1998.

Contreras, M. T., Gironás, J., & Escauriaza, C. (2020). Forecasting flood hazards in real time: a surrogate model for hydrometeorological events in an andean watershed. *Natural Hazards and Earth System Science*, *20*, 3261–3277. doi:10.5194/nhess-20-3261-2020.

Conway, D., Nicholls, R. J., Brown, S., Tebboth, M. G. L., Adger, W. N., Ahmad, B., Biemans, H., Crick, F., Lutz, A. F., de Campos, R. S., Said, M., Singh, C., Zaroug, M. A. H., Ludi, E., New, M., & Wester, P. (2019). The need for bottom-up assessments of climate risks and adaptation in climate-sensitive regions. *Nature Climate Change*, *9*, 503–511. doi:10.1038/s41558-019-0502-0.

Devitt, L., Neal, J., Coxon, G., Savage, J., & Wagener, T. (2023). Flood hazard potential reveals global floodplain settlement patterns. *Nature communications*, *14*, 2801. doi:10.1038/s41467-023-38297-9.

Dutta, D., Herath, S., & Musiake, K. (2003). A mathematical model for flood loss estimation. *Journal of Hydrology*, *277*, 24–49. doi:10.1016/S0022-1694(03)00084-2.

Faranda, D., Bourdin, S., Ginesta, M., Krouma, M., Noyelle, R., Pons, F., Yiou, P., & Messori, G. (2022). A climate-change attribution retrospective of some impactful weather extremes of 2021. *Weather and Climate Dynamics*, *3*, 1311–1340. doi:10.5194/wcd-3-1311-2022.

Fekete, A., & Sandholz, S. (2021). Here comes the flood, but not failure? lessons to learn after the heavy rain and pluvial floods in germany 2021. *Water*, *13*, 3016. doi:10.3390/w13213016.

Felder, G., Paquet, E., Penot, D., Zischg, A., & Weingartner, R. (2019). Consistency of extreme flood estimation approaches. *Journal of Hydrologic Engineering*, *24*. doi:10.1061/(ASCE)HE.1943-5584.0001797.

Felder, G., Zischg, A., & Weingartner, R. (2017). The effect of coupling hydrologic and hydrodynamic models on probable maximum flood estimation. *Journal of Hydrology*, *550*, 157–165. doi:10.1016/j.jhydrol.2017.04.052.

Fischer, E. M., Sippel, S., & Knutti, R. (2021). Increasing probability of record-shattering climate extremes. *Nature Climate Change*, *11*, 689–695. doi:10.1038/s41558-021-01092-9.

FOEN (2021). Stations and data. Federal Office for the Environment FOEN. URL: https://www.hydrodaten.admin.ch/en/stations-and-data.html. Last Accessed: 04.04.2024.

FOEN (2022). Naturgefahren: Flussvermessung. Federal Office for the Environment FOEN. URL: https://www.bafu.admin.ch/bafu/de/home/themen/naturgefahren/fachinformationen/naturgefahrensituation-und-raumnutzung/gefahrengrundlagen/naturgefahren--flussvermessung.html. Last accessed: 04.04.2024.

FOEN (2024a). Forecasts and flood alerts: stations with forecasts. Federal Office for the Environment FOEN. URL: https://www.hydrodaten.admin.ch/en/messstationen-vorhersage. Last accessed: 04.04.2024.

FOEN (2024b). Rivers and lakes: Discharge and water level. Federal Office for the Environment FOEN. URL: https://www.hydrodaten.admin.ch/de/seen-und-fluesse/messstationen-zustand. Last accessed: 04.04.2024.

FSO (2020). Statistik der Unternehmensstruktur. Federal Statistical Office FSO. URL: https://www.bfs.admin.ch/bfs/de/home/statistiken/industrie-dienstleistungen/erhebungen/statent.html. Last accessed: 04.04.2024.

FSO (2021). Buildings and Dwellings statistic. Federal Statistical Office FSO. URL: https://www.bfs.admin.ch/bfs/en/home/statistics/construction-housing/surveys/gws2009.html. Last accessed: 04.04.2024.

Fuchs, S., Heiser, M., Schlögl, M., Zischg, A., Papathoma-Köhle, M., & Keiler, M. (2019). Short communication: A model to predict flood loss in mountain areas. *Environmental Modelling & Software*, *117*, 176–180. doi:10.1016/j.envsoft.2019.03.026.

Horritt, M., & Bates, P. (2001). Effects of spatial resolution on a raster based model of flood flow. *J. Hydrol.*, *253*, 239–249. doi:10.1016/S0022-1694(01)00490-5.

Intergovernmental Panel on Climate Change (2021). *Climate Change 2021: The physical science basis : summary for policymakers : working group I contribution to the sixth Assessment report of the Intergovernmental Panel on Climate Change*. Geneva, Switzerland: Intergovernmental Panel on Climate Change.

Jonkman, S. N., Bočkarjova, M., Kok, M., & Bernardini, P. (2008). Integrated hydrodynamic and economic modelling of flood damage in the netherlands. *Ecological Economics*, *66*, 77–90. doi:10.1016/j.ecolecon.2007.12.022.

Kaltenberger, R., Schaffhauser, A., & Staudinger, M. (2020). "what the weather will do" – results of a survey on impact-oriented and impact-based warnings in european nmhss. *Advances in Science and Research*, *17*, 29–38. doi:10.5194/asr-17-29-2020.

Kelder, T., Wanders, N., van der Wiel, K., Marjoribanks, T. I., Slater, L. J., Wilby, R. L., & Prudhomme, C. (2022). Interpreting extreme climate impacts from large ensemble simulations—are they unseen or unrealistic? *Environmental Research Letters*, *17*, 044052. doi:10.1088/1748-9326/ac5cf4.

Keller, L., Zischg, A. P., Mosimann, M., Rössler, O., Weingartner, R., & Martius, O. (2019). Large ensemble flood loss modelling and uncertainty assessment for future climate conditions for a swiss pre-alpine catchment. *The Science of the total environment*, *693*, 133400. doi:10.1016/j.scitotenv.2019.07.206.

Manzey, D., Gérard, N., & Wiczorek, R. (2014). Decision-making and response strategies in interaction with alarms: the impact of alarm reliability, availability of alarm validity information and workload. *Ergonomics*, *57*, 1833–1855. doi:10.1080/00140139.2014.957732.

Meléndez-Landaverde, E. R., Werner, M., & Verkade, J. (2020). Exploring protective decision–making in the context of impact–based flood warnings. *Journal of Flood Risk Management*, *13*. doi:10.1111/jfr3.12587.

Merwade, V., Olivera, F., Arabi, M., & Edleman, S. (2008). Uncertainty in flood inundation mapping: Current issues and future directions. *Journal of Hydrologic Engineering*, *13*, 608–620. doi:10.1061/(ASCE)1084-0699(2008)13:7(608).

Mosimann, M., Frossard, L., Keiler, M., Weingartner, R., & Zischg, A. (2018). A robust and transferable model for the prediction of flood losses on household contents. *Water*, *10*, 1596. doi:10.3390/w10111596.

Mosimann, M., Kauzlaric, M., Schick, S., Martius, O., & Zischg, A. P. (2023). Evaluation of surrogate flood models for the use in impact-based flood warning systems at national scale. *Environmental Modelling & Software*, (p. 105936). doi:10.1016/j.envsoft.2023.105936.

Mülchi, R., Rössler, O., Schwanbeck, J., Weingartner, R., Martius, O. (). Neue hydrologische szenarien für die schweiz.. Im Auftrag des Bandesamts für Umwelt. doi:10.7892/boris.148715.

Neal, J. C., Odoni, N. A., Trigg, M. A., Freer, J. E., Garcia-Pintado, J., Mason, D. C., Wood, M., & Bates, P. D. (2015). Efficient incorporation of channel cross-section geometry uncertainty into regional and global scale flood inundation models. *Journal of Hydrology*, *529*, 169–183. doi:10.1016/j.jhydrol.2015.07.026.

Potter, S., Harrison, S., & Kreft, P. (2021). The benefits and challenges of implementing impact-based severe weather warning systems: Perspectives of weather, flood, and emergency management personnel. *Weather, Climate, and Society*, *13*, 303–314. doi:10.1175/WCAS-D-20-0110.1.

Potter, S. H., Kreft, P. V., Milojev, P., Noble, C., Montz, B., Dhellemmes, A., Woods, R. J., & Gauden-Ing, S. (2018). The influence of impact-based severe weather warnings on risk perceptions and intended protective actions. *International Journal of Disaster Risk Reduction*, *30*, 34–43. doi:10.1016/j.ijdrr.2018.03.031.

Pregnolato, M., Ford, A., Wilkinson, S. M., & Dawson, R. J. (2017). The impact of flooding on road transport: A depth-disruption function. *Transportation Research Part D: Transport and Environment*, *55*, 67–81. doi:10.1016/j.trd.2017.06.020.

Röthlisberger, V., Zischg, A., Keiler, M., Lang, M., Klijn, F., & Samuels, P. (2016). Spatiotemporal aspects of flood exposure in switzerland. *E3S Web of Conferences*, *7*, 08008. doi:10.1051/e3sconf/20160708008.

Rothlisberger, V., Zischg, A. P., & Keiler, M. (2017). Identifying spatial clusters of flood exposure to support decision making in risk management. *The Science of the total environment*, *598*, 593–603. doi:10.1016/j.scitotenv.2017.03.216.

Röthlisberger, V., Zischg, A. P., & Keiler, M. (2018). A comparison of building value models for flood risk analysis. *Natural Hazards and Earth System Science*, *18*, 2431–2453. doi:10.5194/nhess-18-2431-2018.

RPF (2015). Hydraulische berechnungen hochrhein. Reigierungspräsidium Freiburg. URL: https://rp.baden-wuerttemberg.de/rpf/sgze/hochrheinkommission/. Last accessed: 04.04.2024.

Savage, J. T. S., Bates, P., Freer, J., Neal, J., & Aronica, G. (2016). When does spatial resolution become spurious in probabilistic flood inundation predictions? *Hydrological Processes*, *30*, 2014–2032. doi:10.1002/hyp.10749.

swisstopo (2013). swissALTI3D. Federal Office of Topography, swisstopo. URL: https://www.swisstopo.admin.ch/de/hoehenmodell-swissalti3d. Last accessed: 04.04.2024.

swisstopo (2023). swissTLM3D. Federal Office of Topography swisstopo. URL: https://www.swisstopo.admin.ch/de/geodata/landscape/tlm3d.html. Last accessed: 04.04.2024.

Vetsch, D., Siviglia, A., Caponi, F., Ehrbar, D., Gerke, E., Kammerer, S., Koch, A., Peter, S., Vanzo, D., Vonwiller, L., Facchini, M., Gerber, M., Volz, C., Farshi, D., Mueller, R., Rousselot, P., Veprek, R., & Faeh, R. (2018). Basement - basic simulation environment for computation of environmental flow and natural hazard simulation, version 2.8.1. Laboratory of Hydraulics, Hydrology and Glaciology VAW, ETH Zurich. URL: https://basement.ethz.ch/. Last accessed: 04.04.2024.

Weyrich, P., Scolobig, A., Bresch, D. N., & Patt, A. (2018). Effects of impact-based warnings and behavioral recommendations for extreme weather events. *Weather, Climate, and Society*, *10*, 781–796. doi:10.1175/WCAS-D-18-0038.1.

World Meteorological Organization (2021). *WMO guidelines on multi-hazard impact-based forecast and warning services: Part II: Putting Multi-hazard IBFWS into Practice* volume no. 1150 of *WMO*. Geneva, Switzerland: World Meteorological Organization.

Xu, X., Wang, Y.-C., Kalcic, M., Muenich, R. L., Yang, Y. E., & Scavia, D. (2019). Evaluating the impact of climate change on fluvial flood risk in a mixed-use watershed. *Environmental Modelling & Software*, *122*, 104031. doi:10.1016/j.envsoft.2017.07.013.

Zischg, A. P., & Bermúdez, M. (2020). Mapping the sensitivity of population exposure to changes in flood magnitude: Prospective application from local to global scale. *Frontiers in Earth Science*, *8*. doi:10.3389/feart.2020.534735.

Zischg, A. P., Felder, G., Mosimann, M., Röthlisberger, V., & Weingartner, R. (2018). Extending coupled hydrological-hydraulic model chains with a surrogate model for the estimation of flood losses. *Environmental Modelling & Software*, *108*, 174–185. doi:10.1016/j.envsoft.2018.08.009.

Zischg, A. P., Röthlisberger, V., Mosimann, M., Profico-Kaltenrieder, R., Bresch, D., Fuchs, S., Kauzlaric, M., & Keiler, M. (2021). Evaluating targeted heuristics for vulnerability assessment in flood impact model chains. *Journal of Flood Risk Management*, *5*, 171. doi:10.1111/jfr3.12736.

5 Interactive web-based tools for the visualization of weather and flood event impacts

5.1 Introduction

Existing web-based tools have shown their potential for communicating flood risks (e.g., Mohanty & Karmakar, 2021; Li & Demir, 2022; Copernicus Emergency Management Service, 2024). Interactive maps and data visualizations can communicate complex flood risk information to a broad audience effectively. They enable users to visualize the impacts of potential flood events in near real time and thus enhance their understanding of vulnerabilities and therefore support the planning of mitigation strategies. However, the consensus is that visualization and communication of flood risks, whether in the context of IBFWS or of climate change, are most effective when developed in a participatory process with the target users of such web tools (e.g., Percival et al., 2020; Attems et al., 2020; Maidl et al., 2021; Lumley et al., 2022).

At the Mobiliar Lab for Natural Risks at the University of Bern since March 2016, I have been involved in the development of several web tools embedded in the Flood-Risk Research Initiative (available online: `https://www.floodrisk.ch/`). This initiative aims to bridge the gap between research and practice by developing web-based solutions to address critical aspects of Swiss flood risk management and integrating these in learning modules that support the transfer from understanding to action. In addition to tasks such as supplying data, offering guidance on concepts, and updating the datasets used in various tools, my primary contributions to this initiative, though not directly related to this thesis, are the basis for know-how in developing web-based visualizations for risk communication. These contributions include

- Prototyping the current version of the Flood Damage Potential tool from the findings in Rothlisberger et al. (2017). This prototype (available at `https://hochwasserrisiko.giub.unibe.ch/`), developed in 2016, is the first tool in a series of subsequent developments and attracted considerable media attention and interest across Switzerland; this attention highlighted the relevance of web tools in communicating flood-risk-related topics.
- Developing the Risk Dynamics tool (`https://risikodynamik.hochwasserrisiko.ch/?l=en`) from Zischg et al. (2018) that for instance is used for teaching in geography lessons at the Burgdorf upper secondary school.

The outreach of both tools, along with all other projects in the Flood-Risk Research Initiative, underscores the importance and effectiveness of web tools in transferring flood risk information. Although the development of these two contributions occurred after the publication of the studies and was relatively straightforward, my work on two other web tools, Flood Dynamics and Risk Sensitivity, was conducted with direct input from potential users during the research process presented in Chapters 3 and 4. The studies

and tools both benefitted from this co-development process. Therefore, the metaphorical bridge should not be understood as one-way, from science to practice; this thesis shows that the participatory development of web tools also facilitates the movement of inductive reasoning from practice back to science. The next section provides a concise overview of my involvement in the development of these tools, their outreach, the lessons learned for potential web-based solutions for IBFWS, and future prospects.

5.2 Tool Flood Dynamics - from precipitation to damage

The title of the Flood Dynamics web tool (available online: `https://flooddynamics.ch/`) indicates its overarching goal: to visualize the spatial and temporal relation between extreme weather patterns and the impacts on the floodplain. This is in line with the title of this thesis. The hydrodynamic simulations for the tool (Section 3.2.4.3) are processed with the model setup developed for the surrogate flood models (Section 3.2.2.2). The evaluation of the surrogate model is benchmarked against the results derived from the model chain used and developed for this tool (Section 3.2.4). The graphical user interface was developed by professional software developers. Besides flood and impact modelling, which included the computation of potential detour traffic, I processed the data outputs of the entire model chain to suit the requirements of an integration into a web-based visualization.

The tool allows users to visualize hindcast weather data on a national scale and, by zooming in, to see floodplain-level flood simulations at hourly resolution (Figure 5.1). Users can choose to display either flow depth or the potential impacts according to the hazard classes defined in Table 3.1 and Figure 3.8. Additionally, clicking on any river section or lake displays a summary of the impacts of the selected weather scenario as a table and a graph. The tool was designed to offer physically plausible scenarios for emergency responder training. The participatory development with target users is described in Munz et al. (2023) with findings that align with those of other studies introduced in this chapter.

The Flood Dynamics tool was published in June 2022, again leading to high media interest: the tool was featured in the "Schweiz Aktuell" program on Schweizer Radio und Fernsehen SRF, the Swiss public broadcasting organization. "Schweiz Aktuell" is a news program that covers topics of national interest. The worst-case scenario of the web tool, corresponding to the weather scenario 03-1000y_05 illustrated in Figure 3.4 with a return period of 1000 years (see 3.2.4.1), was of major interest. This is particularly interesting because after the extreme flood event in Germany in July 2021, discussions and questions arose about whether such an event as the Ahr River flood is also possible in Switzerland. This event has led to a shift in societal perception, extending to authorities and policymakers, from primarily questioning the likelihood of such events to focusing on understanding the worst potential impacts. The tool is also used by the Federal Office for Civil Protection for training of the chiefs of regional crisis management staffs for disaster preparedness, and in exercises organized by the Office for Civil Protection, Sports, and Military Affairs of the Canton of Bern.

However, the participatory process documented by Munz et al. (2023) has shown that target users need information tailored to their needs. In addition to long computational

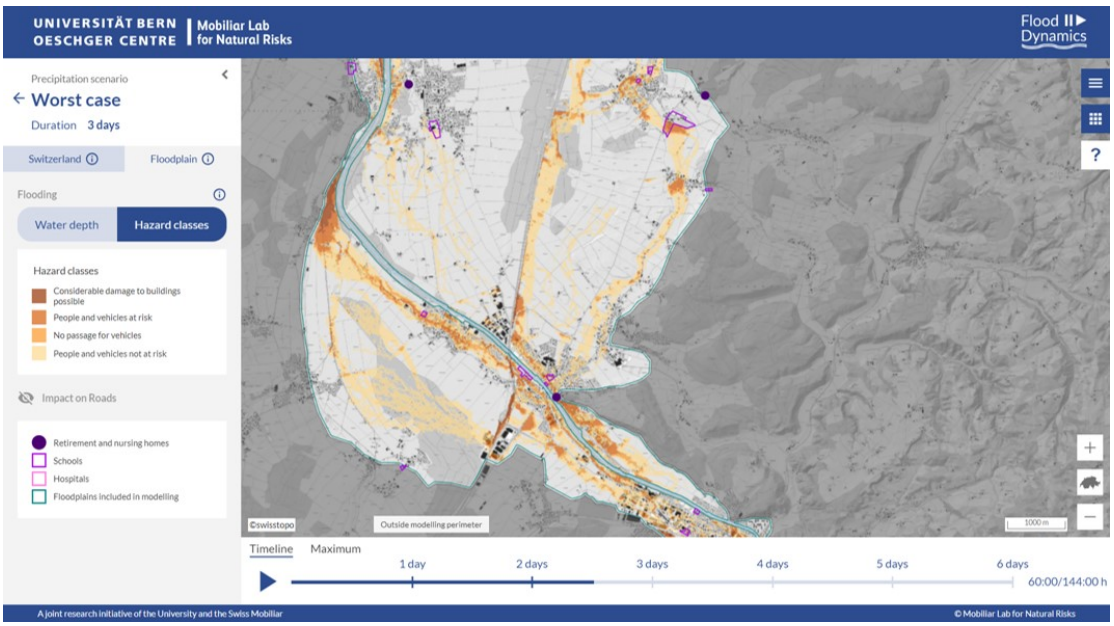

Fig. 5.1: Screenshot of the Flood Dynamics tool showing the worst-case scenario (scenario 03d-1000y_05 in 3.4) after 60 hours simulation time. The hazard classes visualized dynamically are defined in Table 3.1 and Figure 3.8 in Section 3.2.2.3.

time for the transient simulations, the conversion of simulation outputs to the formats used in this web tool requires intensive computing power. Hourly data information stored on triangles first had to be converted to raster format (GeoTIFF), then to an image format (PNG). Finally, the images produced for every hour were converted to WebM video container format. Together with the time for transiently simulating these extreme flood events, where the solution is basically found with the surrogate flood model approach described in Chapter 3, and the time for computing detour roads, this processing does not suit the technical requirements for a web-based IBFWS solution. In any case, the technical efficiency of the postprocessing of flood impact simulations was not the main focus when developing this tool. Nevertheless, the interactive web tool can be used to demonstrate the model chain from a weather forecast simulation to a flood impact simulation. The tool is used to demonstrate a possible extension of flood early warning systems with a cartographic visualization of the areas affected by flood and the impacts of a forecasted weather event.

5.3 Tool Risk Sensitivity - Damaging Floods in Climate Change

The visualization of the impact curves (Figure 4.1) derived from the flood library created for the surrogate flood model (Section 3.2.2) was also prototyped and conceptualized in parallel in the Risk Sensitivity tool (available online: `https://hochwasserrisiko.giub.unibe.ch/up30/?l=en`). Open questions about how the magnitude–impact relationship and specific characteristics of the shape of the impact curve can be derived quantitatively and visualized cartographically finally resulted in the development of the floodplain sensitivity index (FSI) described in Chapter 4. In addition to establishing the scientific

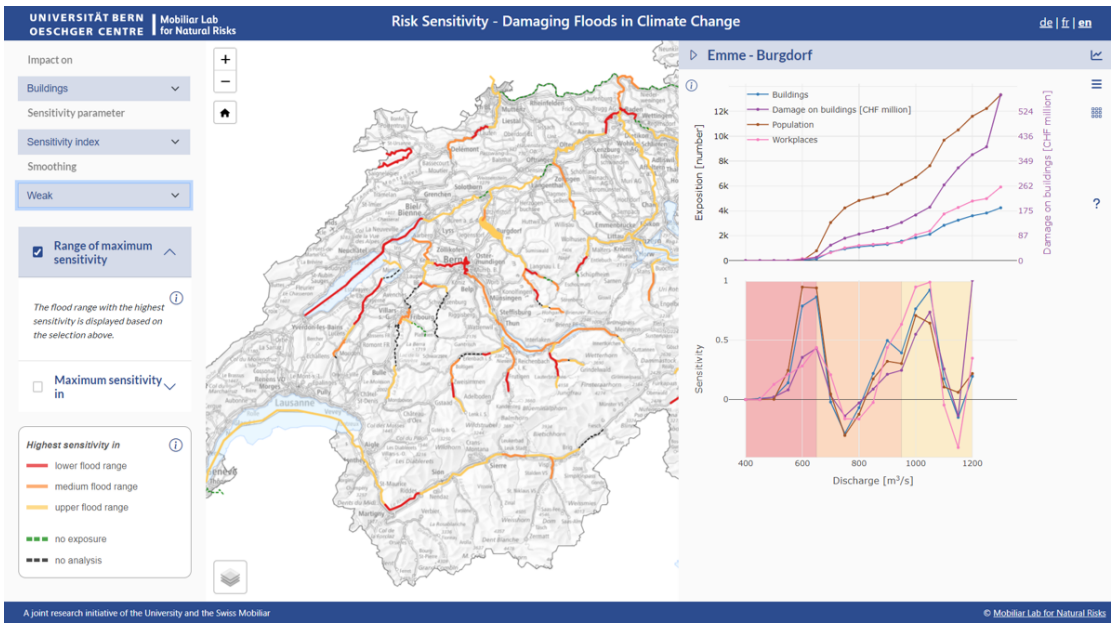

Fig. 5.2: Screenshot of the Risk Dynamics tool. The map shows the same content as presented in Figure 4.6. When clicking on a line indicating a floodplain, the user gains a deeper insight into the impact curves, for instance as shown on the example of the Emme, Burgdorf.

background of this tool, I was also responsible for the front-end development of the user interface, involving HTML, CSS, and JavaScript programming. Both the tool and the study benefitted from its co-development, as internal exchanges and discussions with external experts in flood risk management are included in both. The tool presents the methodology of the FSI mainly in the context of climate change in Swiss flood risk assessment due to the Water Engineering Act; this act came into effect in 2024 and requires the incorporation of climate change in flood risk analyses for Switzerland.

The tool not only contains and visualizes the data presented in Chapter 4; it also enables the formation of the same configurations as outlined in the study, thus providing an even deeper insight into impact analysis. The user has the choice of displaying the sensitivity of exposed buildings, people, workplaces, and building damage on a map and comparing all impact types plotted in one graph. Slope, curvature, or the FSI can be selected to calculate sensitivity and be smoothed according to the window widths used in the study. For example, Figure 5.2 shows a section of the Emme River near Burgdorf, which is also used to present general concepts and ideas in the research article (Figure 4.1 and 4.3).

While presenting this approach at the FAN-Forum in March 2024, an annual conference of natural hazards specialists in Switzerland (*FachleuteNaturgefahrenSchweiz*, FAN), interest in the approach and the results was high. The bottom-up approach focusing on the human–environment relationship well suited the overarching topic of the conference, which was "Past extreme flood events in the countries surrounding Switzerland." The consensus across presentations and the international podium discussion about how to face the anticipated increase in flood hazard due to climate change was that scenario-neutral approaches that depart from return periods and design events and approaches that

increase social resilience require more attention than they have yet received.

Whereas the tool shows important results that should be considered in IBFWS, understanding of the content and approaches presented is not targeted on the general public or decision-makers but on experts in flood risk management. A solution has to be found to reduce the complexity behind the FSI values and how to optimally integrate it with IBFWS.

References

Attems, M.-S., Thaler, T., Snel, K. A., Davids, P., Hartmann, T., & Fuchs, S. (2020). The influence of tailored risk communication on individual adaptive behaviour. *International Journal of Disaster Risk Reduction*, *49*, 101618. doi:10.1016/j.ijdrr.2020.101618.

Copernicus Emergency Management Service (2024). European flood awareness system (efas). URL: https://www.efas.eu/.

Li, Z., & Demir, I. (2022). A comprehensive web-based system for flood inundation map generation and comparative analysis based on height above nearest drainage. *The Science of the total environment*, *828*, 154420. doi:10.1016/j.scitotenv.2022.154420.

Lumley, S., Sieber, R., & Roth, R. (2022). A framework and comparative analysis of web-based climate change visualization tools. *Computers & Graphics*, *103*, 19–30. doi:10.1016/j.cag.2021.12.007.

Maidl, E., Bresch, D. N., & Buchecker, M. (2021). Social integration matters: factors influencing natural hazard risk preparedness—a survey of swiss households. *Natural Hazards*, *105*, 1861–1890. doi:10.1007/s11069-020-04381-2.

Mohanty, M. P., & Karmakar, S. (2021). Webfris: An efficient web-based decision support tool to disseminate end-to-end risk information for flood management. *Journal of environmental management*, *288*, 112456. doi:10.1016/j.jenvman.2021.112456.

Munz, L., Kauzlaric, M., Mosimann, M., Fehlmann, A., Martius, O., & Zischg, A. P. (2023). Participatory development of storymaps to visualize the spatiotemporal dynamics and impacts of extreme flood events for disaster preparedness. *International Journal of Disaster Risk Reduction*, *98*, 104039. doi:10.1016/j.ijdrr.2023.104039.

Percival, S. E., Gaterell, M., & Hutchinson, D. (2020). Effective flood risk visualisation. *Natural Hazards*, *104*, 375–396. doi:10.1007/s11069-020-04173-8.

Rothlisberger, V., Zischg, A. P., & Keiler, M. (2017). Identifying spatial clusters of flood exposure to support decision making in risk management. *The Science of the total environment*, *598*, 593–603. doi:10.1016/j.scitotenv.2017.03.216.

Zischg, A. P., Hofer, P., Mosimann, M., Röthlisberger, V., Ramirez, J. A., Keiler, M., & Weingartner, R. (2018). Flood risk (d)evolution: Disentangling key drivers of flood risk change with a retro-model experiment. *The Science of the total environment*, *639*, 195–207. doi:10.1016/j.scitotenv.2018.05.056.

6 Conclusions and outlook

River floods cause substantial damage globally. As trends in climate change and socio-economic development increase flood risk, flood risk management strategies to mitigate flood impacts need to be reviewed. Long-term measures to mitigate impacts, for instance levees and spatial planning with hazard maps, are designed for a climate that will soon be past. The increased likelihood of extreme flood events will affect supposedly protected areas, demanding alternative solutions. Impact-based forecast and warning services (IBFWSs) are designed to provide tailored information to target users (see Figure 1.1) about the expected impacts by considering exposure and vulnerability at individual and community levels. They optimize short-term prevention and risk management by enhancing the communication between national meteorological and hydrological services (NMHSs) and decision-makers. Despite the proven effectiveness of IBFWSs, technical solutions are still needed to enhance their operational efficacy.

This thesis contributes to addressing this gap by exploring innovative approaches and methodologies. This chapter recapitulates the key findings of the three papers and the development of two web tools and their practical implications for IBFWSs in Switzerland (Chapters 2–5) and places these in their broader context. Then, an outlook provides an overview of potential follow-up research projects and limitations to further elaborate on before concluding this thesis.

6.1 Summary and implications of contributions

6.1.1 Modelling the vulnerability and damage of household contents

In high-resolution flood models, the assessment of flood hazard variables such as flow depth and flow velocity on building levels is feasible, which allows assessments of regions and buildings with a high potential for flood damage. The estimation of damage to building structure is common, and vulnerability functions to assess these are available in various forms and complexity levels, but the number of vulnerability functions for assessing damage to household contents is limited. However, an analysis of over 20,000 claim records arising from a serious flood in 2005 projected the damage to household contents to be approximately CHF 700 million (FOWG, 2005). This represents 23.3% of the total damage (CHF 3 billion) for the entire flood event. We used insurance data available in Cantons Geneva, Uri, Schwyz, Ticino, Appenzell-Innerrhoden, Valais, and Obwalden to show that the contribution of household content damage to the total damage to a building, including structural building damage, in these cantons is up to 32%; the literature review indicates an even higher proportion, of up to 36%. These numbers indicate the relevance of considering content damage in flood risk assessment.

The main contribution of this study is to develop models that derive the vulnerability or the damage of household contents based on the vulnerability or the damage on building

structure. Therefore, besides developing a model to improve the assessment of flood damage, this analysis provides insights into the relationships between building structure, content vulnerability, and damage. When analyzing the best fit of the vulnerability model (green line in Figure 2.3, top), we see that the vulnerability of content is higher for building structure vulnerabilities up than for household content vulnerability to approximately 0.6. The curve of the best fit for the monetary damage model (green line in Figure 2.3, bottom) similarly indicates that the ratio of content to structure damage is higher at lower damage. Following the common interpretation of vulnerability curves for building structures that higher magnitudes lead to higher vulnerabilities, we can infer three main findings:

- Low flow depth and velocity lead to low structural vulnerability, which leads to comparatively higher vulnerabilities to household contents.
- Due to the higher value of building structure compared to household contents, content damage is rarely higher than structural damage in monetary terms.
- Nevertheless, the parabolic shape of the best-fitting curve indicates that in cases of low damage to building structure, the contribution of content damage to total building damage is significant.

This study shows the relevance of damage to household contents and provides a robust and transferable model that can be coupled to any existing vulnerability function for building structure or even to the cost of damage to building structure estimated by insurance companies. The shapes of the curves indicate that, in particular in cases of low flood intensities, damage could most likely be reduced by, for instance, relocating movables upstairs. But such advice should be given carefully and with enough lead time before any flooding occurs, because many cases are known in which people have drowned while attempting to save valuable items from lower floors.

6.1.2 Development of a surrogate flood model for real-time flood impact forecasts

The implementation of hydraulic models in existing early- warning frameworks is often limited to the trade-off between computational efficiency and spatial resolution. Highly resolved flood models for large regions covering multiple rivers and capable of analyzing impacts at the building level require more time to simulate a flood than the time in which hydrometeorological forecasts are updated. This means that they cannot be used for IBFWSs. Approaches considering the use of deep learning techniques or running models on GPUs rather than CPUs bear the potential to simulate floods in time frames suitable for early warnings. However, the use of these approaches in IBFWSs is also limited at a national scale in Switzerland for several reasons. Firstly, the definition of high resolution has to be interpreted relative to the environment. A 10m raster-based flood model (e.g., Apel et al., 2022) will tend to overestimate floods in Switzerland, as levees usually have a width lower than 10 meters. A 10m-resolved flood model will therefore underestimate the height of the levee, and therefore also the river capacity, leading to more intense flooding on the floodplain. So far, machine learning techniques require extensive preprocessing and large amounts of training data, mostly stemming from high-resolution flood simulations conducted in the regions where they should be applied later, and such machine learning models therefore lack transferability to other regions (Bentivoglio et al., 2022).

The library-based flood surrogate model optimizes the trade-off between spatial resolution and computational efficiency (Chapter 3), providing an impact assessment similar to that of a high-resolution transient flood model. The backbone of the surrogate model is a flood library with information for every triangle mesh element about flow depth, velocity, potential hazard (Table 3.1 and Figure 3.2) over time and the peak discharge and lake level for which these variables were simulated (see 3.2.2). Compared to other computationally efficient flood modelling techniques, the surrogate flood model offers several benefits:

- Instead of using a raster-based approach, we use the BASEMENT modelling software (Vetsch et al., 2018) to simulate floods with a triangular irregular mesh. The flexibility of the computational mesh allows a spatially explicit discretization of hydraulically relevant structures such as levees from highly resolved digital elevation models (50cm to 200cm used in this study).
- Using a 1D model to simulate flow in river channels is more efficient, because 2D approaches must consider a high spatial resolution to represent river capacity adequately. Additionally, structures built for flood defense such as walls that are not entirely covered by a high-resolution digital elevation model (DEM) containing gridded elevation information are measured and stored in the cross-section data used for the 1D model. BASEMENT can determine whether the 1D-2D coupling boundary, which defines the top edge of the river channel and thus whether flooding occurs, should use the elevation stemming from the 1D model or the 2D model. However, 1D approaches do not consider superelevation in river bends and do not allow for varying velocities within river cross-sections.
- Supposedly high impacts (hazard levels 3 and 4 in Figure 3.8) are well represented by the surrogate flood models when they replace a transient flood model (area $> 83\%$, buildings $> 86\%$, population $\approx 89\%$, workplaces $> 88\%$). The difference in damage estimations across all nine scenarios and the entire study area is 7%.
- Because the flood simulations and the impacts are stored on the same PostGIS database, the spatial relation between single mesh elements and the impact locations can be preprocessed and stored as a matching table that only contains the IDs of the elements at risk with the IDs of intersecting mesh elements. This allows processing of hazard and impact information in only a few minutes even for very extreme events such as the scenario 03d-1000y_05 shown in Figure 3.4. This demonstrates that application to a hydrometeorological ensemble forecast or an analysis of potential flood events beyond a forecasted ensemble is feasible at national scale.

This work represents the thesis's core achievement and fundamental contribution: demonstrating the feasibility of acquiring detailed spatial and temporal insights into potential flood intensities and impacts from hydrometeorological forecasts. There is potential for straightforward application in existing NMHSs, as represented in Switzerland by the Federal Institute for Meteorology and Climate MeteoSwiss for weather and the Federal Office for the Environment for hydrological forecasts. The surrogate model uses only the peak magnitude of a hydrological forecast to deliver information at the same resolution as a transient model, but in minutes instead of hours or days. This provides a proof of concept that the library-based surrogate flood model approach can provide specific information on the potential impacts of anticipated flood events tailored to the

target users of IBFWSs.

6.1.3 Assessment of impact sensitivity in floodplains

As discussed in the previous section, studies focusing on the model chain in a top-down manner are often limited by computational or resolution constraints. Recent studies show the potential of bottom-up approaches on a global scale and thus concentrate on the relationship in human–environment systems (Devitt et al., 2023; Zischg et al., 2021).

Chapter 4 describes the development of the floodplain sensitivity index (FSI). Impact curves represent the relationship between flood magnitude, such as river discharge and lake levels, and its effects on the built environment of floodplains from magnitudes with potential flooding to the probable maximum flood.

By integrating the slope and curvature of the impact curve, the FSI indicates magnitude ranges and the thresholds at which impacts are sensitive to increases of magnitude. Within the model chain from weather forecasts to impact assessment, this bottom-up approach facilitates understanding of whether hydrometeorological uncertainties or uncertainties due to climate change projections at the beginning of the chain are relevant to the impact assessment. In addition to introducing the FSI, which offers a metric for understanding the sensitivity of floodplain impacts to changes in magnitude, the results highlight the following key points:

- The application of the FSI for the main rivers and lakes of Switzerland highlights floodplains that show high sensitivity to increasing magnitudes in the lower part of the spectrum of potential flood events.
- No spatial or regional pattern allows impact curves to be generalized. Additionally, the sensitivity of flood impacts is specific to buildings, workplaces, and people. Therefore, the assessment of the impact sensitivity of floodplains is specific.
- Low values for the FSI indicate magnitude ranges with low sensitivity of impacts to increases in magnitudes, potentially lowering the uncertainties in a model chain, whereas high values for the FSI indicate magnitude ranges with high impact sensitivity, which potentially amplify uncertainties along the entire model chain.
- The FSI is to be interpreted as a value that describes sensitivity relative to the highest sensitivity measured in the impact curve, maximized at 1.0. This means that, for instance, moderate sensitivity indicated by a FSI between 0.0 and 0.2 signifies that the floodplain has a threshold somewhere else on the magnitude spectrum, where a similar change in magnitude will have a much larger effect on the impact.

In summary, the FSI supports the integration of the sensitivity of impact assessment specific to different impact types with changes or uncertainties in climate change projections and in hydrometeorological ensemble forecasts. Through this, IBFWSs can be formulated more precisely and adapted to remaining uncertainties. Additionally, floodplains subject to severe increases of impact in the lower part of the magnitude spectrum can be prioritized for predisaster planning of flood mitigation measures. Lastly, the need to interpret FSI values relative to the highest sensitivity appears to be a disadvantage. However, when low FSI values within forecasted magnitude ranges coincide with high absolute numbers of impact, it signals a crucial threshold at higher magnitudes not covered by the forecast. Past events have shown that looking beyond forecasted

magnitudes is necessary.

6.1.4 Enhancing flood risk awareness through interactive web tools

Existing web-based tools have demonstrated the potential for communicating flood risks effectively through interactive maps and data visualizations by enabling near real-time visualization of potential flood impacts and thus supporting mitigation.

At the Mobiliar Lab for Natural Risks at the University of Bern, I contributed to the development of web tools within the Flood-Risk Research Initiative . My involvement included prototyping the Flood Damage Potential tool and developing Risk Dynamics, both of which received significant attention and underscored the relevance of web tools to communicating flood risk.

My involvement in the development of those web tools laid the foundation for the subsequent development of two new web tools during my PhD. These tools, Flood Dynamics and Risk Sensitivity, are closely linked to the studies described in Chapters 3 and 4. The development of such tools for IBWFS requires consideration of three key messages:

- Web tools are a two-way bridge between research and practice. Co-development of web-tools through participatory processes is beneficial. This is shown by implementation of the Flood Dynamics tool in training for emergency responders conducted by federal and cantonal authorities nearly two years after the tool was published. Discussions with, for instance, the fire brigade of the town of Burgdorf about the display of content in both tools revealed that the impact-oriented view of potential flood events is new and leads to moments of insight. Moreover, the consideration and communication of modelling uncertainties is important, because non-experts often understand the content presented as reality.
- Web tools offer the opportunity to obtain deeper insights into aggregated content presented in research papers (e.g., Figure 4.4) by providing access to to a diverse and extensive range of examples, surpassing the limitations of analyzing only a single instance (e.g., Figure 4.3) or a limited few. Web tools featuring simple graphical user interfaces facilitate straightforward analysis without presuming any programming skills.
- Furthermore, storing detailed data on a web platform allows for interactively aggregating and visualizing these to suit the specific needs of target users .

In summary, the web tools and the feedback received during participatory development highlight that the research presented in Chapters 2 to 4 are relevant to practical issues in Switzerland. Even though certain technical limitations, such as the time-consuming preprocessing required by the Flood Dynamics tool, do not allow one-to-one i ntegration of the processing chain into web-based solutions for IBFWSs, the web tools developed demonstrate the potential for such solutions.

6.2 Limitations and outlook

This chapter provides a summary of the limitations encountered in Chapters 2 to 5 and outlines future work necessary to mitigate these limitations.

Vulnerability

A general pitfall in vulnerability assessments is the uncertainties of vulnerability models. This is underlined by the spread of single observations in data used to fit vulnerability functions, for instance in Figure 2.3. One major aspect that could not be covered by the analysis in Chapter 2 is described in Fuchs et al. (2019). Besides vulnerability, this study also analyzes the general probability that a building is damaged if it is exposed. Another uncovered aspect is the frequency with which building structure was damaged without any damage to household contents. Further studies could elaborate on this relationship.

Furthermore, studies such as Keller et al. (2019) and Molinari et al. (2020) discuss how the choice of vulnerability function strongly influences the damage predicted. As mentioned, warnings and recommendations to individuals may differ according to the expected intensity of an anticipated flood. This means that it might be worth recommending that valuables from lower floors be safeguarded — if the risk to life is not raised through this. The formulation of warnings and recommendations was not the focus of this thesis, but from the modellers' perspective, it might also be interesting to analyze the extent to which the choice of a vulnerability function influences flood risk perception and consequent decision-making processes. In general, it would be interesting to further elaborate on prioritization mechanisms in decision-making processes at federal, regional, and communal governmental levels, especially for critical infrastructure such as power grids, water supply systems, and transportation networks.

Hydrodynamic modelling and sensitivity of impacts

The optimization of hydrodynamic modelling in Switzerland remains an open task, because the resolution of today's national DEMs is higher than the resolution at which it is feasible to simulate floods at national scale even with flood surrogate models. The flexible mesh approach used in these studies at least allows consideration of the major hydraulically relevant structures at the highest resolution possible. However, a more sophisticated version of the model used here could incorporate bridges in the 1D hydrodynamic model and culverts and road and railway underpasses in the 2D model not currently covered by the DEM. The integration of these structures is not straightforward. For bridges, the height of freeboard, from the space between the lower edge of the bridge and the water surface used to consider wood transport and nonlinear flow induced by turbulence , influences the discharge capacity of bridges. Additionally, the options for integrating bridges into hydrodynamic models are limited, in particular because the construction of bridges influences backwater effects, and bridges have often been observed not to resist the water pressure and collapse. The issue with culverts and underpasses is that the geometry of such structures is difficult to assess, and it is questionable whether these structures can be integrated with their full capacity into 2D models . Culverts are often subject to log-jams, and underpasses are not hydraulic structures that are constructed to transport water. The question is not whether the consideration of bridges, culverts, and underpasses can influence the propagation of floods in reality but whether their integration into the models improves flood hazard and impact assessments or merely increases the number of assumptions to be made.

The flood simulations in this thesis assume stable levees without suspension load. The lifespan of levees is limited, and those constructed decades ago might have a higher risk of collapsing, especially if overtopped. It would be interesting to analyze the extent

to which a flood simulated at the upper limit of the magnitude spectrum, ideally the probable maximum flood, might resemble a dam breach scenario in its impact.

Surrogate models derived with synthetic hydrographs have been shown to tend to underestimate the flood volume, which leads to a slightly negative bias of the impact assessment compared to transient models. It would be interesting to elaborate whether the vertexes from the FSI curve of floodplains could be used to define volume-sensitive flood magnitude ranges. I hypothesize that the magnitude ranges between vertexes at the positive Y-axis and the next vertex at the negative Y-axis are mostly sensitive to different flood volumes because they are proxies for the beginnings and ends of flood processes that lead to impacts.

Furthermore, the flood library could be tested for use with machine learning applications. The flood library consists of more than 3000 flood simulations for 179 floodplains. This dataset is suitable for testing machine learning approaches, may well solve the volume issue. The library could also be used to train machine learning models to support the downscaling of, for instance, the flood hazard and impact models of the EFAS (Copernicus Emergency Management Service, 2024), whose resolutions are currently too low for IBFWSs in Switzerland. Such a model might even be trained to entirely replace hydrodynamic models in regions without calibration; this would be a milestone because the transferability of such models is probably the remaining issue and the reason why numerical models are still used to train machine learning models.

Expanding the early warning framework of Switzerland

This thesis elaborates how to bridge the gap between NMHSs and their target users and focuses on the development of methods for integrating flood and impact modelling in early warning frameworks. The methods developed in this thesis have been shown to meet the requirements for expanding the Swiss early warning framework from the point where it currently ends, probabilistic hydrometeorological forecasts (Figure 1.2). Interactive web applications have also been shown to be suitable for communicating and distributing flood-risk-related information to the public and experts. However, some technical steps remain on the way to deriving information from a flood hazard and impact library. GeoServer is an open-source platform for sharing and editing spatial data and enables the Web Map Tile Service (WMTS) to reformat and provide spatial data to web applications as high-resolution images. Additionally, it allows the formulation of queries through the Web Feature Service (WFS) to retrieve specific data from databases, thus facilitating the integration and manipulation of spatial information in visual presentations and analyses. First tests have shown that GeoServer is able to deliver highly resolved flood hazard and impact data to web applications. This means that data stored on the database can be queried via GeoServer using QGIS, Python, JavaScript, or any other programming language or software tool that supports the OGC standards, such as WFS, WMTS, and WMS, for accessing, querying, and manipulating spatial data. Therefore, GeoServer's integration into the national flood early warning system should be possible and could be tested.

6.3 Concluding remarks

By developing a flood vulnerability function for household contents relative to building damage, this thesis provides a novel approach to improving the accuracy of damage assessments. The approach aids response planning by insurance companies and by public target groups because it shows that at low flood intensities, and therefore low vulnerabilities for buildings, the proportion of damage to household contents can be substantial (Chapter 2).

Furthermore, I evaluated an innovative approach to embedding hydrodynamic analysis in model chains that optimizes the trade-off between computational efficiency and spatial resolution. This surrogate flood modelling approach allows high-resolution impact analysis to be used in IBFWSs; it is similar to transient models but better suited to the requirements of early warning applications (Chapter 3). Surrogate flood models allow impact analysis within a few minutes, and they may also be implemented in probabilistic forecasts at national scale (see Section 1.2) from NMHS.

This thesis introduces floodplain sensitivity index (FSI), a metric that can transmit the uncertainties of a hydrological ensemble forecast to the sensitivity of impacts in a floodplain (Chapter 4). The FSI is derived from the relationship between flood magnitude, here taken as peak discharge or lake level, and impacts on the floodplain. A low FSI signals low impact sensitivity to the ensemble forecast and thus indicates that warnings may be formulated more precisely; a high FSI signals that warnings must be formulated more generally. Nonetheless, providing information on the impacts and making flood maps available remains indispensable (Chapter 3).

The development of two web tools in collaboration with experts in flood risk management and potential target users shows the potential of integrating the entire scientific contribution into practice. This integration could occur within the existing web-based framework of the Federal Office for Meteorology and Climatology, MeteoSwiss, and the Federal Office for the Environment, FOEN, to enhance the impact-based warning of flood events. Although some minor technical implementation steps remain to entirely incorporating the modelling perspective gained in this thesis and extending the weather forecasts with impact forecasts, the path to resolving these issues and preparing model outputs for cartographic near-real-time visualizations is clear. This represents a significant milestone.

References

Apel, H., Vorogushyn, S., & Merz, B. (2022). Brief communication: Impact forecasting could substantially improve the emergency management of deadly floods: case study july 2021 floods in germany. *Natural Hazards and Earth System Science*, *22*, 3005–3014. doi:10.5194/nhess-22-3005-2022.

Bentivoglio, R., Isufi, E., Jonkman, S. N., & Taormina, R. (2022). *Deep Learning Methods for Flood Mapping: A Review of Existing Applications and Future Research Directions*. doi:10.5194/hess-2022-83.

Copernicus Emergency Management Service (2024). European flood awareness system (efas). URL: https://www.efas.eu/.

Devitt, L., Neal, J., Coxon, G., Savage, J., & Wagener, T. (2023). Flood hazard potential reveals global floodplain settlement patterns. *Nature communications*, *14*, 2801. doi:10.1038/s41467-023-38297-9.

FOWG (2005). Bericht über die hochwasserereignisse 2005. *Federal Office for Water and Geology*, . URL: http://www.news.admin.ch/NSBSubscriber/message/attachments/1123.pdf.

Fuchs, S., Heiser, M., Schlögl, M., Zischg, A., Papathoma-Köhle, M., & Keiler, M. (2019). Short communication: A model to predict flood loss in mountain areas. *Environmental Modelling & Software*, *117*, 176–180. doi:10.1016/j.envsoft.2019.03.026.

Keller, L., Zischg, A. P., Mosimann, M., Rössler, O., Weingartner, R., & Martius, O. (2019). Large ensemble flood loss modelling and uncertainty assessment for future climate conditions for a swiss pre-alpine catchment. *The Science of the total environment*, *693*, 133400. doi:10.1016/j.scitotenv.2019.07.206.

Molinari, D., Scorzini, A. R., Arrighi, C., Carisi, F., Castelli, F., Domeneghetti, A., Gallazzi, A., Galliani, M., Grelot, F., Kellermann, P., Kreibich, H., Mohor, G. S., Mosimann, M., Natho, S., Richert, C., Schroeter, K., Thieken, A. H., Zischg, A. P., & Ballio, F. (2020). Are flood damage models converging to "reality"? lessons learnt from a blind test. *Natural Hazards and Earth System Sciences*, *20*, 2997–3017. URL: https://nhess.copernicus.org/articles/20/2997/2020/. doi:10.5194/nhess-20-2997-2020.

Vetsch, D., Siviglia, A., Caponi, F., Ehrbar, D., Gerke, E., Kammerer, S., Koch, A., Peter, S., Vanzo, D., Vonwiller, L., Facchini, M., Gerber, M., Volz, C., Farshi, D., Mueller, R., Rousselot, P., Veprek, R., & Faeh, R. (2018). Basement - basic simulation environment for computation of environmental flow and natural hazard simulation..

Zischg, A. P., Röthlisberger, V., Mosimann, M., Profico-Kaltenrieder, R., Bresch, D., Fuchs, S., Kauzlaric, M., & Keiler, M. (2021). Evaluating targeted heuristics for vulnerability assessment in flood impact model chains. *Journal of Flood Risk Management*, *5*, 171. doi:10.1111/jfr3.12736.

Acknowledgements

Being in the right place at the right time, or in other words, meeting the right people at the right time. That's how it feels regarding the journey of my PhD and my work at the Mobiliar Lab for Natural Risks, which are closely intertwined. I am profoundly grateful for the support and encouragement I have received over the last years. This achievement would not have been possible without the support of a number of individuals and institutions.

First and foremost, I extend my deepest gratitude to my supervisor, and mentor of almost 10 years, Andreas Zischg. His great trust and patience, insightful feedback, and brilliance and expertise have provided me with an excellent environment and the motivation to shape my research and academic growth. I am also thankful to my co-supervisor, Olivia Romppainen-Martius, whose inputs and perspectives were invaluable for the successful completion of this work. Her suggestions and constructive criticism have significantly contributed to the quality of my work.

I am also grateful to the Oeschger Centre for Climate Change Research and the Mobiliar Insurance Company, especially Luzius Thomi. Their joint research initiative, the Mobiliar Lab for Natural Risks, created the foundation and environment for this dissertation to come about at all. This dissertation shows that knowledge transfer is not one-sided but that science itself benefits from practical insights —- and that the standards for the projects at the Mobiliar Lab are no less than those for scientific works.

A special thanks also to all former and current team members of the Mobiliar Lab and the groups of hydrology and geomorphology for numerous inputs, interesting discussions, and varied coffee breaks and lunches.

Furthermore, I am deeply thankful to the entire GIUB domain for providing me with a welcoming and productive workspace over the years. My gratitude extends to everyone working behind the scenes, ensuring that everything operates seamlessly.

Lastly, it's not taken for granted to be able to write a dissertation with three young children. My heartfelt thank goes to my wife, Patricia, who, during my entire challenging activity at the Mobiliar Lab, and especially in the last weeks and months, has supported me and made writing this thesis possible. To my children Zoë, Amelie, and Michelle, your endless love has given me strength and kept me grounded.

Declaration of consent

on the basis of Article 18 of the PromR Phil.-nat. 19

Name/First name	Mosimann, Markus
Registration number	10-120-491
Study program	PhD in Geography Bachelor ☐ Master ☐ Dissertation ☒
Title of the thesis	From Weather Forecasts to Impact-Based Flood Warning Systems - a Modelling Perspective
Supervisors	Prof. Dr. A. Zischg and Prof. Dr. O. Romppainen-Martius

I declare herewith that this thesis is my own work and that I have not used any sources other than those stated. I have indicated the adoption of quotations as well as thoughts taken from other authors as such in the thesis. I am aware that the Senate pursuant to Article 36 paragraph 1 litera r of the University Act of September 5th, 1996 and Article 69 of the University Statute of June 7th, 2011 is authorized to revoke the doctoral degree awarded on the basis of this thesis.

For the purposes of evaluation and verification of compliance with the declaration of originality and the regulations governing plagiarism, I hereby grant the University of Bern the right to process my personal data and to perform the acts of use this requires, in particular, to reproduce the written thesis and to store it permanently in a database, and to use said database, or to make said database available, to enable comparison with theses submitted by others.

Bern, 2 May 2024 Markus Mosimann